UNIVERSITY
OF TASMANIA

Performance of an Auger Dredging Cutter for Subsea Dredging and Mining

by

Mridul Kumar Sarkar

National Centre for Maritime Engineering and Hydrodynamics

Australian Maritime College

Submitted in fulfilment of the requirements for the Doctor of Philosophy

University of Tasmania January, 2013

DEDICATION

Dedicated to

Sri Aurobindo

and

The Mother

Acknowledgement

At the onset I must express my thanks and gratitude to Prof. Neil Bose. Without his initiation, constant inspiration and guidance, this research would not have been possible. Dr. Shuhong Chai and Dr. Kim Dowling always encouraged and helped me to focus on the subject and my thanks are due to them. Dr. Jonathon Binns always looked after even my trifle requirements about research and I would like to thank him. Dr. Ranmuthugala Dev helped me a lot by providing many information and literature whenever I approached him and I thank him in this occasion. My young colleagues always helped and taught me all the tricks essential for research and I am taking the opportunity to thank them all. I am remembering all the people at AMC, and thanking all of them, who made my time at Launceston pleasant and helped directly or indirectly in my research.

The research was funded jointly by the Australian Maritime College, Australia and Excavation & Equipment Manufacturing (P) Ltd. India. I thank them for their support.

I thank my daughter Dr. Ir. Sritama Sarkar, who supplied me a lot of latest information about the dredging and subsea technology. Lastly, I am giving my heartfelt thanks to my wife Mamata Sarkar, who always motivated and inspired me and took all the burden of the mundane household chores during my research.

January 2013

Australian Maritime College

University of Tasmania, Launceston,

Tasmania, Australia

Declaration of Originality

This thesis contains no material which has been accepted for a degree or diploma by the University or any other institution, except by way of background information and duly acknowledged in the thesis, and to the best of the my knowledge and belief no material previously published or written by another person except where due acknowledgement is made in the text of the thesis, nor does the thesis contain any material that infringes copyright.

(MRIDUL KUMAR SARKAR)

Student ID: 117510

Dated: 24 January 2013

Australian Maritime College,

University of Tasmania,

Newnham, Launceston,

Australia

Authority of Access

1. This thesis may be made available for loan and limited copying and communication in accordance with the Copyright Act 1968.

2. This thesis may be made available for loan. Copying of any part of this thesis is prohibited for two years from the date this statement was signed; after that time limited copying and communication is permitted in accordance with the Copyright Act 1968.

3. This thesis is not to be made available for loan or copying for two years following the date this statement was signed. Following that time the thesis may be made available for loan and limited copying and communication in accordance with the Copyright Act 1968.

4. (A statement of conditions applying to loan and access for copying which is consistent with any existing (intellectual property or other kind of) agreements relating to the thesis or work reported in it.)

(Mridul Kumar Sarkar)
Student ID: 117510
Date: 24 January 2013

Australian Maritime College,
University of Tasmania,
Newnham, Launceston,
Australia

Statement regarding Published Work contained in Thesis

The publisher of the paper, 'Conceptual Design of a Submersible Remotely Operated Swimming Dredger (SROSD) - [49868]', comprising Chapter 3 hold the copyright for the content, and access to the material should be sought from the respective journal. The remaining non published content of the thesis may be made available for loan and limited copying and communication in accordance with the Copyright Act 1968.

(MRIDUL KUMAR SARKAR)

Student ID: 117510

Dated: 24 January 2013

Australian Maritime College,

University of Tasmania,

Newnham, Launceston,

Australia

Abstract

Increasing use of deep-water dredger and miner vehicles has been anticipated for resource collection, engineering construction and environmental protection. Among existing deep-dredging equipment designs submersible dredgers have advantages over others such as surface designs.

Considering the limitations of commercially available and conceptualised submersible dredgers, a different type - the 'Swimming Remotely Operated Submersible Dredger' (SROSD) is conceptualised in this research. In its working mode, it imitates a walking motion by using spuds that are also used for station keeping during dredging. When required, the vehicle can swim by means of vector thrusters. The vector thrusters also help in position-keeping and motion-control during swimming. To offset high forces generated during excavation of hard materials, spuds, variable buoyancy tanks and control planes are included as secondary station-keeping devices. The general arrangement and the sub-systems of the conceptualised vehicle are described.

For swimming and control in a submerged condition, the vehicle is ballasted to a neutrally buoyant condition. Balancing of the excavation forces is necessary for efficient production and this is a design problem with submersible dredgers. A transverse axis auger cutter capable of surgical cutting with low force fluctuations is used in the design. A theoretical model of the cutting forces in vertical and horizontal directions generated by this type of cutter is proposed.

An experiment was designed to measure the cutting forces generated by this cutter. Comparisons between the power requirements derived from the experiment and the theoretical model were done to validate the model. The measured experimental power requirements were found to be within the calculated power ranges for dredging loose to slightly compacted sand in similar operating conditions.

In a further experiment to assess the spillage from the cutter in operation, near and far field turbidity generation by the auger was measured by using turbidity sensors. Measurements of turbidity were taken to indicate the environmental impact of the auger. It was observed that the turbidity increase was dependent on the relative position between the probes and the auger and its shroud.

It is hoped that, through this work, a new design of vehicle, along with the reaction force analysis of the excavation and the turbidity measurements will significantly contribute to the evolution of existing deep-dredging and mining equipment leading to improved efficiency, increased mobility and position control while minimising environmental disturbance.

Table of contents

Table of Figures

Table of Tables

Table of Symbols

A	Representative area
A_{fs}	Area of flight straight cutting edge
A_{ff}	Area of flight fold cutting edge
A_{vs}	Area of shear for vane edge cutting
a_h	Coefficient
a_v	Coefficient
b_b	Width of cutting blade
b_{fs}	Straight flight cutting edge width
b_{ff}	Fold flight cutting edge width
b_h	Coefficient
b_v	Coefficient
C_D	Drag coefficient
C_s	Clearance between auger and soil
C_v	Clearance between auger and virtual casing
C_w	Virtual clearance between auger and water
c	Cohesion in Coulomb's equation, $\tau_f = \sigma \tan \varphi + c$
c_h	Coefficient
c_0	Material resistance coefficient
c_v	Coefficient
D_a	Diameter of cutter or auger (m)
D_r	Relative density
d_a	Diameter of auger shaft
d_{10}	Grain size at 10% passing
E_{spec}	Specific energy of cutting
E_{spec_c}	Specific energy for granular material under cavitating condition
$E_{spec_{nc}}$	Specific energy for granular material under non-cavitating condition
e	Porosity, Actual pore volume present in the field
$e_{\max}$	Pore volume in the loosest state
$e_{\min}$	Pore volume in the densest state
F_{ai}	Shaking forces and moments due to various actuators (hydraulic cylinders, electrical motors)

F_b Buoyancy forces due to total submergence in water, acting along '-Z' axis

F_c Excavation forces acting at the cutter circumference, resolved into 'X', 'Y' and 'Z' axes as F_{ca}, F_{ch}, F_{cv} respectively

F_{ci} Cutting force

F_f Total cutting force at the flight straight and fold cutting edge

F_{g_a} Weight force of the actuator assembly, acting along 'Z' axis

F_{g_D} Weight force due of the vehicle acting along 'Z' axis at its centre of gravity

F_{HC} Horizontal force component, Excavation force

F_{HL} Horizontal force component measured at Load cell

F_O Force due to the overburden of sand and water

F_p Transport forces as vibrations felt at the mountings of the dredge pump, and the delivery pipeline

F_R Tangential force supplied by the auger drive motor

F_s Force due to the currents at the place of operation

F_T Horizontal force to auger by hydraulic cylinder (feed force)

F_u Circumferential force used for sand cutting

$F_{u_{av}}$ Average tangential force

F_{uh} Horizontal force component

F_{uv} Vertical force component

F_v Force required for vane edge cutting

F_{VC} Vertical force component, Excavation force

F_{VL} Vertical force component measured at Load cell

F_W Warping force, provided by the swing hydraulic cylinder to give necessary feed to the cutter

g Acceleration due to gravity

h Depth of cut (m)

h_i Initial layer thickness

h_w Water depth

I_R Relative dilatancy index

k Permeability of granular soil

k_{if} Inclination factor (for horizontal configuration, k=1)

L_b Blade length

L_v Total length of vane engaged in cutting,

L_{vp}	Length of vane engaged in cutting in one pitch length
M_{ai}	Shaking moments due to various actuators (hydraulic cylinders, electrical motors)
N	Revolutions per minute
n	In-situ pore volume, porosity
n_f	Number of flights
n_p	Number of pitches in the auger
P_e	Cutter power for cutting
P_{se}	Cutting power on Specific Energy
p_a	Pitch of auger
P_H	Soil transport power of auger
P_n	Powers lost due to friction for a screw conveyor
Q	Actual volumetric transport output of an auger
Q_e	Excavation production of cutter
Q_{loss}	Volume loss during transport
Q_{se}	Excavated volume on Specific Energy
Q_{th}	Theoretical volume of transported material
q	Uniform surcharge pressure
q_c	Cone resistance
R	Resistance
R_a	Radius of auger
r_a	Radius of auger shaft
t_{ff}	Thickness of flight fold cutting edge
t_{fs}	Thickness of flight straight cutting edge
t_i	Instantaneous time
t_v	Thickness of vane edge
t_{vb}	Thickness of auger vane blade
U	Speed of the body
u	Pore pressure
v_t	Operating velocity of blade
v_c	Cutting velocity
v_T	Warping/ Horizontal velocity
X_C	Distance between cutter centre and cutter vertical component
X_L	Distance between cutter centre and Load cell vertical component

Y_C	Distance between cutter centre and cutter horizontal component
Y_L	Distance between cutter centre and Load cell horizontal component
z	Number of cutter blades
α	Flight angular spacing of auger
α_{br}	Blade rake angle
α_f	Angle between the critical plane and the major principal plane
$\left(\frac{\delta s}{\delta t}\right)$	Deformation rate
ϕ	Internal friction angle of soil
φ	Flight phase angle between two consecutive flights
ψ	Angle of dilatancy
Γ	Coefficient for transported volume by an auger
γ_s	Soil bulk density
γ_r	Relative density of granular soil
η_F	Fullness efficiency
η_v	Volumetric efficiency
η_{VR}	Vortex efficiency
μ	Coefficient of sand to metal friction
ω	Angular velocity of auger = $2\pi n$
θ_e	Effective angle at which the average tangential cutting force acts
θ_i	Angle of tangential cutting force with the horizontal
ρ_w	Density of water
σ	Normal stress of soil
σ_1	Major normal stress
σ_3	Minor normal stress
τ	Shear strength
τ_u	Undrained shear strength
τ_f	Failure stress of soil
τ_p	Peak undrained shear strength of soil
τ_F	Total shear force
ξ	Ratio of depth of cut to cutter diameter

List of Abbreviations

AUV	Autonomous underwater vehicle
CEDA	Central Dredging Association
CEMA	Conveyor Equipment Manufacturers Association
DAQ	Data acquisition system
DOF	Degrees of freedom
DPC	'Dredging and Port Construction' Magazine
EBA	European Boating Association
EBI	European Boating Industry
ECSA	European Community Ship-owners Association
EDF	Environmental defence fund
EEM	Excavation & Equipment Manufacturing (P) Ltd
EIA	Environmental impact analysis
ESPO	European Seaports Organization
EuDA	European Dredging Association
GES	Good Environmental Status
IADC	International Association for Dredging Companies
ICOMEA	International Council of Marine Industry Associations
ISU	International Salvage Union
LARS	Launching and Recovery System
lps	Litre per sec
MSFD	Marine Strategy Framework Directive
MSNG	Marine Strategy Navigation Group
NTS	Not to scale
PIANC	International Navigation Association
PDS	Product Design Specifications
PSD	Particle size distribution
ROV	Remotely operated vehicle
RPM	Revolutions per minute
rpm	Revolutions per minute
SMT	Sea Mining Tool
SROSD	Submersible remotely operated swimming dredger
TSHD	Trailing Suction Hopper Dredger

TSS	Total suspended solid
VBT	Variable buoyancy tank
WHO	World health organization

CHAPTER 1 INTRODUCTION

1.1. Preamble

Dredging is now essentially used for, deepening navigation channels, reclamation and creation of new lands, collection of sands and boulders, harvesting of mussels and clean up contaminated sediments. Future extension of this technology will require dredging at increased depths for creation of new land (Endicott 2001; Nakheel 2009), resource collection under the sea (Department of Sustainability 1981; Desa 1999; Gooch 2012; IADC 2012; Paragon International 1993; Parr et al. 2009) construction of wind and wave power generating stations (Piere et al. 2009), cable and pipeline burials, oil and gas extraction, underwater agriculture to meet the future food demands, controlled aquaculture within specific areas, drawing out of subsea health and cosmetic ingredients, such as red sea clay, underwater tourist spot development and environmental issues. This list is not exhaustive.

Among the existing deep dredging equipment, submersible dredgers are more suitable than others (Sarkar2007). Submersible crawlers and walkers work in a submerged terrain-contact condition and depend on their apparent weight and ground reactions to counteract the excavation forces. Crawlers are inefficient in negotiating difficult sub-sea terrain and walking submersibles are slow moving over long-distances. Considering the constraints of dredging depth, negotiation of uneven terrain, slow motion, interchange ability of excavation or transport sub-system components and station keeping during operation, a new type of submersible dredger or miner was conceived. To overcome the limitations of the existing submersible dredgers a new submersible remotely operated swimming dredger (SROSD) was conceptualized.

Dredgers loosen materials either by plain suction or by water jets or mechanical excavating tools for hard materials. All the rotary cutters including crown, basket, chain buckets and dredging wheels generate fluctuating impact reaction forces during excavation. Transverse axis auger cutters are better in this respect for their almost constant excavation reactive forces. The swimming submersibles being marginally neutrally buoyant need appliances to counterbalance the excavation forces for efficient dredging.

The objective of this research was to investigate the nature of the excavating force components in vertical and horizontal directions produced by a transverse axis auger when dredging sand. The possibility of counterbalancing the reaction force components by vector thrusters, otherwise used for propulsion was investigated. If thruster balancing is found insufficient, then additional methods for counter balancing, (e.g. anchoring by spuds, variable buoyancy tanks, control surfaces) were also discussed. Environmental impact is an issue for dredging. Near and far-field turbidity generated during dredging by an auger is a suitable indicator for environmental impact assessment. A test tank was designed and built to measure the excavating force components and near and far-field turbidity generation, during dredging loose and slightly compacted fully saturated sand. The experimental results of force components were validated by comparing the experimental power requirements, to those based on specific energy for dredging sand. The results are discussed in relation to a typical design of the submersible remotely operated swimming dredger (SROSD).

1.2. Motivation and Research Questions

As land-based natural resources become depleted with the increasing demands of global population (Wikipedia 2010), underwater excavation at greater depths is projected to be an increasing interest for the purposes stated above. Underwater excavation at greater depths is possible either with, (i) diver assisted dredging equipment, (ii) surface floating dredgers having long actuating arms (ladder boom) (iii) modified commercial remotely operated vehicles (ROV) or with iv) submersible dredgers.

Diver assisted dredging equipment is limited in capacity and involves human risk. Surface floating dredgers can dredge to specific maximum water depths, depending on their size and ladder length. Mobilization, interchange ability of components required for different working conditions are expensive for the big surface floating dredgers. Waves and swells also shift the mechanical cutter from its desired trajectory, affecting excavation production. In some cases, the operating accessories such as wires, pipelines and cables may be a hazard to navigation. Submersible vehicles are not limited to a specific operational depth. Hence, increased utilisation of submersible dredgers and miners is expected, with increasing use in subsea mining for valuable minerals (Nautilus 2009), construction materials, land creation by reclamation, underwater tourism (Primidi 2009)

and construction of green power stations with the help of wind, current or wave energy. Submersible dredgers and miners used for commercial purposes are tracked vehicles. Tracked vehicles may move more quickly, but are unable to traverse on high gradients and uneven terrain. Limited research has been done on legged submersible dredgers and miners, which are suitable for locomotion on uneven and undulating terrain (Hisao et al. 1999; NIOT 2002; Verheul et al. 2004; Sarkar 2007). Legged submersible dredgers are slow moving, hence unsuitable to work in disjointed underwater work spaces, separated by uneven terrains.

With the above background, the main research question was:

"Can a submersible dredger be designed to exceed existing parameters with respect to locomotion, interchange ability of tools, precision, position keeping and minimal environmental impact potentials with comparatively lower cost?"

A free-swimming vehicle that can also come in ground-contact condition when required is a suitable design that can overcome the above limitations. Free swimming vehicles can fly at relatively high speeds compared to tracked vehicles and their mobility is not restricted by the terrain topography. Also, free swimming vehicles can be moved relatively easily and quickly between different working zones when compared to tracked and legged vehicles. Modular design of the vehicle can provide interchange ability of working tools and with small size, the production cost can be reasonable. For higher dredging or mining rates, a number of these machines could run in parallel operations.

Free-swimming vehicles include a) the work class ROVs used primarily in inspection and maintenance works for the oil and gas industries and b) the ROVs with jetting tools (i.e. for hydraulic excavation) used for subsea cable and pipeline burial applications. Mechanical excavation devices (i.e. cutters) are currently not used with free swimming vehicles. Mechanical excavation is highly efficient compared to hydraulic excavation in soils of higher strength and in rock. Mechanical excavation forces are however higher in magnitude and more dynamic in nature compared to hydraulic excavation forces. The free-swimming vehicles are neutrally or marginally neutrally buoyant. High excavation forces encountered during dredging or mining may disturb the position keeping of the vehicle and the cutter could move away from the desired trajectory. With uncontrolled cutter motion, the production would be affected and the system would be inefficient.

Furthermore, the choice of cutter is also important for the mechanical excavation under water. For position-keeping of the vehicle almost constant excavation forces are desired, rather than fluctuating periodic loads. To minimise environmental disturbances, the cutting should be closely controlled with less dispersion of the excavation materials. The dispersed materials increase turbidity in the near and far-field of the cutter. The turbidity flume is an indicator of the environmental impact. The next research sub-question was obviously,

"How can the excavation forces be counteracted and what type of cutter produces the least variance in excavating forces with minimal dispersion of the spilled dredged material?"

The mechanical excavation devices used for surface floating dredgers include axial cutters e.g. dredge cutter head, previously also known as crown/ basket cutter head and transverse cutters e.g. augers, rotovator (Figure 1- reproduced with permission from EEM Pvt. Ltd.).

Crown cutter **Auger cutter**

Figure 1 Mechanical cutter for dredging

The forces generated by axial cutter heads continuously change because of the contour of the cutter head, which has been optimised for efficient gathering. In order to counteract the cutting forces, a significantly heavy ladder structure is required (Figure 2- reproduced from the lecture notes of TID given to the author in 1993). Weight is a major concern for any submersible vehicle. Transverse cutters are cylindrical in shape and remove soil in thin layers (surgical cutting). As a result, the cutting force variation is much lower when compared with axial cutters. For surface floating dredgers, the length of the auger is the same as the width of the dredger, which reduces the reset time of the cutter.

For tracked or legged submersible vehicles, the hydraulic or mechanical excavation forces are balanced by the traction generated at the terrain interface and the weight of the vehicle. For free swimming jetting machines, the hydraulic excavation forces are balanced by thrusters.

Figure 2 Ladder structure for dredge cutter head

Taking into account the restrictions of dredging depth, negotiation of uneven terrain, slow motion, the interchange ability of sub-system components and station keeping of a vehicle during operation, a new type of submersible remotely operated swimming dredger (SROSD) or miner was conceived in this work. The vehicle is small, modular and incorporated with excavation force counter acting devices, described later. A transverse axis cutter was used as the excavating tool that produces almost constant excavation forces. A shroud was provided surrounding the cutter, to reduce turbidity dispersions.

Extensive research has been done by the dredging industry to determine the forces generated while excavating granular and cohesive soils and rock with axial dredge cutter heads (He 2005; Hofstra et al. 2000; Joanknecht 1976; Joanknecht 1975; Joanknecht 1974; Ma & Miedema 2006; Miedema 2010a; Miedema 2010b; Miedema 2009; Miedema et al. 2004; Miedema 2003; Miedema 1994; Miedema 1989; Miedema 1987; Miedema 1985a; Miedema 1985b; Miedema 1983; Van Os 1987; Van Os 1977). No such work has been found in published literature on augers or transverse cutters. For the efficient workability of the conceptual design, it is important to consider the following issues:

"What is the nature of the excavation force created by an auger during dredging and how efficient is the cutter system to control the dispersion of the dredged spilled out materials?"

1.3. Research Aim

Given the expansion of industry needs, for which submersible mining and dredging machines are necessary, the following research aims were formulated:

a) To visualise a conceptual design of a submersible dredger to exceed existing parameters with respect to locomotion, slow mobility, position keeping and environmental impact

b) To conduct an experimental program, with a full size auger dredging cutter, to assess the generated important excavation force components, which affect position-keeping of the conceptualised dredger

c) To assess the environmental impact of the auger, by using turbidity as an indicator during dredging.

This thesis is divided into nine chapters and the contents are stated below:

In Chapter 2, a literature review was done to locate the possible areas, where submersible dredgers could be used. To know about the current technology about surface floating dredgers with deep dredging capability, submersible vehicles for deep underwater excavation, propulsion and control of dredgers, counterbalancing of dredging excavation forces and dredging environmental issues, literature surveys were done. In Chapter 3, a conceptual design of a Submersible Remotely Operated Swimming Dredger (SROSD) is presented. Existing theoretical excavation models of dry as well as saturated granular soils are described in Chapter 4. A theoretical excavation model related to an auger for dredging saturated sand is developed in this research and presented in Chapter 5. To validate the theoretical model, an experimental set-up was designed, fabricated and instrumented by the author. The experiment is described in Chapter 6. The experimental results are discussed along with the validation and presented in Chapter 7. Environmental impact of submersible dredging vehicles is described in Chapter 8. Turbidity being a suitable indicator for environmental impact assessment, the near-field and far-field turbidity generated during dredging sand by an auger was investigated. The efficiency in

controlling the turbidity by a shroud, fitted partly covering the auger was also experimented. The results of this experiment were also shown in Chapter 8. Lastly, in Chapter 9 a conclusion was made with the limitations of the present work and recommendations for future works.

CHAPTER 2 LITERATURE SURVEY

2.1. Scope of Literature review

As this work is related to deep dredging hence, literature survey was done on the possible areas, where submersible dredges could be potentially used. In order to identify and summarize current technology related to deep water dredging, the significance of this research, and research already pursued by other researchers, literature reviews have also been done on, a) surface floating dredgers with deep dredging capability, b) submersible vehicles for subsea excavation, c) propulsion and locomotion of submersible vehicles including control and d) counterbalancing of excavation forces.

2.1.1. Possible use of deep dredging

Underwater excavations are necessary for loosening of soil, deepening, exploitation or by selective deposition. These processes could be used for, a) burials of cables and pipelines (Goldewijk 2001; Reece et al. 1986), b) creation of new land (Endicott 2001), c) exploitation of beneficial resources available under water, shown in Figure 3, d) mining of engineering materials, minerals (Desa 1999; Jackson et al. 2007; Mero 1964; NIOT 2002), oils and gases, e) setting of alternate sustainable power plants (Peire et al. 2009), f) supply of foods (Damen 2010; Zwanenburg 2004), g) source for cosmetic and health care related materials e.g. red sea clay (Fichter 1978), h) development of spots for tourism, entertainment and recreation (Primidi 2009), i) aquaculture and agriculture under water due to global warming (EDF 2009), and j) supply of unpolluted drinking water with increased surface water storage by deepening reservoirs (IWMI 2009; Smedley & Kinniburgh 2009; WHO 2001). A list of the resources that can be exploited with the deployment of submersible dredgers/ miners is shown in Figure 3.

2.1.2. Surface floating dredgers with deep dredging capability

Herbich (1992) and TID (1993) classify surface floating dredgers. A general classification is proposed by the author as shown in Figure 4. Dredging depth of surface-floating dredgers is increasing with industry demand. For excavation of subsea soils to a limited depth, different types of normal surface floating dredgers with long ladder booms and attachments are commercially available (Winkelman 2011). The following paragraphs present a brief literature survey on surface floating dredger with deep dredging capability.

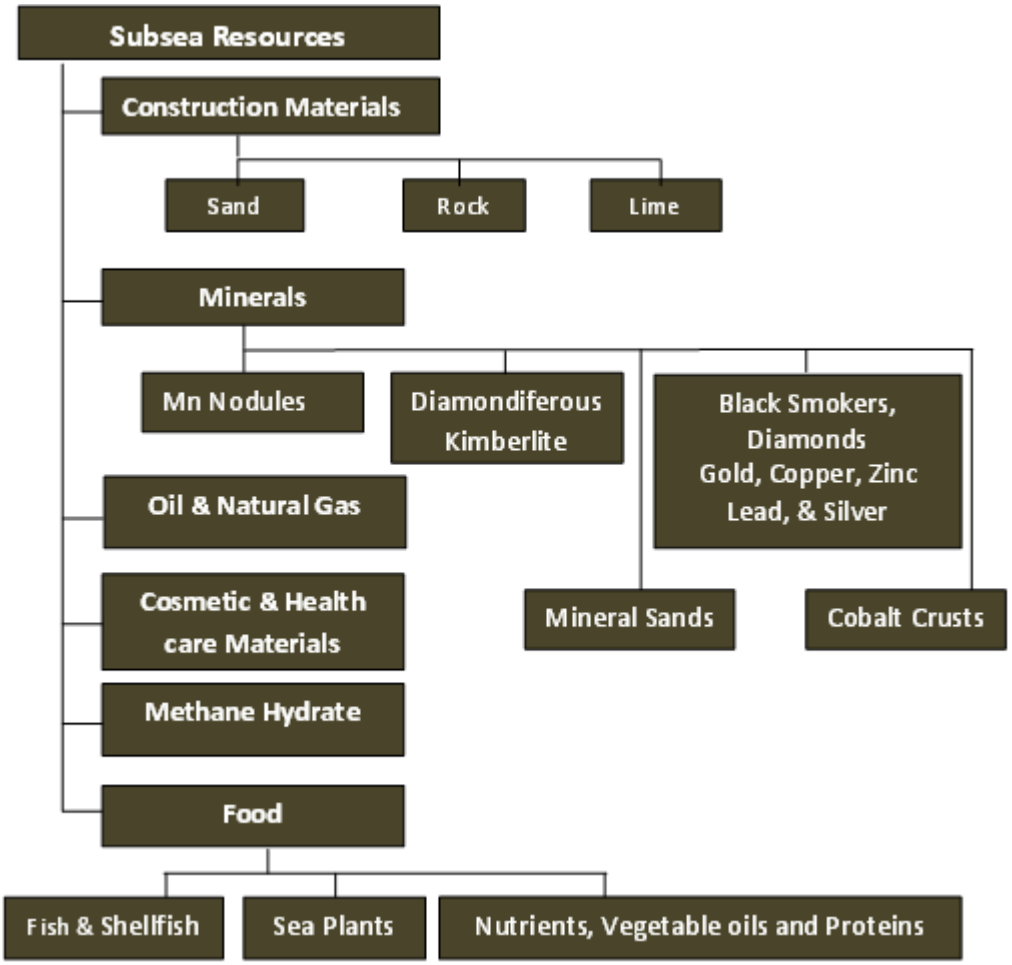

Figure 3 Resource exploitations – potential submersible dredger/ miner deployment

In 1994, Kurimoto Ltd. Osaka, Tokyo, Japan (Kurimoto 1994) developed 'an electrically powered dredge pump system known as Amaluza 1', with a travelling reel and flexible hose to work up to a depth of 110 m. The system placed on board of a vessel was first used in the Amaluza Dam, INECEL, Ecuador and later used in Singapore to reclaim the area for expansion of the Changi airport (Kurimoto 1994).

Some examples of surface floating deep dredging equipment are shown in Table 1 (Adrian 1999). Development of the deep dredging capability of surface floating dredgers during the last two decades is cited by Van de Velde (2008).

Huge quantities of sand, clay and rock are required for the big projects done for reclamation from the sea. Examples are the formation of the Lap Kok airport in Hong Kong, (Endicott 2001), creation of the islands 'Palm Island' (Wikipedia 2009), 'The World' (Nakheel 2009) in the Middle East. For these dredging projects mega sized trailing suction hopper dredgers (TSHD) with deep dredging capabilities were used. Jan De Nul, the

Belgian contractor now possesses the dredger Leiv Eiriksson capable to dredge to a depth of 155 m (Slinn 2009).

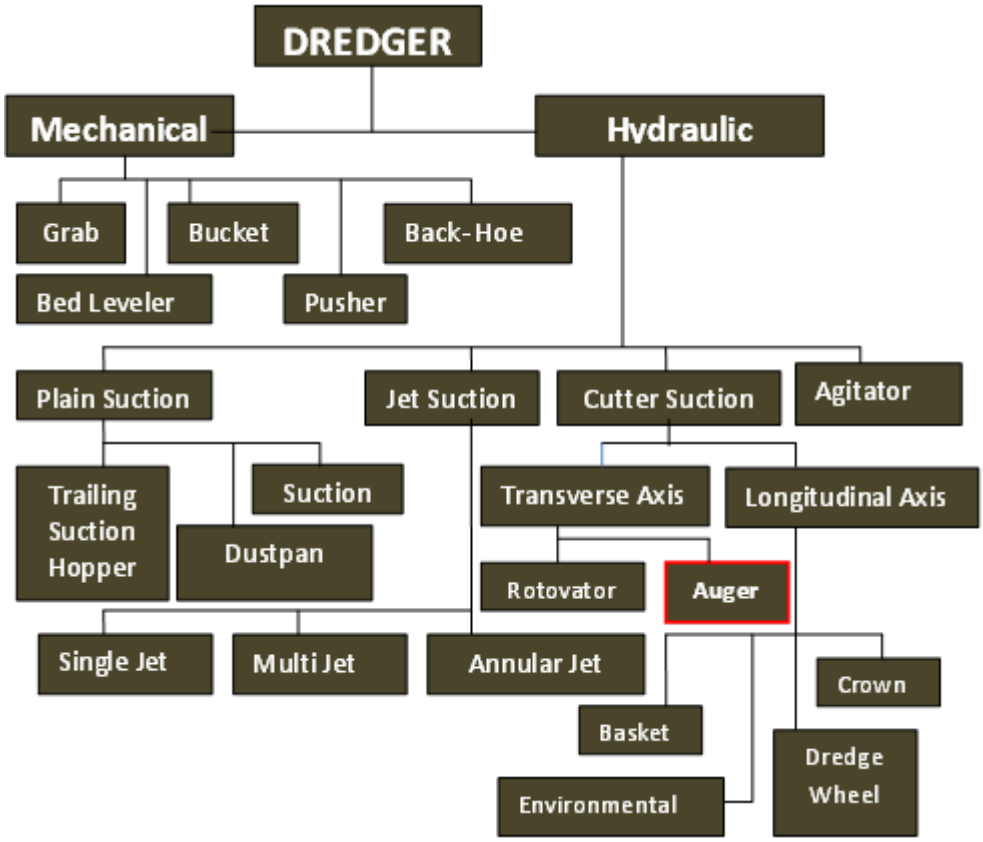

Figure 4 Classification of surface floating dredgers

Grab dredgers are sometimes used for deep dredging operations. A classic example is the 'White Rose glory holes' project at a water depth of 120 metres in Canada (Boskalis 2000). In the offshore oilfields near Newfoundland, the huge floating icebergs can damage the submerged oil pipes if exposed. To protect the top of the oil pipes from the sliding icebergs, grabs were used to dig holes. The pipe ends are kept below the existing subsea ground level, within the holes created by the grab dredger, so that those are not damaged by the icebergs (Figure 5-reproduced with permission from Boskalis Offshore BV and Tideway). De Beers Group is famous for diamond exploration, mining and trading. In 1967, they used a drilling vessel to mine kimberlitic from shelf areas. Later, they acquired more sophisticated mining vessels with processing equipment on board. One such vessel was used to mine of diamonds, off the coast of Namibia. In 2007 De Beers launched a 260 ton seabed crawler unit, working from a diamond mining ship (Krugger 2007).

Table 1 Dredger with deep dredging capability

Name of Vessel	Owner	Year Built	Hopper Capacity (m3)	Max. dredging depth (m)
Amsterdam	Ballast Nadam Dredging	1996	18,000	70.0
Goryo Ho No. 5	Hyundai Dredging Engineering & Construction	1999	10,000	70.0
JFJ De Nul	Jan De Nul NV	1992	11,750	78.3
Volvox Terranova	van Oord ACZ	1999	20,000	105.0
Gerardus Mercator	Jan De Nul NV	1997	18,000	112.0
Queen of the Netherlands	Royal Boskalis Westminster NV	1998	23,350	120.0
WD Fairway	Royal Boskalis Westminster NV	1997	23,425	120.0
Vasco Da Gama	Jan De Nul NV	2000	33,000	131.5

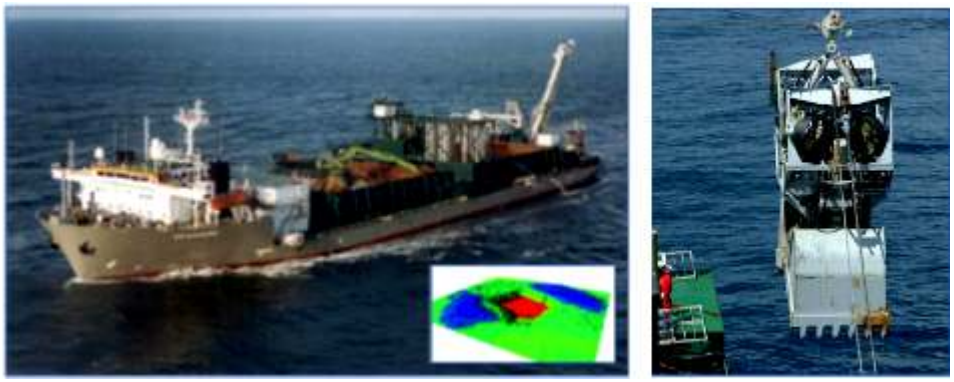

Figure 5 Deep dredging by grab dredger

2.1.3. Submersible vehicles for subsea excavation

A detail description of submersible trenchers and ploughs was given by Palmer & King (2008). Pictures of a trencher with tracks (SMD 2009) and a plough with skids are shown in Figure 6. Submersible dredgers can be classified depending on locomotion system as shown in Figure 7.

Remotely operated water tight submerged fixed pumping systems known as “Punaise” (Williams & Visser 1997) can dredge sediments from the sea floor without affecting the navigation by any ropes, cables or pipelines, floating above water. It remains undisturbed by the impact of storm or wave (Figure 8). This system is suitable for by-passing, beach nourishment and dredging of silt in large harbours and near the intakes of power stations.

Figure 6 Subsea tracked trencher and plough with skids

The submersible dredger 'Namsol', operates from a support vessel fitted with the mining system to operate to a depth of 200 meter. The crawler dredger mines the kimberlites in the shelf area of Namibia (Paragon International 1993).The National Institute of Ocean Technology, in India designed and built a subsea crawler. It is fitted with a small reciprocating solid handling pump and a small rotary cutter (NIOT 2002) (Figure 9). For the walking varieties of submersible dredgers two types are noticed – i) sliding frame and ii) leg walking. The oldest one in the sliding frame type was named as 'Futuba 2' (Hisao Sadayoshi 1999), being designed and built by Japanese engineers (Figure 10). The conceptual design of the other design is known as "Tripod' (Verheul et al. 2004) and was done by The Delft University of Technology, the Netherlands (Figure 11).

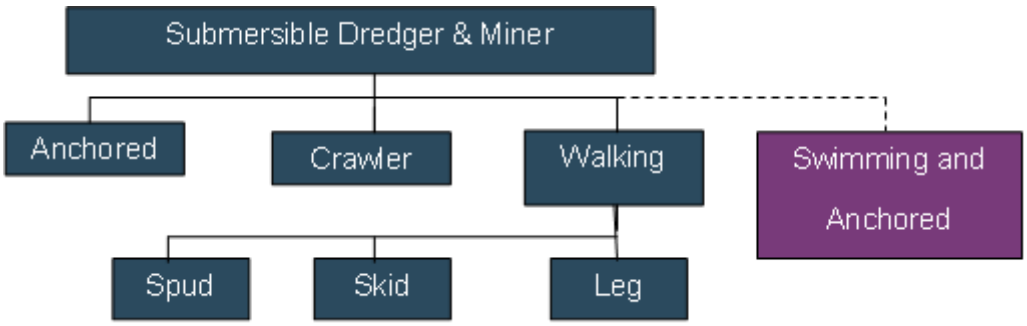

Figure 7 Different locomotion systems for submersible dredgers or miner

Figure 8 “PUNAISE” submerged stationary dredging system

Figure 9 Subsea crawler

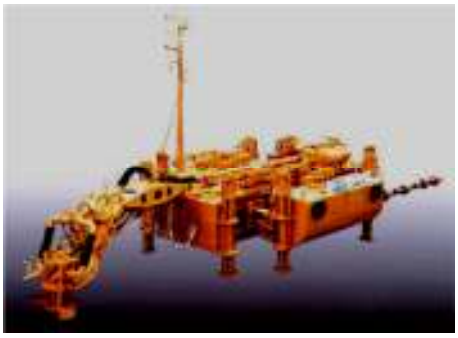

Figure 10 'Futuba 2'

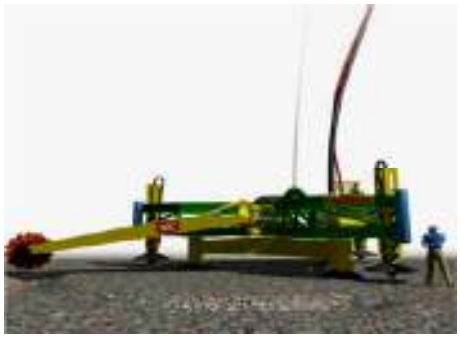

Figure 11 ‘Tripod’ conceptual design

A walking submersible dredger ‘Golden Tortoise 01’ was designed and built jointly by Sarkar (2007), and EEM (P) Ltd. (Figure 12). A most recent subsea mining venture is being undertaken in the region of Papua New Guinea by Nautilus Minerals Inc., a Canadian company to mine polymetallic sulphides or ‘Black smokers’ (Nautilus 2009). No technical details have been published but they have contracted SMD of UK to assist in development, to design and build the sea mining tool (SMT). An artist’s impression of the system

(reproduced with permission from Nautilus Minerals) is shown in (Figure 13). The new dredger type is shown as the 'swimming and anchored' in Figure 7.

Figure 12 'Golden Tortoise 01'

Figure 13 Artist's impression for the subsea SMT (Sea Mining Tool)

2.1.2. Propulsion, control and counterbalancing of excavation forces

Launching is an issue for submersible vehicles launched from a support vessel. During launching, a vehicle has free fall and stability depends on the end forms of hull. Behaviours of cylindrical objects with various end forms during free fall under water were

reported by Abelev (2007) where blunt end forms were found more stable during launching.

Various propulsion and locomotion systems are used for surface floating vessels and submersible vessels, in swimming as well as ground contact modes. The literature review for propulsion and locomotion was categorised into a) Surface floating propulsion and b) Submersible propulsion and locomotion. Submersible propulsion is divided into, (i) Swimming propulsion and (ii) Ground contact locomotion.

Surface floating propulsion, control and force counterbalancing

Surface floating dredgers may be dumb or self-propelled. Dumb- dredgers are towed by tugs or other ships. Self- propelled dredger propulsion and control is the same as ship propulsion, with an extra resistance for appendages and hull forms. The discussion of the same is not included in this work. The excavation forces for surface-floating dredgers are counterbalanced by the weight of the vessel, specially the weight of the ladder, the grounded spud and swing wires.

Swimming propulsion and control and force counterbalancing

Position and orientation of submersible vehicles are described with reference to an inertial coordinate system fixed to earth. Equations of motion for free swimming vehicles are expressed with a body fixed coordinate system having its origin at the centre of gravity of the vehicle and are based on Euler's equation of motion (Negahban 2002) having six degrees of freedom (DOF). The forces and moments are defined according to SNAME (1950) notation (Figure 14).

Thruster equations of motion are non-linear. For remotely operated vehicles (ROV) bilinear (four quadrant) models including actuator dynamics were discussed by Fossen & Ross (2002). An accurate four quadrant non-linear model was proposed by Bachmayer (2000). Non- linear dynamic models for propellers were designed and experimented by Whitcomb & Yoerger (1999) at Woods Hole Oceanographic Institution.

For velocity transformation, either a) Euler angle representation, b) Euler parameters consisting of four parameters representation based on quaternion (four quadrants), or c) Rodrigues parameters can be used (Fossen et al. 1994). For pitching when the angle is (+/-) 90^0 then there is a problem of singularity with Euler angle representation. In case of a

remotely operated vehicle, connected to a support vessel through tether, this situation may not arise.

To calculate the static and dynamic forces during propulsion and control of a submersible vehicle, Evans & Nahon (2004) model is noteworthy. In this model, the external forces during propulsion are divided into groups according to: gravitational, buoyancy, hydrodynamic, propulsion and control forces.

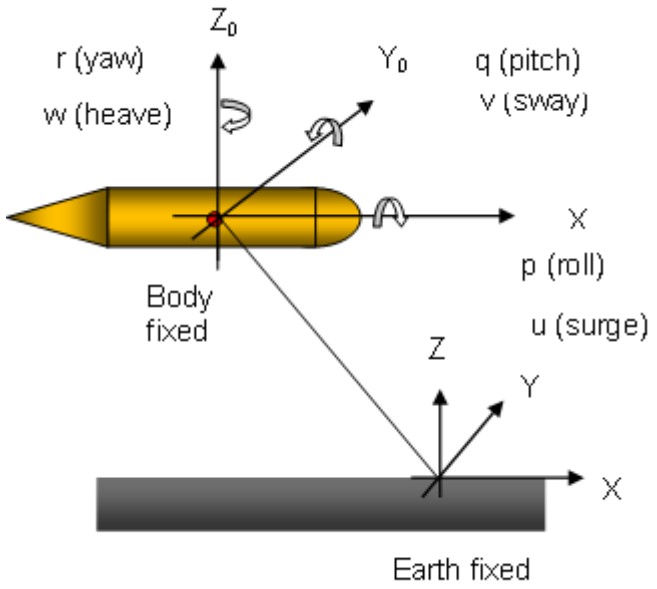

Figure 14 Position and orientation of free swimming vehicle

Gravitational force and the centre of gravity are calculated in an associative (separately calculated and added afterwards) way for all the components. Buoyancy forces are calculated for fully submerged condition with the respective water density for fresh or sea water as required. Total submerged drag or resistance can be divided into a) skin friction drag and (b) form drag. Hydrodynamic coefficients contribute more to the skin friction drags that are very important for the propulsion and control of free swimming vehicles. Various theoretical models are available to calculate the drag coefficient, but experimental determination for a particular shape is widely used. Methods to calculate hydrodynamic coefficients have been discussed by Jones et al. (2000). Hydrodynamic force or resistance of a body to motion within water can be expressed as,

$$R = \frac{1}{2}\left(C_D \rho_w A U^2\right)$$

Equation 1

A = representative area

C_D = Drag coefficient

ρ_w = Density of water

U = Speed of the body.

Hope (2000) suggested the selection procedure of propeller for small vessels, from standard series, with the help of computer that can be used as a preliminary selection guide for thrusters. Dewijs (2000) described some commercial AUV/ ROV thrusters made by Subsea Propulsion Company. There is loss of efficiency due to (a) interactions of two closely spaced thrusters (Brandner 1998), (b) 'Coanda effect' for closely placed hull (Faltinsen 2003) and (c) current. Small working ROVs with jets for excavation are propelled and counterbalanced by thrusters.

Ground-contact locomotion, control and Force counterbalancing

Like the onshore excavation machines, crawling tracks are mostly used for locomotion in subsea ground-contact vehicles (SMD 2009). The control of the crawler vehicles are described by Wong (2001). A snake like neural oscillator based motion controlled underwater robot was developed by Matsuo & Ishii (2007). A wheel with grousers (projected plates to increase gripping forces) type crawler (MARUM crawler) was tested for subsea research work by ECOR (2011). An underwater wheel for traction on submerged ground was tested by Waldmann (2007). 'Archimedean screw' locomotion is proposed by Alvarez Grima (2011) for submersible vehicles. Gait and motion planning of a walking submersible vehicle was tested and described by Sarkar (2007).

For terrain contact vehicles moving with tracks or skids or legs, the excavation forces are counterbalanced by their apparent weight and track/ skid/ leg- terrain contact reactions. Excluding the thrusters, other possible methods of counteracting the excavation forces are, a) Spuds, b) VBT (Variable Buoyancy Tank) and c) control surfaces. Spud is a pole like structure with pointed ends. It is a familiar device for surface floating dredgers for station keeping during dredging. It is used as a common temporary anchoring device by the surface floating dredgers. It also partly counterbalances the excavation and natural forces due to current and waves. It can be embedded within soil when lowered and lifted when

necessary. Variable buoyancy tanks (VBT) are a common system adopted in submarines (Burcher et al. 1998) for diving or surfacing. A variable buoyancy control system for a large autonomous underwater vehicle (AUV) has been designed, constructed and tested by Pennsylvania State University (Tangirala et al. 2007). Control surfaces are used in aircrafts (air brakes) to increase drags during landing (Kermode 1963) and in ships (stabilizers) to equalize rolling actions. Control surfaces are used to generate drag forces in the opposite direction of motion.

Chapter 3 has been removed for copyright or proprietary reasons.

It has been published as: Sarkar, M. K., Bose, N., Chai, S., Dowling, K. Conceptual design of a submersible remotely operated swimming dredger (SROSD). ASME. International Conference on offshore mechanics and arctic engineering, volume 6: Ocean engineering, 671-679. doi:10.1115/OMAE2011-49868

CHAPTER 4 THEORETICAL EXCAVATION MODELS FOR GRANULAR SOIL

4.1. Introduction

In order to assess station keeping ability of the Submersible Remotely Operated Swimming Dredger, work was done to accurately assess loading on the transverse axis dredging cutter during operation. Depending on the orientation of the axis of a cutter, to the longitudinal axis of a dredger, the cutter can be described as an axial or transverse axis cutter. There is a difference between the excavation process of axial and transverse axis dredging cutters (auger), which is described in this chapter.

Soil properties have got a significant role.in the dredging excavation process. Soil properties that are important in the dredging excavation process are reported here. Existing theories of soil cutting with axial cutters, related to exposed land surface as well as to dredging, are also discussed. An excavation model is developed for an auger dredging cutter, based on the geometry of an auger.

4.2. Dredging excavation process

Some percentage of the power supplied by the motor to the dredging cutter through the drive is lost in the transmission process. The remaining power is available to the dredging cutter for excavation. Part of this available power is consumed for overcoming hydrodynamic friction and part is utilized for other causes such as transporting materials to suction mouth, centrifuging and friction between soil and the cutter blades, that depends on the cutter geometry. The residual power is available for soil cutting. This residual power produces a torque depending on the rpm of the cutter. The force available at the cutter cutting edges is dependent on the torque produced from the residual power and depends on the cutter circumference. The excavation process is dependent on the direction of cutter rotation during feeding (under-cutting or over-cutting) and also with the type of cutter.

With a longitudinal axial cutter, the cutter arm swings in an arc, whereas the cutter rotates about its own axis (Figure 23). The transverse cutter rotates around its own axis while moving in a forward and backward motion (Figure 24). The axial and transverse cutters thus have two simultaneous motions, a) rotational motion about its own axis and

b) translational motion or 'feed' into the soil. The rotational and translational motion generates a cycloidal trajectory for the cutting tools (figure 25).

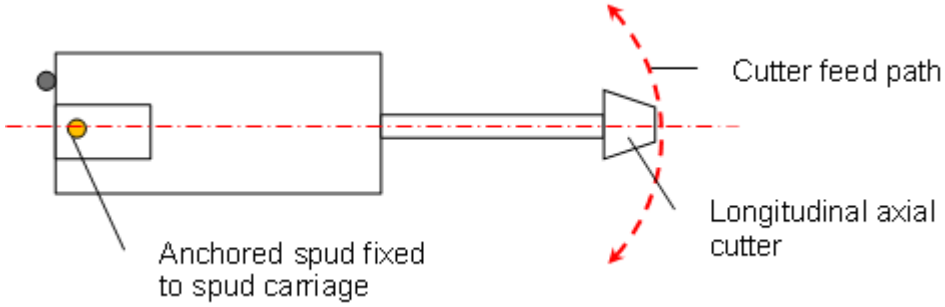

Figure 23 Operational method of longitudinal axial cutter

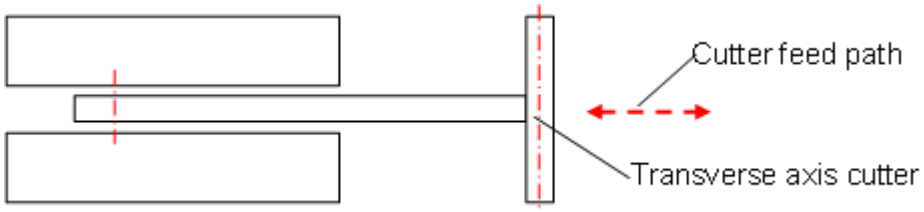

Figure 24 Operational method of transverse axis cutter

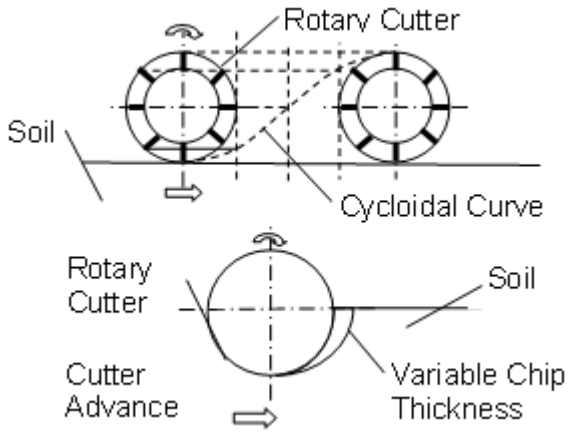

Figure 25 Cutter motion and chip formation

The shape and characteristics of the cycloidal curve is determined by the ratio between the rotational velocity and translational velocity and the cutter geometry (Yatsuk et al. 1984). Due to variable chip thickness and finite number of rotating cutter blades and variation in soil properties, the cutting force is variable and cyclic in nature.

4.3. Soil properties influencing cutting of saturated granular soils

Failure of saturated granular soil in ground is described as an elasto-plastic phenomenon by Payne (1954). During excavation by a straight blade, the three physical properties listed as important by him are, a) soil bulk density (γ_s), b) undrained shear strength (τ_u) and c) coefficient of sand to metal friction (μ). Luth & Wismer (1969) predict force response equations of plane soil cutting blades in sand and considers the additional variables, a) blade width (b_b), b) blade length (L_b), c) blade operating water depth (z), d) blade rake angle (α_{br}), e) operating velocity (v_t), f) internal friction angle of soil (ϕ), g) cohesion in Coulomb's equation $\tau_f = \sigma \tan\phi + c$, and h) acceleration due to gravity (g). Hettiartchi et al. (1974) calculated the passive soil resistance through dimensional analysis and used the same variables as above with the additional variable-uniform surcharge pressure (q). McKyes & Ali (1977) investigates soil cutting by narrow blades from the dynamic equation viewpoint and proposed equations to predict force factors to fit Reece's general earthmoving equation (Hettiaratchi 1966). Excavation force varies with blade width/ blade depth) ratio, blade rake angle and the friction angle of the soil.

The dredging soil cutting force in granular soil is dependent on soil properties (PIANC 1984). Research by Leussen et al. (1984) shows that the parameters important in dredging saturated sand are, a) permeability coefficient (k), b) porosity (n), c) relative density (γ_r), d) angle of dilatancy (ψ), e) relative dilatancy index (I_R) and f) pore pressure (u). Van Os (1977) shows how the saturated sand excavation force is dependent on the 'deformation rate' $\left(\frac{\partial s}{\partial t}\right)$ in addition to the above factors.

4.4. Important soil parameters affecting dredging of sand

Although all the soil properties affect the cutting process of sand during dredging, to some extent, three properties of granular soil mostly influence the sand cutting process during dredging. These are a) dilatancy, which is the increase of volume of compacted sand during excavation, b) permeability, the flow rate of water through soil and c) relative

density, which depends on the porosity of the soil. Influences of these three important properties during dredging of saturated sand are described in the following sections.

4.4.1. Dilatancy

When mechanical cutters are used in cutting soils a shear stress is exerted on the soil mass. At increasing shear strain, loose sand has the tendency to decrease in volume (Craig 1992), which result in denser packing of the grain structure (Figure 26).

When cutting dense sand the opposite occurs i.e. the packing becomes looser. This phenomenon is known as 'dilatancy' (Figure 27). If the dense sand is saturated with water, then due to the flow resistance in the soil, the change of pore volume cannot be compensated quickly enough by an equal change in water volume, and hydrostatic under-pressure or negative pore pressure occurs (Whitlow 1998). Hence the effective stress will increase until the vapour pressure of water is reached and cavitation occurs, limiting the pore pressure.

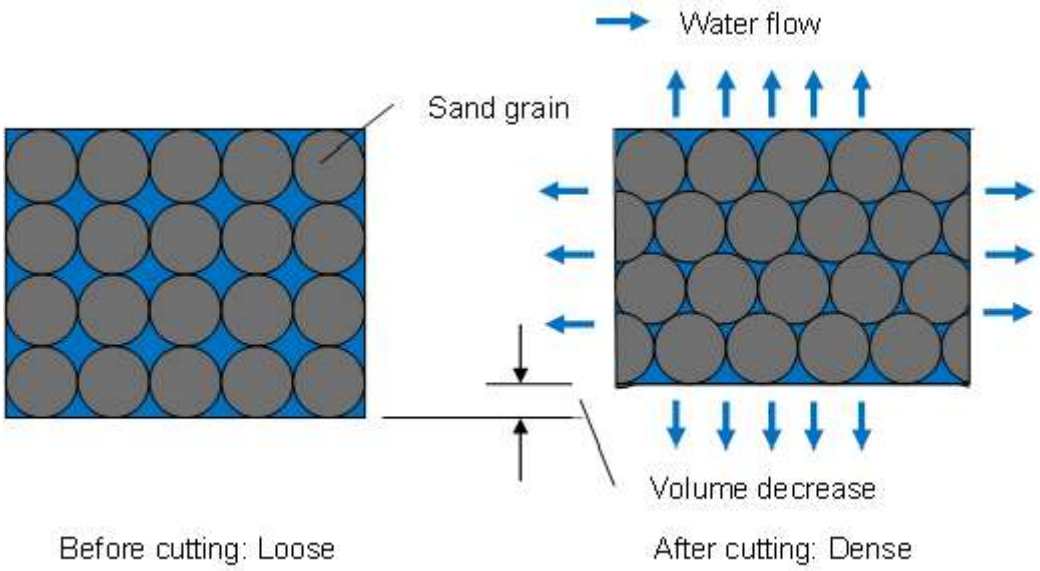

Figure 26 Condition of loose sand during excavation

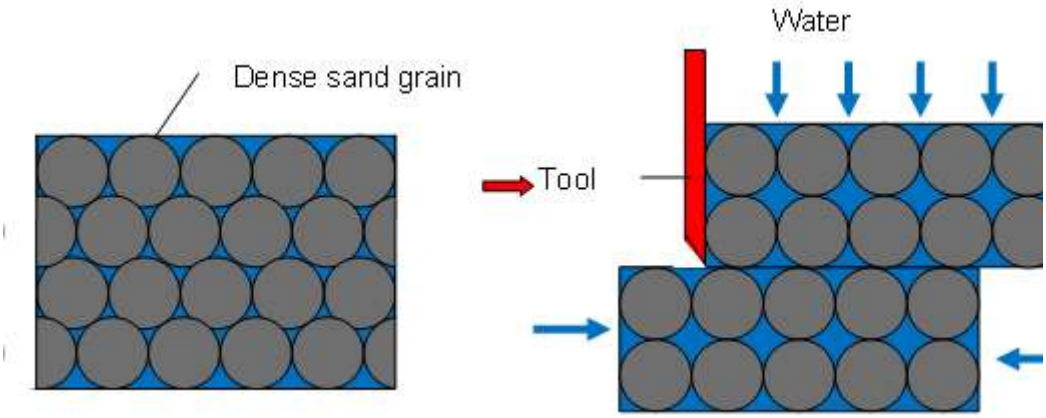

Figure 27 Dilatancy of dense sand during excavation

4.4.2. Permeability of soil

As described above, the flow of water through the sand forms a major aspect of the excavation process. The flow rate of water through a certain material is known as its permeability. As a consequence, the permeability of the soil is an important parameter for soil cutting. The permeability determines if pore pressures can build up and how it disperses, influencing cutting forces and the stability of the grain skeleton. Usually no direct measurements of permeability are made during a soil survey, but different correlations are used to estimate the values. Terzaghi (1925) gives a wide range of permeability according to the following equation:

$$k = 5450\left[\frac{n-0.13}{\sqrt[3]{1-n}}\right]d_{10} \qquad \text{Equation 2}$$

where,

d_{10} Grain size at 10% passing [mm]

k $k = v/\left(\Delta h/\Delta L\right)$, Coefficient of permeability [m/day]

(Whitlow 1998 pp. 91-92)

Δh Difference in total head over a flow path of ΔL

n In-situ pore volume, which is the volume percentage filled with liquid or sometimes with air/ gas within the soil in the natural condition, [%].

Empirical formulae for the correlation between permeability grain size distribution and in-situ pore volume are discussed in detail by Odong (2007).

4.4.3. Relative density

Another important parameter which must be determined for sand is relative density. The relative density is a measure for the compaction of a granular soil. Its value is related to the loosest and densest state in which the particular material can exist. Natural soil is not homogenously packed. It varies from a loosest to a densest state. The relative density is therefore expressed in terms of the porosity number as:

$$\gamma_r = \frac{e_{\max} - e}{e_{\max} - e_{\min}} \qquad \text{Equation 3}$$

where,

γ_r Relative density [%]

e Actual pore volume present in the field [%]

$e_{\max}$ Pore volume loosest state [%]

$e_{\min}$ Pore volume densest state [%].

As the in-situ pore volume is extremely difficult to determine, Teferra (1975) and Lunne & Robrtson (1997) correlated the cone resistance to the relative density as shown in Figure 28. The relation between relative density and cone resistance is given by the empirical equation:

$$\gamma_r = 9.33 q_c^{0.78} \qquad \text{Equation 4}$$

q_c Cone resistance in MPa.

Cone resistance is the maximum force recorded during penetration of a standardised cone ((Whitlow 1998 pp. 482). The correlation between relative density γ_r, the grain size and the angle of internal friction can be represented (Schmertmann 1978) as shown in Figure 29. The figure shows the influence of the grain size in relation to the relative density (γ_r) at a constant angle of friction ϕ.

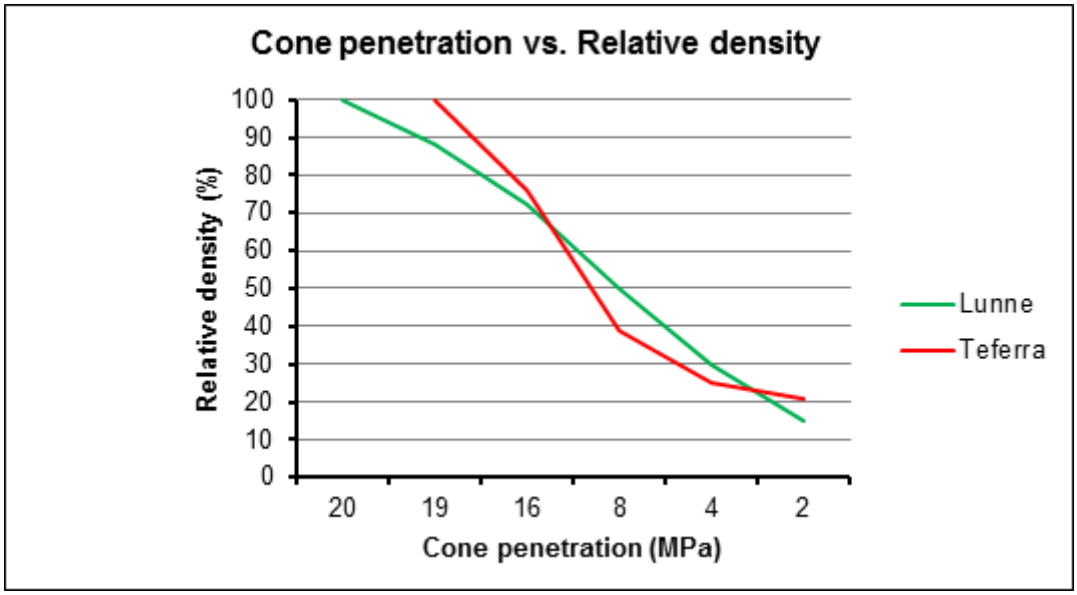

Figure 28 Relation between cone penetration and relative density of sand

4.5 Theoretical models in dry granular soils

The first notable experimentation to predict the excavation forces in agricultural soils by simple implements were done by Payne (1954) and Payne et al. (1959). Hanson et al. (1966) experimented to define a relationship between the strain rates and shear strength of soil, which is relevant to dredging excavation.

Luth et al. (1969) applied dimensional analysis to make a theoretical model about the performance of plane soil cutting blades that is validated by experiments. Theoretical models to predict the passive soil resistances and mechanism of soil cutting are proposed by Hettiaratchi (1965, 1966, 1967, 1974, 1975) and Hatamura et al. (1975, 1976, 1976a, 1976b, 1977a, 1977b). Based on the works of Hettiaratchi et al., McKyes et al. (1977) investigated the cutting of soil by narrow blades. Reece et al. (1989) proposed a slip-line method for estimating passive earth pressure on soil cutting blades, to simplify Sokolovski's solutions (1960) to partial differential equations, related to the equilibrium for rigid-plastic Mohr-Coulomb materials.

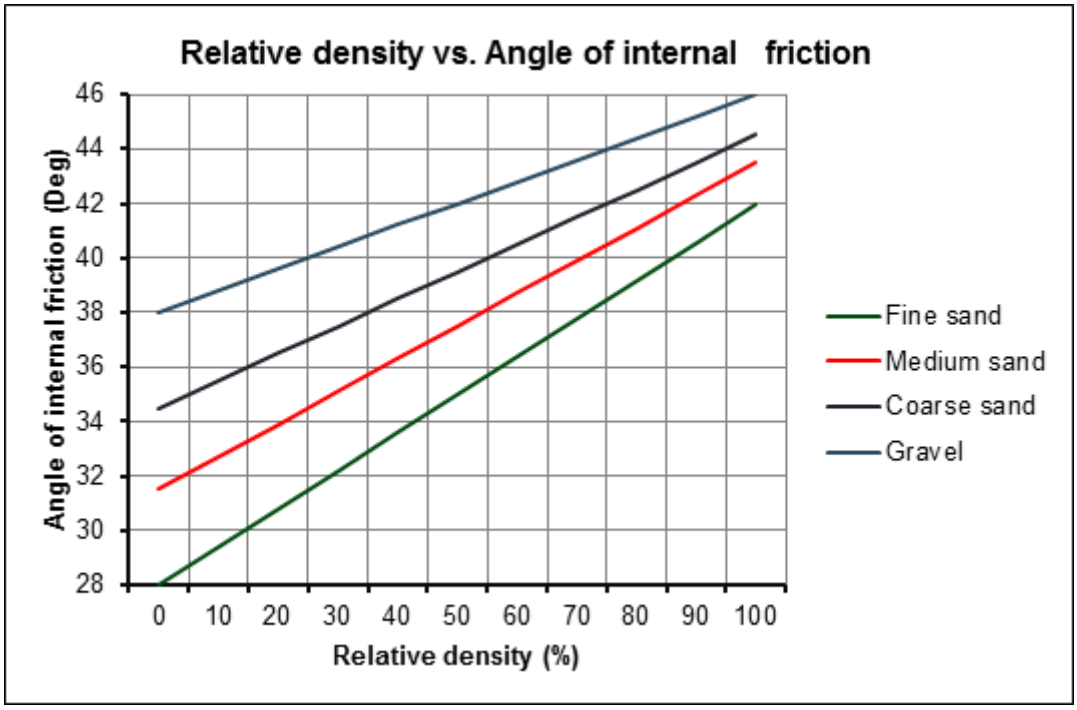

Figure 29 Correlation between relative density angles of friction

4.6 Theoretical models in saturated granular soils

Theoretical and experimental work on excavation processes in saturated sands was started in the late seventies in Holland at the Waterloopkundig Laboratorium in Delft (WL), Technische Hogeschool in Delft and at the Mineraal Technologisch Instituut (MTI). The relation between cutting forces, soil properties and cutting blade geometry was described by Joanknecht (1974) and Van Os (1977).

Joanknecht indicated the different roles played by inertia forces, pressure reduction behind cutting blade and the soil properties in case of cutting saturated soils. He proposed the following equation for the soil cutting force for a straight blade moving perpendicular to soil:

$$F_{ci} \propto v_c h_i^2 b_b \qquad \text{Equation 5}$$

where,

F_{ci} Cutting force (kN)

b_b Width of cutting blade [m]

h_i Initial layer thickness [m]

v_c Cutting velocity [m/sec].

The initial density of soil, the saturated soil and blade friction angle and the variation of cutting forces at greater depths were not considered in his work. Miedema (2000) argued that the type and geometry of the cutting tool, operational parameters i.e. rpm, feed rate, depth of cut and excavation process during dredging influences the cutting process. Miedema (1983) modified Equation 5, by including permeability of soil (k) in the equation. The modified equation is:

$$F_{ci} \propto \frac{\rho_w g v_c h_i^2 b_b e}{k} \qquad \text{Equation 6}$$

where,

e Porosity

k Permeability of granular soil (m/sec)

ρ_w Unit weight of water (kN/m3).

The influence of pore water pressures and permeability on cutting saturated sands at depths was derived by Miedema (1985a). Miedema subdivided the cutting processes of saturated sand into five separate groups based on cutting velocities. The cutting process and hence the cutting forces are significantly different at low cutting velocities than at high cutting velocities.

Procedures to calculate the vertical and horizontal components of cutting forces were described by Bindt et al. (1994), Miedema (1987, 1989, 2000) and Van Os (1987). These theories were developed for longitudinal axis dredge cutter head i.e. crown cutters.

The offshore soil mechanics background of Verruijt (1983, 1985, 1999, 2001) was used by Miedema (1985,1987,1989), Van Os (1987), Van Leussen et al. (1983) to develop the two-dimensional dredging cutting theories for sand. The two-dimensional cutting theories have imperfections, since cutting is a three dimensional process. Miedema (1994) proposed a three dimensional cutting theory for saturated sand at water depths. This theory is complex, and requires a large number of inputs for many soil mechanical

parameters, in order to estimate the cutting forces, cutting power and dredging production.

For practical purposes, the concept of 'specific energy' is used to determine the cutter power. Cutting force required for soil failure can be derived from this cutter power if the cutter diameter and cutter RPM are known. Specific energy (kJ/m^3) is defined as the energy required for excavating unit volume of soil. The specific energy is given as:

$$E_{spec} = \frac{P_a}{Q_e}$$ Equation 7

where,

E_{spec} Specific energy for cutting [kJ/m^3]

P_a Cutter power for cutting [kW]

Q_e Excavation production of cutter [m^3/sec].

Miedema (1994) deduced the specific energy required to dredge saturated sand from Standard Penetrometer Tests (SPT). This relation however predicts the upper limit of the specific energy and hence lower limit of production.

The specific energy for granular material under non-cavitating conditions (when no cavitation occurs during excavation) is given as (Paragon International 1991):

$$E_{spec\_nc} = 0.013 * \gamma_r^{1.15} * \frac{v_T * D_a}{z * k}$$ Equation 8

The specific energy for granular material under cavitating condition (when there is cavitation during excavation) is given as (paragon International 1991):

$$E_{spec\_c} = [1.8 * h_w + 17.6] * \gamma_r^{0.7}$$ Equation 9

where,

E_{spec_nc} Specific energy for sand under non-cavitating condition [kJ/m3]

E_{spec_c} Specific energy for granular material under cavitating condition [kJ/m3]

D_a Average diameter of cutter head [m]

h_w	Water depth [m]
k	Permeability of granular soil [m/sec]
v_T	Warping/ Horizontal velocity [m/sec]
z	Number of cutter blades [-]
γ_r	Relative density of granular soil [%]

The cutter power can be estimated based on the specific energy concept. Vlasblom (2000) deduced the relationship between swing force and axial force acting on an axial dredge cutter head based on the total cutter power. Sarkar (2007) also used the concept of specific energy to derive the cutter forces for a twin counter-rotating axial cutter head system.

4.7. Conclusion

Theoretical models for excavating dry and saturated granular soils on land and excavation models for saturated granular soils in the case of dredging with axial cutters are discussed. Vertical, horizontal and axial force components for axial cutters were developed. No published literature was found about dredging of saturated sand with an auger. For an auger, the failure mechanism of saturated sand is the same as the axial cutter, but the process is different due to different geometry and feeding direction of the auger than that of the axial cutter. The practical approach of specific energy related to dredging is more straightforward to apply and that method was adopted in this work to validate the experimental results for an auger.

CHAPTER 5 EXCAVATION OF SAND MODEL BY AUGERS

5.1. Introduction

Power is supplied to the auger during dredging, through its drives. Part of the input power is spent for the hydrodynamic forces and the frictional forces in the joints. Hydrodynamic drag forces are produced by the rotation of the auger and by the forward translational motion of the auger under water. Frictional forces in the joints are dependent on the normal forces and associated coefficient of friction. The rest of the power is used for the excavation of soil. The excavation power available to a transverse-axis auger are used for, a) cutting the soil and b) transport of soil by the auger spiral vane, towards the suction mouth. The soil cutting power available to the auger produces a torque in the cutter leading to forces at the cutting points of the auger. The cutting force is dependent on the radial distance of the cutting points from the axis of rotation of the auger.

The failure mechanism of sand with the application of cutting force is an existing knowledge. The development in the method to calculate soil cutting power by an auger in the dredging was done in the present study. The method to calculate the cutting power by specific energy is a standard practice in dredging industry (Paragon International 1991). The method to calculate the transport power by a screw conveyor was done by (Roberts 2000), but the factor for dredging underwater by an auger was developed in this research.

5.2. Failure mechanism and cutting force for sand

In dredging, sand is a three phase model comprising of solid grains, with water and air or gas in the inter-granular spaces or pores. Failure of sand without any cohesion is always a shear failure (Terzaghi 1925) along the shear plane (Garg 2010). When a cutter blade applies gradually increasing force to loose sand, the following successive phenomena take place (Figure 30). With the start of cut, the loose sand is packed and the pore volume is reduced. With the application of more cutting force, the interlocked portions of the sand grains are crushed and the volume is decreased further with soil failure by shearing at constant volume. For dense sand the sequences are shown in Figure 31. In this case the volume is increased (dilatancy effect) and the pore pressure is reduced. The interlocked portions of the sand grains are crushed with soil failure by shearing at constant volume.

Failure in sand occurs when the mobilized shear stress exceeds the limit that the soil can sustain. Failure of soil is an elasto-plastic phenomenon. The failure pattern for dense and loose sand is represented in Figure 32 (Barnes 2000). With soil failure, there is a change in volume, which is different in case of loose and dense sands as shown in Figure 33 (Whitlow 1998).

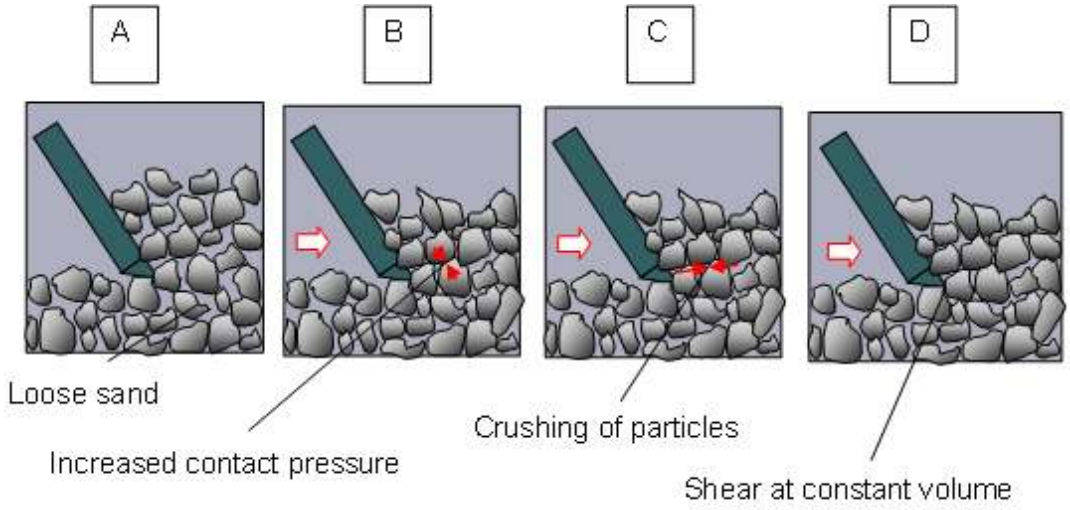

Figure 30 Cutting of loose sand

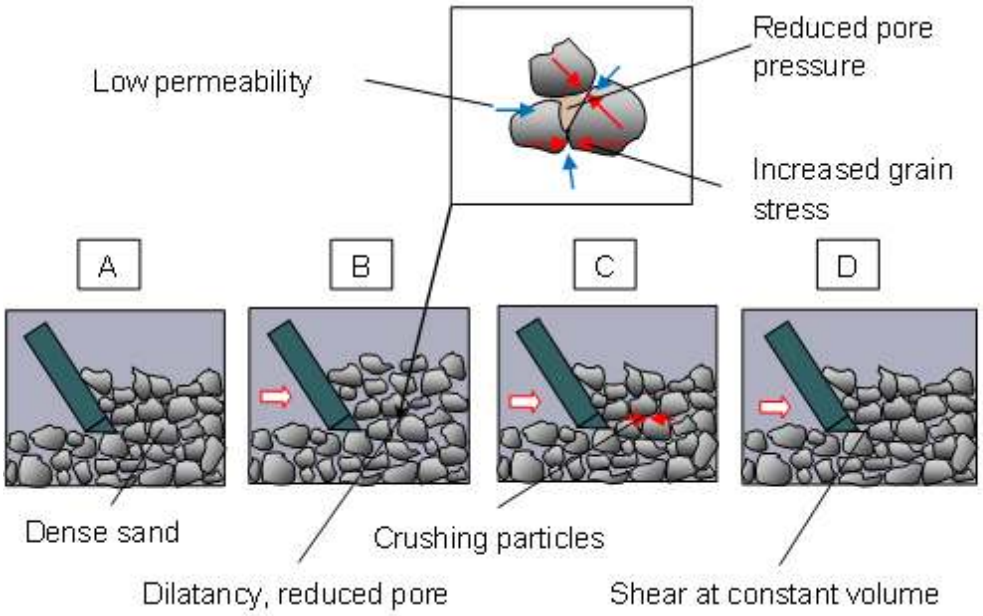

Figure 31 Cutting of dense sand

Legend:

A Loose or Dense sand before cutting

B Loose sand: Packing with volume decrease and increased contact pressure and force. Dense sand: Slight packing with volume decrease, reduced pore pressure, increased effective or grain pressure and force

C Crushing of contact point, volume decrease, increased forces for both loose and dense sand

D Equilibrium condition, cutting at constant volume and forces for either loose or dense sand

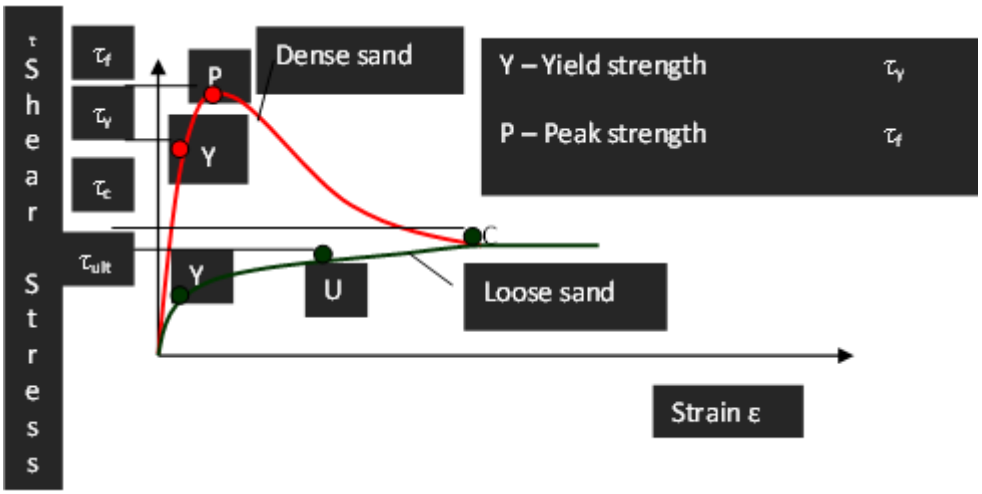

Figure 32 Different failure strengths of sand

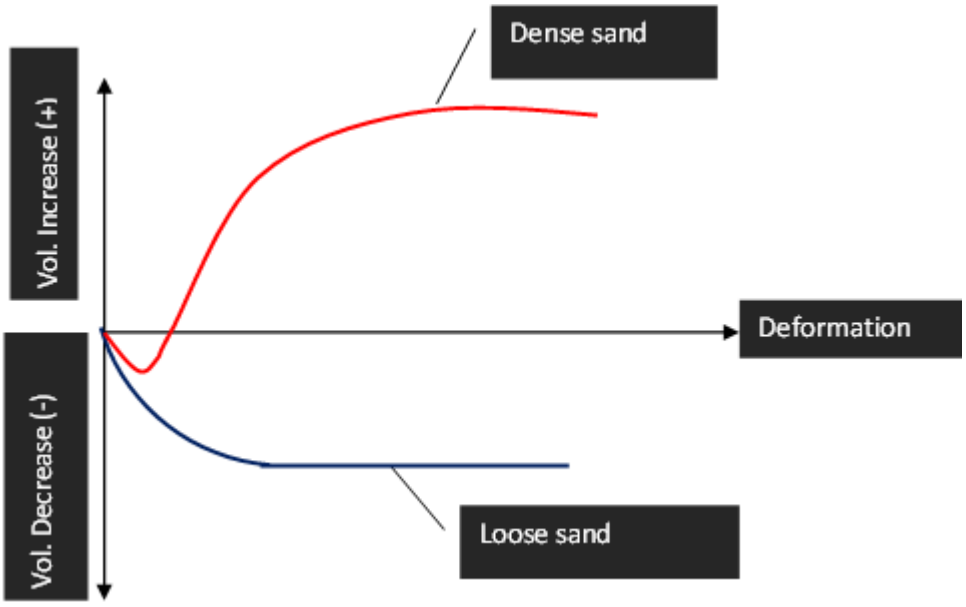

Figure 33 Volume-change of sands during cutting

5.3. Soil cutting by an auger

The available cutting energy is divided to the vane and flights depending on the instantaneous position of the vane and flights within the soil. During the cutting process of dredging, a point on the vane or flight of the auger is loaded with a variable force. The force depends on the shear strength of the soil from the peak to the critical state for constant volume cutting value, during the soil contact period. The cutter torque should be fixed depending on the peak shear strength of the soil and all other operational factors and efficiencies.

In a dredging auger, soil failure occurs in three separate ways, a) Soil failure by the edges of the two halves of the vane, b) Soil failure by the straight edges of the flights and Soil failure by the folded tips of the flights. The cutting edges of auger vane and flights are shown in Figure 34. The flights are spaced at an angular distance of φ^0 and folded alternatively in opposite directions. The geometry of the cutter is shown in Figure 35.

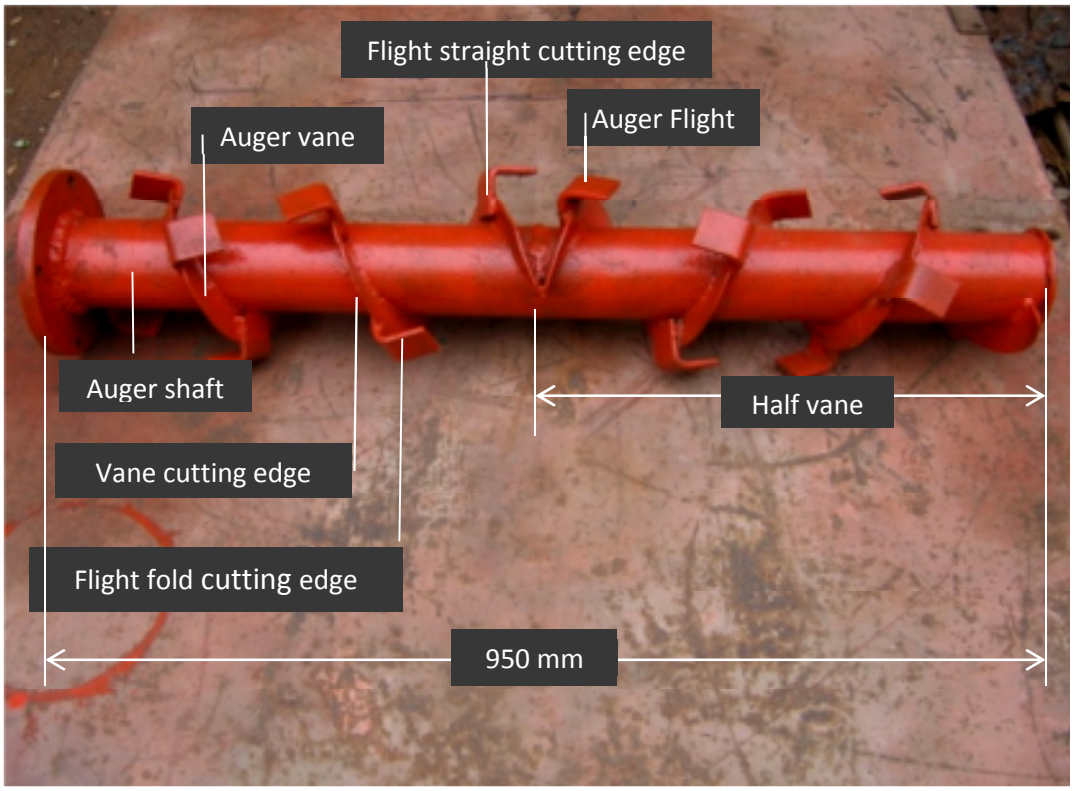

Figure 34 Cutting edges of vane and flights

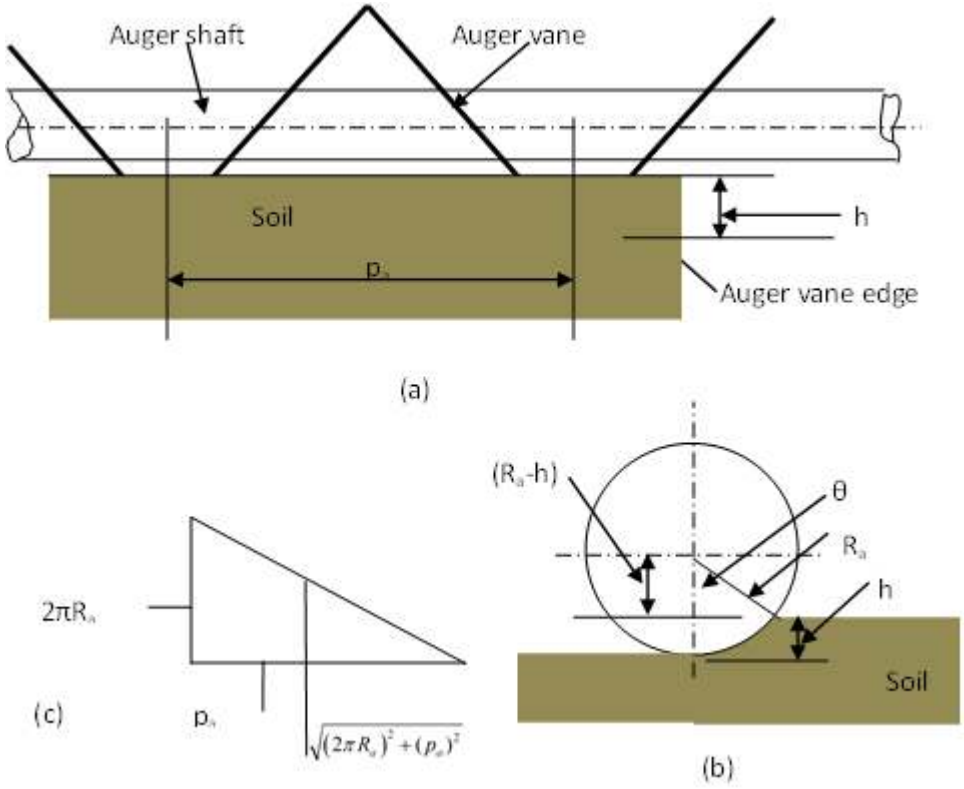

Figure 35 Geometry of an auger

Figure 35(a) is the longitudinal schematic sketch of the auger, Figure 35(b) is the side view of the auger cutting process and Figure 35(c) shows the developed length of a pitch of an auger. The auger vane is submerged within soil, depending on the depth of cut (h) and the angle of cutting is (θ) as shown in Figure 35(b). The developed length of the vane edge within a pitch (p_a) of the auger is shown in Figure 35(c).

5.3.1. Failure by the vane edge

Failure by the edge is primarily a punching shear or rearrangement failure. Soil grains are either compressed or slightly moved along the surface of the cutter and movement is restricted in other directions. Energy available in the vane is used for the purposes of, a) failure of soil at the vane edge b) overcoming frictional forces between the vane surface and soil (included in the transport of soil described later) and c) centrifuging (throwing of soil by centrifugal force) of the loose soil particles (neglected in this analysis).

In Figure 36, ABCD represents a sand section affected by the vane edge (Figure 34 and Figure 35) during cutting. There are two forces acting on the sand section; F_T provided by the feed acting horizontally and F_R supplied by the auger drive motor torque acting normally with the auger axis of rotation at an angle θ_i with the horizontal at any point of time t_i. F_R is resolved normal and along AD to obtain F_{RX} and F_{RZ} respectively. F_O is the force due to the overburden of sand and water above the sectional element.

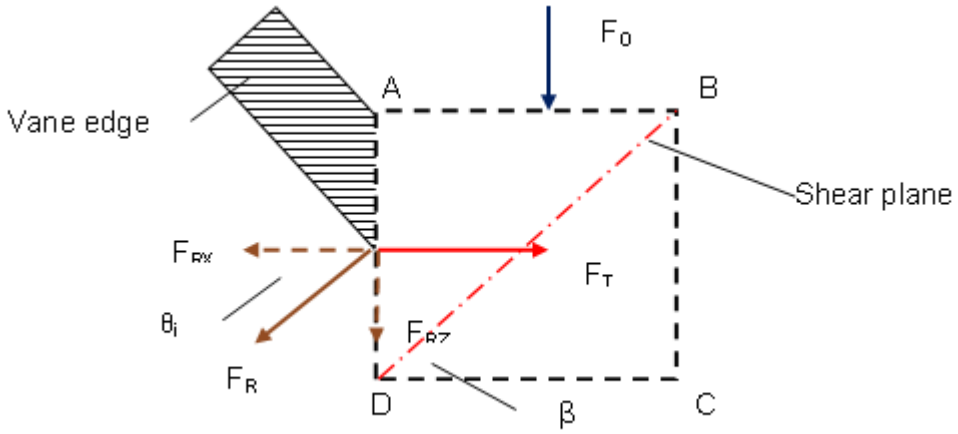

Figure 36 Failure of sand by vane edge

Normal force acting on AB is $F_Z = F_O + F_{RZ}$ and on AD is $F_X = F_T - F_{RX}$. The major normal stress σ_1 along AD and the minor normal stress σ_3 along AB can be calculated and the shear stress is given as Garg (2000),

$$\tau = \left(\frac{\sigma_1 - \sigma_3}{2}\right).\sin 2\beta$$

Equation 10

Failure occurs when, $\beta = \beta_m$ and

$$\sin \beta_m = \left(\frac{\sigma_1 - \sigma_3}{\sigma_1 + \sigma_3}\right)$$

Equation 11

The angle between the critical plane (when failure occurs) and the major principal plane AD is,

$$\alpha_f = 45^0 + \left(\frac{\beta_m}{2}\right)$$

Equation 12

Referring to Figure 35, Figure 36 and Figure 37, with unit depth of cut, area of shear is, 2*(length of vane edge engaged in cutting + vane thickness). Length of vane edge engaged in cutting and the length of vane edge travel within soil during cutting are constant for a specific depth of cut. If,

p_a Pitch of auger (m)

R_a Radius of auger (m)

r_a Radius of auger shaft (m)

h Depth of cut (m)

θ Soil contact angle as shown (radian)

L_{vp} Length of vane engaged in cutting in one pitch length

α Angle made by the cutting edge with the horizontal

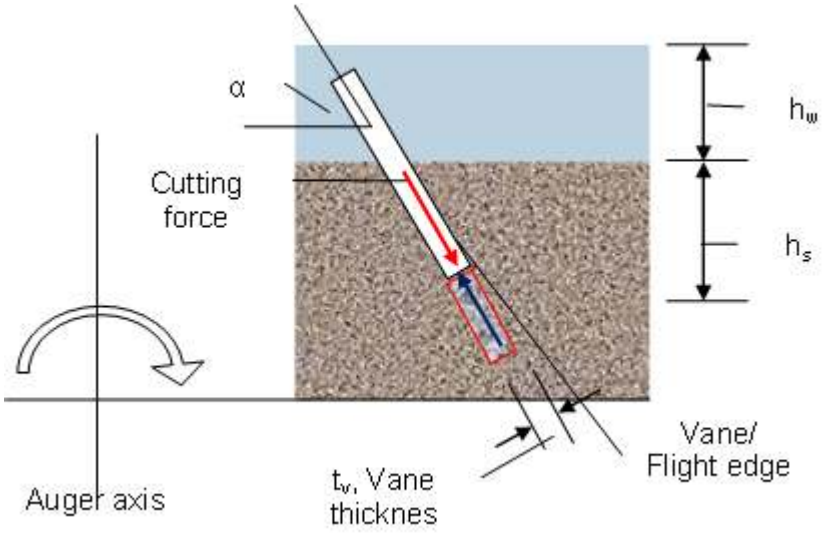

Figure 37 Soil-failure by the edges of auger vanes and flights

$$L_{vp} = \sqrt{{p_a}^2 + \left(R_a * 2\pi\right)^2} * \frac{\theta}{2\pi}$$

Equation 13

If n_p is the number of pitches in the auger and L_v the total length of vane engaged in cutting,

$$L_v = L_{vp} * n_p = \sqrt{p_a{}^2 + \left(R_a * 2\pi\right)^2} * \frac{\theta}{2\pi} * n_p$$ Equation 14

If,

$$h < \left(R_a - r_a\right)$$

Then,

$$\theta = \sin^{-1}\left[\frac{\left(R_a - h\right)}{R_a}\right]$$

If,

$$h = \left(R_a - r_a\right)$$

Then,

$$\theta = 90^0$$

If,

$$h > \left(R_a - r_a\right)$$

then

$$\theta = \frac{\pi}{2} + \sin^{-1}\left[\frac{\left(h - R_a\right)}{R_a}\right]$$

A_{vs} Area of shear for vane edge cutting for unit depth of cut

t_v Vane thickness

τ_p Peak undrained shear strength of the soil

$$A_{vs} = 2 * \left(L_v + t_v\right)$$ Equation 15

Assuming for a normal depth of cut (Shear plane ≈ Normal plane), the force required is,

$$F_v = A_{vs} * \tau_p = \left(L_v * t_v\right) * \tau_p$$ Equation 16

5.3.2. Failure by the flight edges

Energy available in a particular flight is used for, a) the failure of soil at the straight cutting edge of the flight b) the failure of soil at the folded cutting edge of the flight, c) overcoming frictional forces between the flight surface and soil, d) centrifuging of the loose soil particles.

The forces for overcoming friction and centrifuging are neglected. Failure at the edge of a flight is a punching failure. It can be simplified with the assumptions that, a) full length of a flight edge enters soil at a time, b) flight edge soil failure is mainly reorganization of soil particles and c) forces at the straight and fold cutting edge of a flight are acting at a single point and at the same direction. Assuming a flight phase angle (φ) between two consecutive flights the total number of flights (n_f) is given by,

$$n_f = \left[\left(\frac{2\pi}{\varphi}\right) * n_p\right] + 1 \qquad \text{Equation 17}$$

Number of flights in phase is the number of pitch n_p and soil contact angle is (θ) for a specific depth of cut (h). If the straight flight cutting edge width and thickness of the plate are b_{fs} and t_{fs}, then area of shear for all the flight straight cutting edge is,

$$A_{fs} = n_f * (b_{fs} * t_{fs}) \qquad \text{Equation 18}$$

Force acting on the straight flight cutting edges is,

$$F_{fs} = A_{fs} * \tau_p = n_f * (b_{fs} * t_{fs}) * \tau_p \qquad \text{Equation 19}$$

Similarly, the force acting on the fold flight cutting edges is,

$$F_{ff} = A_{ff} * \tau = 2 * n_f * (b_{ff} + t_{ff}) * l_{cf} * \tau \qquad \text{Equation 20}$$

Total cutting force at the flight straight and fold cutting edges is,

$$F_f = F_{fs} + F_{ff} = n_{f*}(b_{fs} * t_{fs} + b_{ff} * t_{ff}) * \tau_p \qquad \text{Equation 21}$$

The force acts through a time of, $\frac{\theta}{2\pi N}$

N is the revolution of the auger per second. The same situation repeats at a phase difference φ (Figure 38).

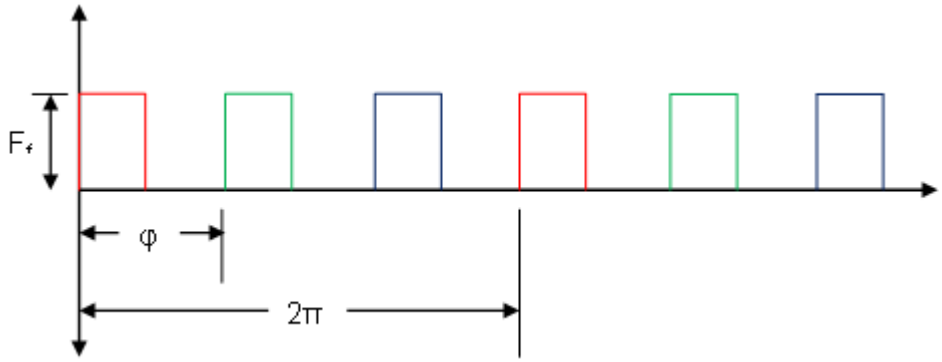

Figure 38 Forces acting at the flight edges of an auger

5.4. Auger transport forces

Transport force calculation and the auger design are based on the recommendations of (KWS 2008). Steps of the design are, a) establishing the characteristics of the material to be conveyed, b) locating auger capacity (size and speed) depending on the excavation production required c) selection of conveyor components, d) calculation of required horsepower and e) checking of component torque capacities (including selection of shaft types and sizes).

5.4.1. Material characteristics

As per screw conveyor design consideration, density of damp sand = 1758 kg/ m^3, the material is highly abrasive-Class III and the power (HP/ kW) factor is 2.8 (CEMA 2009).

5.4.2. Auger conveying capacity

Cross- sectional area of the material cut is calculated for two conditions, a) depth of cut is less than the difference between the auger radius and auger shaft, i.e. $\left[h<\left(R_a - r_a\right)\right]$ and b) depth of cut is more than the difference between the auger radius and auger shaft, i.e. $\left[h \geq \left(R_a - r_a\right)\right]$.

Referring to Figure 39 and Figure 40, h = Depth of cut (m), $\mathrm{R_a}$ = Auger radius (m), shown as OA, r_a = Auger shaft radius (m), shown as OA', p = Pitch of the auger (m), θ_1 = (Angle circumscribed by auger circumference with a depth of cut (*h*) when $\mathrm{h}<\left(\mathrm{R_a}-r_a\right)$, θ_2 = (Angle circumscribed by auger shaft circumference with a depth of cut h) when $h \geq \left(R_a - r_a\right)$, A_{s1} = Cross- sectional area of the soil when $\mathrm{h}<\left(\mathrm{R_a}-r_a\right)$, A_{s2} = Cross-sectional area of the soil when $h \geq \left(R_a - r_a\right)$.

Condition: I (Figure 39)

When, $\mathrm{h}<\left(\mathrm{R_a}-r_a\right)$, then the cross-sectional area of the soil, A_{s1} = ½ (Area of Segment AKG)

Area of segment AKG =

$$\tfrac{1}{2}\left[\left(\theta_1 - \sin\theta_1\right) * R_a^2\right]$$

Cross-sectional area of the soil,

$$A_{s1} = \tfrac{1}{4}\left[\left(\theta_1 - \sin\theta_1\right) * R_a^2\right] \qquad \text{Equation 22}$$

where,

$\theta_1 = 2 * \cos^{-1}\left[\dfrac{\left(R_a - h\right)}{R_a}\right]$, ($\theta_1$ is in radians).

Condition: II (Figure 40)

When $h \geq \left(R_a - r_a\right)$, then cross-sectional area of the soil = ½[(area of segment AKG) – (area of segment A'K'G')]. Here, angle $\theta_2 \leq AOG$, angle $\theta_3 \leq A'O'G'$.

$$\cos\left(\theta_2 / 2\right) = \left[\frac{\left(R_a - h\right)}{R_a}\right]$$

and

$$\cos\left(\theta_3 / 2\right) = \left[\frac{\left(R_a - h\right)}{r_a}\right].$$

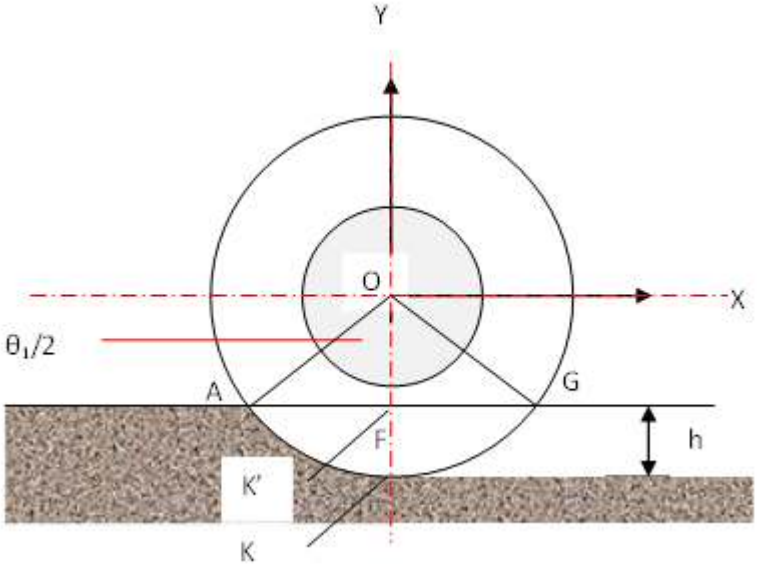

Figure 39 Cross-sectional area of captured soil in auger for ($h<(R_a - r_a)$)

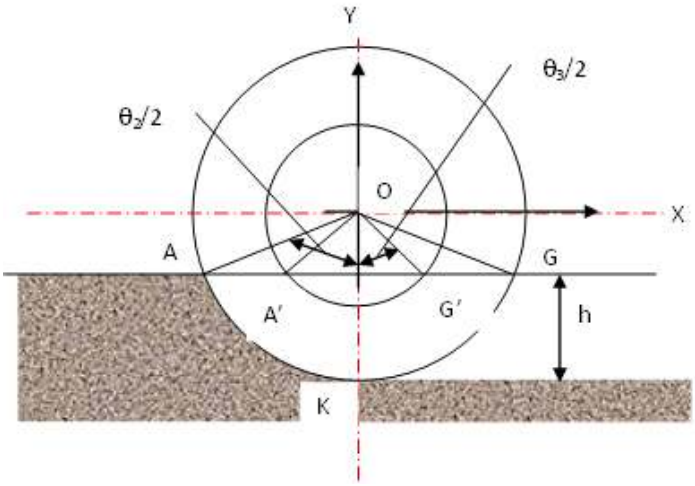

Figure 40 Cross-sectional area of captured soil in an auger for ($h=>(R_a - r_a)$)

Area of segment AKG = $\frac{1}{2}\left[(\theta_2 - \sin\theta_2) * R_a^2\right]$ and area of segment A'K'G' = $\frac{1}{2}\left[(\theta_3 - \sin\theta_3) * r_a^2\right]$.

The cross-sectional area of the soil,

$$A_{s2} = \frac{1}{4} * \left[(\theta_2 - \sin\theta_2) * R_a^2 - (\theta_3 - \sin\theta_3) * r_a^2\right] \quad \text{Equation 23}$$

Theoretical volume of transported material (cu. m/ s) is,

$$Q_{th} = \Gamma * A_s * k_{if} * v = \frac{\Gamma * A_s * k_{if} * p_a * N}{60}$$ Equation 24

Value of Γ suggested by Roberts (2000) is,

$$\Gamma = \frac{1}{8}\left[\left(1 + 2\frac{C_v}{D_a}\right)^2 - \left(\frac{d_a}{D_a}\right)^2\right] * \left[\frac{p_a}{D_a} - \frac{t_{vb}}{D_a}\right]$$ Equation 25

C_v Virtual clearance, explained later in detail (m),

D_a Diameter of the auger (m),

d_a Diameter of the auger shaft (m),

t_{vb} Vane blade thickness (m),

A_s Cross sectional area of cut (m^2),

$A_s = A_{s1}$ or $A_s = A_{s2}$

depending on the condition (depth of cut).

k_{if} Inclination factor; for horizontal configuration, k=1 (Carlos III University 2010),

p_a Pitch of auger (m),

N Revolutions per minute (-).

A virtual clearance C_v is considered surrounding the auger. The auger has no casing, but the part where the cutting is done, a virtual casing can be imagined where the material is not disturbed by cutting. The portion of the auger exposed to water creates turbulence in the surrounding water. Due to the turbulence, there is some disturbance up to a certain disturbed radial limit depending on the auger geometry and material spillage to the disturbed zone. An imaginary boundary can be assumed at the radial distance for the circumferential portion of the auger in contact with water. By weighted average the virtual average casing clearance is,

$$C_v = \frac{\left[\left(C_s * \theta_C\right) + \left(C_w * \left(2\pi - \theta_C\right)\right)\right]}{\left(2\pi\right)}$$ Equation 26

$\theta_c = \theta_1$ or $\theta_c = \theta_2$ depending on the condition

C_s and C_w are the clearances between the auger and the soil for the cutting portions of the auger and between the auger and water for the non-cutting portions of the auger respectively.

Now the actual volumetric transport output of an auger is (Roberts 2000),

$$Q = Q_{th} * \eta_v$$

η_v Volumetric efficiency (%),

Q_{loss} Volumetric loss (m^3).

The volumetric efficiency depends on the ratio,

$$\eta_v = \frac{\left(Q_{th} - Q_{loss}\right)}{Q_{th}}$$

Volumetric efficiency η_v consists of two parts, vortex efficiency η_{VR} and fullness efficiency η_F.

$$\eta_v = \eta_{VR} * \eta_F$$

$$\eta_F = \frac{h}{p_a}$$

$$\eta_v = \eta_{VR} * \left(\frac{h}{p_a}\right)$$

η_{VR} depends on the type of material, angular velocity (centrifugal force) and outside forces such as water drag and water current. In the case of non-cohesive soil, a portion of the materials will be thrown away by centrifugal force outside the conveying zone. The frictional force between sand and auger blade and the water drag force act opposite the centrifugal force. Force produced by water current act only on the portion of the auger exposed to water and modifies the resultant force, depending on the direction of current. In the case of cohesive materials percentage of overthrown material would be less due to

cohesiveness. These factors will affect the volumetric conveying efficiency η_v. No published data is available about loss or spillage for an auger dredging cutter. These may be derived by experiment with complex set-up.

For conveying the material power required is,

$$P_H = c_0 * \frac{Q * \gamma_s * L_a * g}{3600} kW$$ Equation 27

(Carlos III University 2010)

c_0 Material resistance coefficient, taken as 4 for sand

L_a Length of auger in meter

g Acceleration due to gravity

γ_s Bulk density of sand (t/m3).

The powers lost due to friction for a screw conveyor $\left(P_n = \frac{D_a * L_a}{20} \right)$, as is given by the equation (Carlos III University 2010) is negligible, hence excluded from the total power calculation.

5.5. Soil-cutting power of an auger.

For the validation of the experiment, attention was focused on the soil cutting power. Soil cutting powers derived from the experiment and calculated from the 'Specific Energy' are addressed in this section.

5.5.1. Soil cutting power from the experiment

In the experiment, powers were supplied to two actuators for excavation of soil by the auger. One is the auger-drive power for its rotation and another is hydraulic cylinder power for the feed of the auger into the soil. The feed force does not change the direction during the excavation process and it is assumed constant. The feed force is included within the hydrodynamic and frictional forces. Hence, only the force supplied by the auger-drive motor is taken into consideration. The force from the auger torque varies depending on the depth of cut, engagement of the auger flights with soil and also with the position of the flight within the sand during cutting.

When only the vane edges are engaged in sand cutting then the area of cutting is constant for a particular depth of cut. Depending on the number of flights engaged in cutting and the position of the flight within the soil, the available power is divided between the vane edges and the flights thus reducing the cutting force available at the vane edges. The cutting process of a single flight demands a varying force starting from zero to a maximum. With fixed phase angle of the auger flights (number of flights in a pitch) and the pitch of the auger, cutting condition of the auger is constant. It can be assumed that the circumferential force is acting at a distance of [auger radius – ½(flight height)]. In the experiment, soil cutting power was derived from the actuator power after deducting the power loss and the transport power as shown in the flow chart (Figure 41).

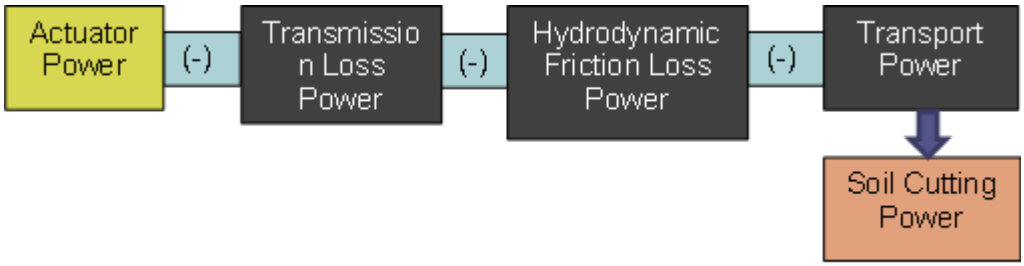

Figure 41 Flow chart of 'Actuator power' to 'Auger soil cutting power'.

5.5.2. Soil cutting power from the experiment

The specific energy for dredging is the power required to dredge a unit volume of a specific type of soil. With the volume rate of excavated material the power necessary for soil cutting can be calculated if the 'specific energy' for the type of soil is known. Specific energies for different types of soil are given in Table 6 (Paragon International 1991; Vlasblom 1999).

Table 6 Specific energy values for different types of soil

Soil Type	Consistency (Whitlow 1998)	Specific Energy [kWh/ m^3]
Sand	Loose	0.04 – 0.10
Sand	Slightly Packed	0.10 – 0.30
Clay	Dense	0.10 – 0.20
Clay	Very Dense	0.30 – 0.70
Soft Rock	Fissured	0.70 – 1.00

The volume of soil excavated per unit time by an auger is given by,

$$Q_{se} = \frac{\pi * D_a * N * L_a * h}{60}$$ Equation 28

D_a = Auger Diameter

N = Auger RPM

L_a = Auger length

h = Depth of cut.

$$\left(E_{spec} = \frac{P_{se}}{Q_{se}} \right)$$ Equation 29

E_{spec} Specific energy (kWh / m^3)

P_{se} Power based on *specific Energy (*kW)

Q_{se} Excavated volume per hour - calculated (m^3 / hour)

5.6. Auger components

Three important dimensions of screw conveyors are depicted in (CEMA 2009) They are auger outer diameter, tube diameter and pitch. The auger had to cater for cutting forces and drag forces hence the auger tube diameter was made bigger than the standard screw conveyor. The following dimensions were taken for the auger

D_a Auger diameter: 190 mm

d_a Auger shaft diameter: 90 mm N. B. heavy pipe

t_{ff} Flight thickness: Base: 3 mm, Tip: 1.5 mm

p_a Pitch: standard $\left(p_a = D_a \right)$.

5.7. Conclusion

An existing soil cutting mechanism model was discussed in this chapter. Soil cutting by an auger, depending on the auger geometry is developed in this research. The supplied power to an auger is used for three different purposes; hydrodynamic friction, soil cutting and transport of soil by the auger. Hydrodynamic frictional power losses are auger specific

and to be derived by experiment for a particular auger. Transport power of an auger was calculated theoretically taking the auger as a screw conveyor. Theoretical correction factors for the transport power were assigned for the screw conveyor working under water. As discussed in Chapter 4, theoretical determination of soil cutting power is complex. In this research, the soil cutting powers of loose to slightly compacted sand with an auger of specific dimensions were determined by the available values of *specific energy*.

CHAPTER 6 EXPERIMENTAL SET UP

6.1. Introduction

A neutrally buoyant swimming submersible dredger is a plausible alternative to the available deep dredging equipment. It can surpass the limitations of the existing submersible dredgers, provided the excavation forces are counterbalanced by suitable devices. Compared to other types of dredging cutters, a transverse axis auger cutter can dredge thin slices of material and if fitted with a shroud, produces minimal environmental disturbance during gathering of soil or ore (Hoagland et al. 2010). Hence, a neutrally buoyant submersible swimming dredger with transverse axis cutter, incorporating devices for counterbalancing the dredging forces, is a suitable contender for controlled surgical cuts that are necessary for mining and environmental sustainable dredging. For station keeping during dredging accurate prediction of the level of generated excavation force components is essential for design. The forces along the axis of the cutter are balanced between each side of the cutter, hence vertical and horizontal force components play the major roles in station-keeping. An experimental set up made to investigate these two force components, for cutting saturated sand with an auger and the method of experiment as well as the results of the experiment are presented in this chapter.

The experiment was done in India in the workshop of Excavation & Equipment Manufacturing (P) Ltd. (EEM) at Suri, West Bengal, India. Expertise of EEM in designing, building and operating different types of dredgers for inland applications was used in this research. The different types of dredgers designed, built and operated by EEM are shown in Figure 1, which is an auger dredger and also in Figure 42, Figure 43 and Figure 44.

An auger cutter dredger is used in places where much dispersion of dredged materials is not permitted and closely controlled surgical cuts are necessary. Where the sediment is composed of different types of organic and inorganic large sized particles, then the sediments can be dozed by a pusher dredger to a suitable location and then re-handled by an excavator. For dredging in locations with deep rooted underwater weed growths, rotovator cutter dredger is ideal. The rotovator chops the weeds to pieces so that they could be pumped by the dredge pump. An axial crown cutter dredger is a general purpose dredger used in places without any contamination or foreign matters.

Figure 42 Pusher dredger

Figure 43 Rotovator cutter dredger

Figure 44 Axial cutter dredger

6.2. Design of experiment

The experimental design follows the methodology of Figliola & Beasley (1995). The steps are described in the following sections.

6.2.1. Objective

Two main objectives were targeted in this experiment. The first objective of the experiment was, to quantify the nature and magnitude of the excavation force components generated in vertical and horizontal directions during dredging loose to slightly-compacted saturated sand by an auger. The second objective was to measure the near-field and far-field turbidity generated during dredging by this cutter, fitted with a shroud. Turbidity could be an indicator to assess the environmental impact of dredging. Only the force components measurement is described in this Chapter. Turbidity generation and measurement aspects are addressed in Chapter 8.

The variables (output) sensed as signals were vertical upward/ downward and horizontal forward/ backward force components, tabulated in Table 7. The control parameters (factors) that affected the dependent variables were the a) cutter rpm, b) cutter feed rate and c) depth of cut to cutter diameter ratio (ξ).

Table 7 Variables recorded by sensors

Serial No.	Variable	Sensor	Remarks
1	Vertical upward or downward force components - Z axis	Load cell	The axis orientation is shown in Figure 48
2	Horizontal forward or backward force components - X axis	Load cell	

6.2.2. Test plan and matrix

Three levels of rpm of the cutter, two levels of feed, and four levels of depth of cut to cutter diameter ratio were tested as shown in Table 8. The cutting edges of the auger vane and the flights are visible in Figure 45.

Cutter rpm

Minimum and maximum values of rpm were selected based on standard industry practice used for these dredging cutters, although some limit was imposed by the design of the testing equipment. Test tank dimensions, feed hydraulic cylinder and cutter hydraulic motor specifications were the constraints for the test equipment. Low rpm is required for

highly compacted materials and obviously the production rate is lower. On the contrary, with higher rpm there is a possibility of more dispersion of the excavated material (spillage).

Table 8 Parameters and their levels

Factor code	Factor description	Level				Unit
		1	2	3	4	
X_1	Cutter RPM	11	25	-	40	-
X_2	Feed rate	2	-	-	6	m/min
X_3	Cutter diameter/ depth of cut ratio (ξ)	0	0.12	0.24	0.48	-

Feed rate

The relation between the cutter angular velocity and the translational velocity is important for excavation production from a rotary cutter (Yatsuk et al. 1984). The feed rates were selected based on the installed capacity of the hydraulic cylinders and the dredge pump capacity. For effective dredging and minimal dispersion of the spillage flume, the excavation capacity and the pumping capacity should match. If the excavation capacity is more than the pumping capacity then some excavated materials would be left. With left over excavated soil, there would be repetitive cutting of the same soil mass. This could produce additional signals for re-excavation of the same soil mass, making the analysis difficult. On the other hand, if the pumping capacity is higher than the excavation capacity, a thinner mixture would be pumped reducing effective production. For example if 1 cu m of soil is excavated per minute, theoretically the dredge pump should also handle 1 cum of soil per minute. If the concentration of soil by volume is 20%, then the dredge pump mixture capacity should be 5 cum per minute.

Ratio of depth of cut and cutter diameter (ξ)

The lowest level selected was without any depth of cut $(\xi = 0)$. This allowed the hydrodynamic force for rotation and translation of the auger in water to be recorded. The frictional force of the auger and its drive during rotation, for a specific feed rate and rpm of the cutter was also calculated. Effective cutting was possible, when the ratio of cutter diameter and depth of cut did not exceed 0.24 $(\xi < 0.24)$. During this range, the depth of cut was equal to or less than the depth of the vane and flights (**Error! Reference source not found.**). If the ratio of cutter diameter and depth of cut exceeded 0.24 $(\xi > 0.24)$,

then the cutter shaft was immersed partly or fully in soil. For scale, the length of the cutter is 0.95 metre.

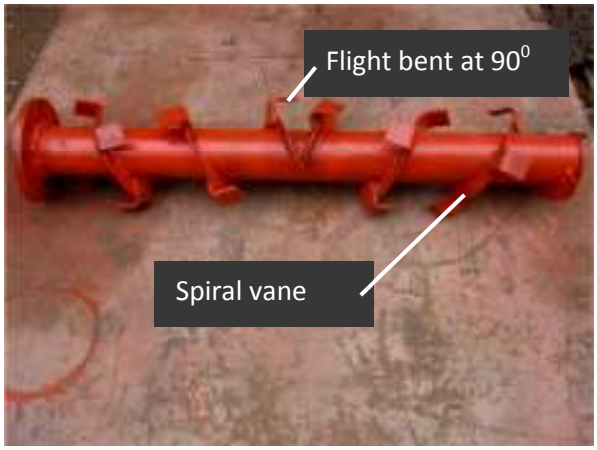

Figure 45 Auger 'Vane' and 'Flight'

A test was done when the ratio of cutter diameter and depth of cut was 0.48 $(\xi = 0.48)$ to observe the nature of forces when the vane and flight including half of the cutter shaft was within the soil. In practical situations, the dredge operator may unwillingly put a higher depth of cut or there may be undulations in the ground that may cause the submergence of the cutter shaft into the soil.

6.2.3. Assessment of methodology

The following aspects were considered for assessing the methodology of the experiment.

Testing environment and uniqueness of this experiment

A purpose-built test tank made up of steel plate with reinforcements was fabricated. To approximate natural conditions, the test tank was filled with river sand collected from the nearby riverbed of the river *Mayurakshi,* at the downstream side of a barrage. The particle size distribution of the soil was classified by a sand scale. The clastic (carried away) sediment was saturated by keeping it in water for two days after excavation. Before the excavation force components tests, compaction of the sand was done manually with a flat hand rammer. Compaction at different points within the tank was tested by a hand-held penetrometer to assure the state of the sand was within the range of loose to slightly-compacted. All other soil properties were assumed constant during the tests (Figure 46).

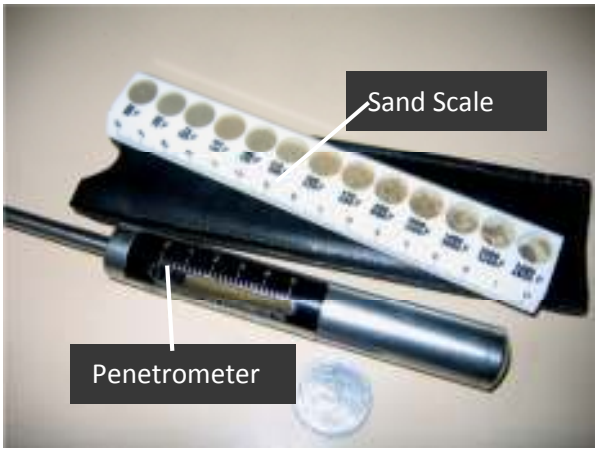

Figure 46 Sand scale and Hand Penetrometer

The differences in this experiment from the work of Joanknecht (1974), Van Os (1987) and Henriksen (2009) are, a) the type of cutter for the excavation force test, b) the objective of the test and c) the type of set up and transducers used for this test.

The cutter used for this test was a transverse axis auger instead of the axial cutters used in previous experimental designs (Henriksen 2009; Joanknecht 1974; Van Os & Van Leussen 1987). Instead of analysis of the excavation forces related to soil cutting, one aim of this experiment was to investigate the reaction force components produced from excavation in dredging that affect position keeping of the dredger itself. The positioning arrangement of the cutter in this experiment was achieved by a two-directional translational motion in place of a hinged ladder positioning system for axial cutters. In the case of previous experiments the cutter was attached to the end of a ladder, which was hinged to the carriage. The cutter along with the ladder rotated in a vertical plane around the fixed hinge. The depth of cut depended on the angle of rotation of the ladder. In this experiment, the cutter had a translatory motion in a vertical plane and the depth of cut depended on the linear motion. In the case of cutting force experiments for axial cutters, strain gauges are normally fixed on the cutting surfaces. These exposed strain gauges can be easily damaged. The transducers used in this test were placed apart from the cutting surfaces and were of a dismountable type, permitting easy and quick maintenance or replacement if necessary. In this test the force transducers showed the load-directions as well. Two transducers were used and placed at a distance from the cutter above water to measure the vertical and horizontal force components.

For experiments on dredging cutters in the past, both a scaled-down model and a full scale cutter have been tested (Henriksen 2009, Dekker et.al. 2003, Van Os 1987). EEM had experience with comparatively small dredging cutters used in inland situations. A small full scale auger cutter was used for this research based on a design developed by the author during his work for EEM for use in closely controlled inland dredging situations. From experience it was observed that the auger could cut thin slices of material when required and the vibrations felt during excavation were more uniform and less than with other designs.

Test set up

A picture and a schematic diagram (not to scale) of the test set up are shown in Figure 47 and Figure 48 respectively.

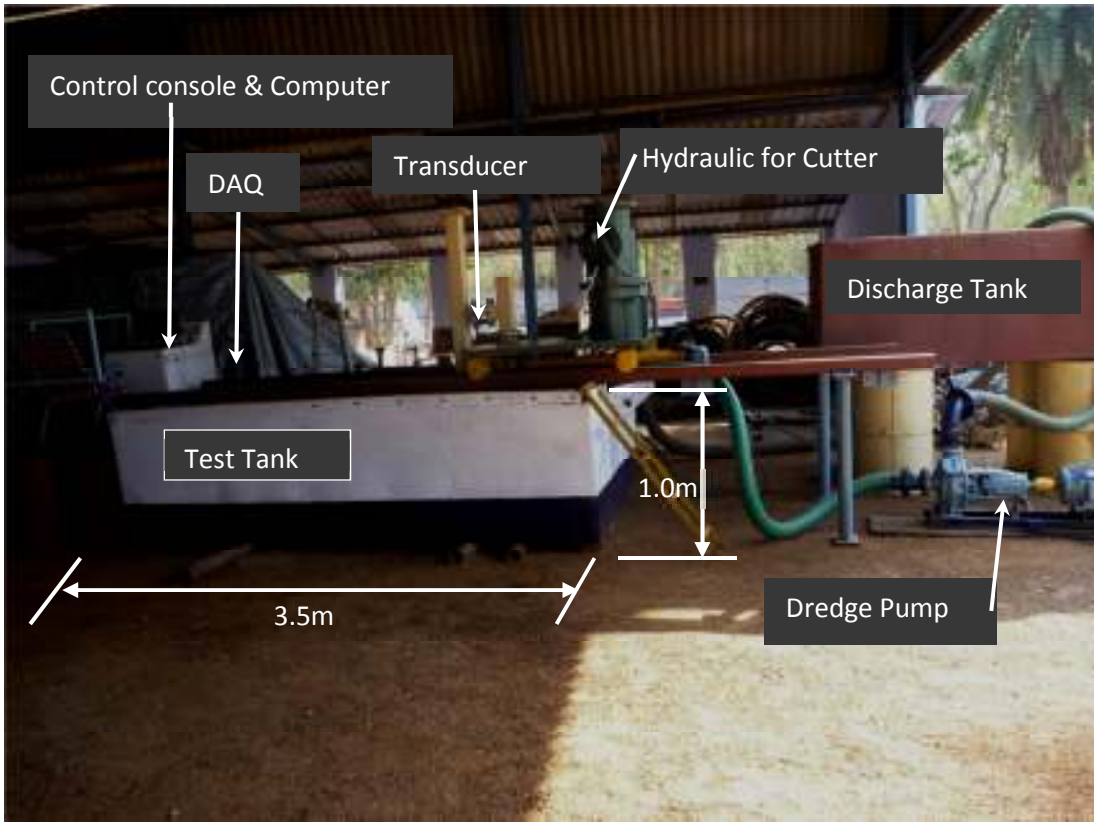

Figure 47 Dredging test tank at the workshop of EEM in India

A steel test tank was fabricated with length 3.5 metre, width 1.5 metre and an approximate depth 1.0 metre. On the top of the test tank, two parallel rails of 100mm square steel cross section and 5.7 metre long, were fixed by welding, at a centre distance

of 1.2 meter. A rectangular platform like carriage with length of 1.2 metre and width of 1.6 metre was designed to roll on the two rails on four flanged wheels. The wheel diameter was 76 mm with 110 mm diameter flange. Each wheel was fitted with ball bearings to reduce friction and provide smooth operation. The load transducer structure was fixed at the front of the carriage. On the front of the carriage a small flanged square-sectioned steel member (100mm sq.) was welded, on which the side-flanged horizontal transducer was fixed vertically with nuts and bolts. The flanged square-sectioned column (100mm sq.) was joined with nuts and bolts to the top of the horizontal transducer. The vertical transducer placed horizontally, was bolted on either side to two small square-sectioned (100mm sq.) short pieces. One of these short pieces was welded to the vertical column and the other to the vertical guide. The guide was 1.2 metre long with the same cross section (100mm sq.).

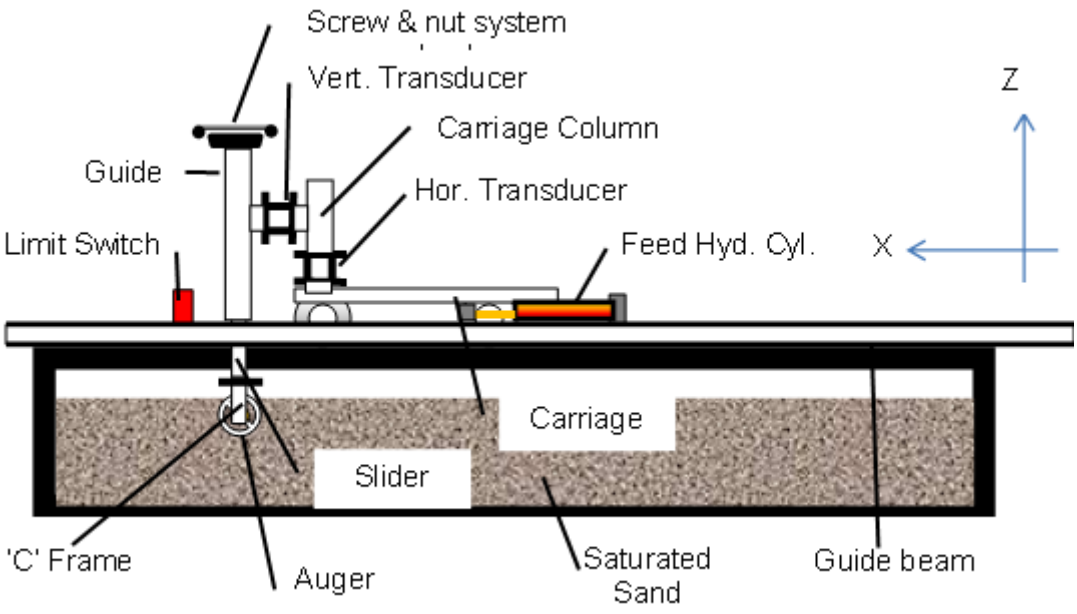

Figure 48 Schematic test set up

A steel slider with a smaller cross section (93mm sq.) was designed to slide up and down through the fixed guide. The sliding was achieved by means of a screw and nut mechanism with a rod diameter of 38 mm, length of 500 mm and having a square thread of 3 mm pitch. The screw and nut mechanism was operated by a hand wheel fixed on plates on the top of the guide. There were thrust bearings fitted with the screw and nut mechanism to overcome the vertical thrusts.

The flanged lower part of the slider was fixed by nuts and bolts to the centre of a 'C' frame having the same cross section as that of the slider (93mm sq.). The auger was made of mild steel with all- welded construction, having a length 950 mm, shaft diameter 90 mm, outside diameter 200 mm, with 90^0 bent flights of 40 mm. width and height. The auger had a pitch of 150 mm. The cutter rotated within two bearings fitted to the lower ends of the 'C' frame. A hydraulic motor (Make: 'EATON' Hydraulic; Model: H 290; Displacement (cm^3/rev): 293; Selected rpm: 11 to 40) was coupled directly through a flexible coupling to drive the auger (Figure 49). The auger was partly covered on the top and the back by a removable shroud, which controlled the dispersion of the spillage flume. The back side of the shroud was formed as the suction bell mouth of the dredge pump and the suction pipe was attached to it through a flanged connection (Figure 50).

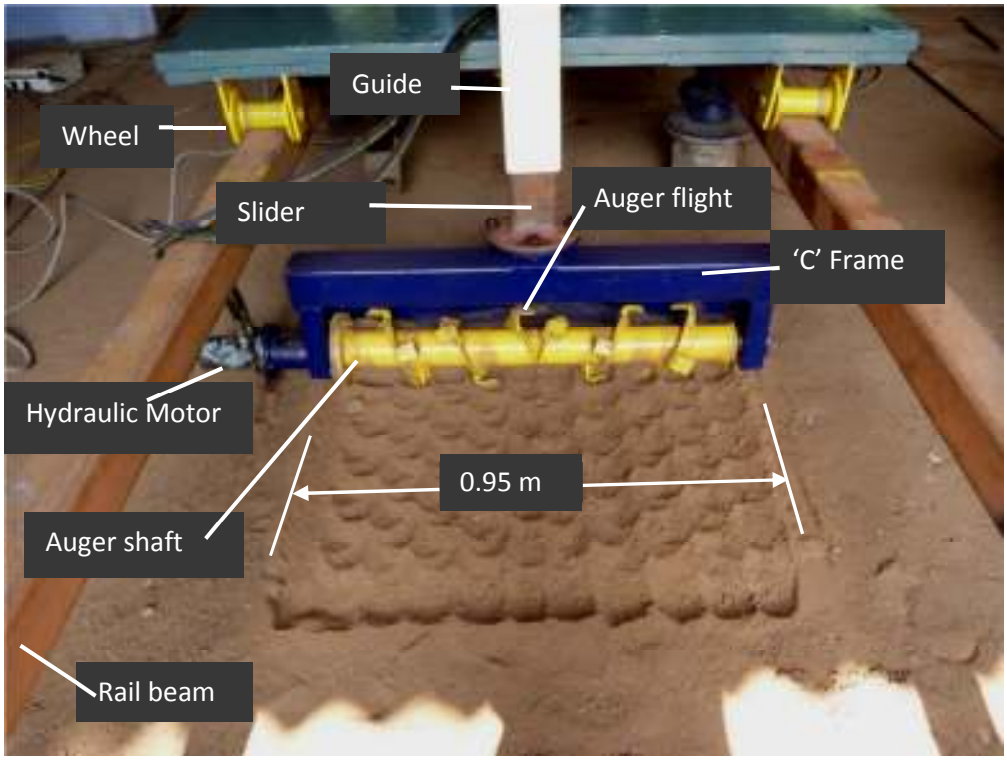

Figure 49 Auger cutting dry soil

The cutter hydraulic motor driving power pack was fixed on the back of the carriage. The hydraulic gear pump (Make: 'MICO'; discharge: $8cm^3$/rev; Pressure: 9.12 MPa; rpm: 1500) within the power-pack was driven by a 'KIRLOSKAR' make 3.7 kW @ 1500 rpm squirrel-cage induction electrical motor. The flow was controlled by a 220V solenoid operated 4-way directional control valve and a manually operated flow control valve.

There were two cross beams fixed with gusset plates and bolts and nuts between the two rails at their ends. Another removable cross beam could be relocated at locations separated by a distance, slightly longer than the stroke of the hydraulic cylinder. One end of a hydraulic cylinder was connected to the centre of the removable cross beam and the other end was attached to the centre of the carriage at the front (Figure 50) for movement of the carriage along with the auger. With the relocation of the removable cross beam, fresh areas of uncut sand in the tank are available to the auger. Hence, different sets of excavation tests could be done.

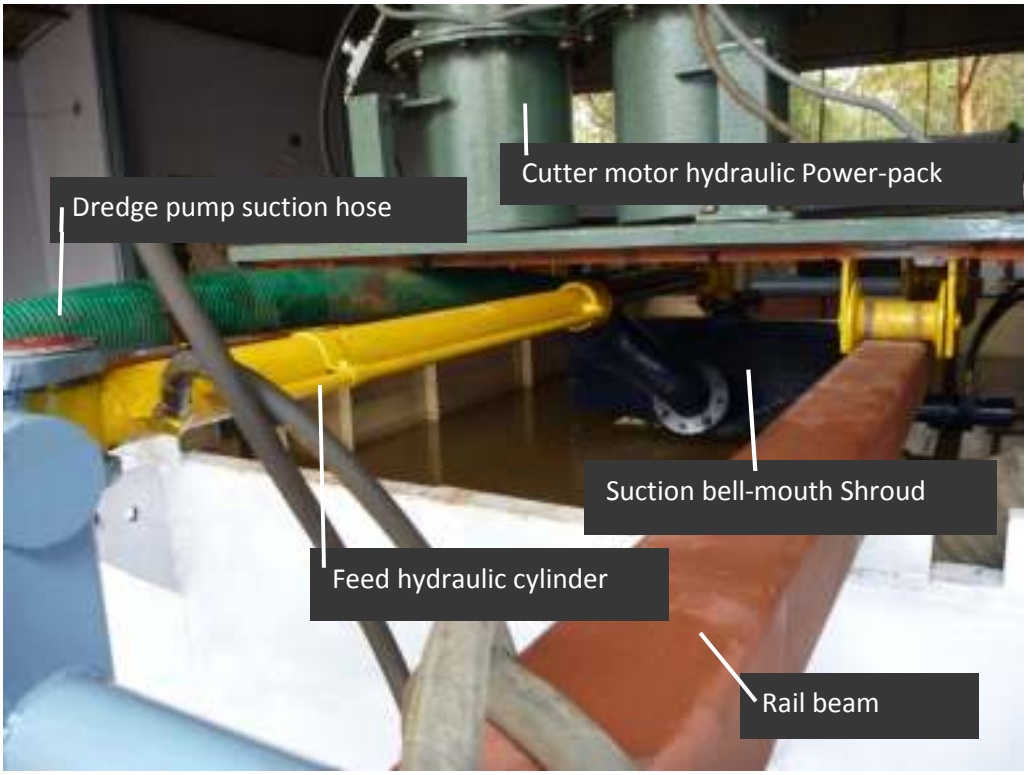

Figure 50 Feed hydraulic cylinder and suction pipe of dredge pump

The hydraulic cylinder with an operating pressure of 10.1 MPa and effective stroke of 900 mm was built by EEM. There was a limit switch that activated at the end of feed, to stop the electric motor, used to drive the hydraulic pump, operating the hydraulic cylinder. There was a separate power pack to drive the feed hydraulic cylinder. The hydraulic cylinder was controlled by a 220V solenoid operated 3 position 4-way directional control valve and a manually operated flow control valve. The cylinder driving hydraulic pump ('MICO' make) had a discharge of 16cm^3/rev. and a working pressure of 10.1 MPa. The

hydraulic pump was powered by a 'KIRLOSKAR' make, 440V squirrel-cage induction motor of 5.5 kW @ 1500 RPM.

The dredge pump was a 'KIRLOSKAR' make solid handling pump, model: SHN 50/ 26 N with a total head of 21.5 (MWC), suction (mm) / delivery (mm): 65 / 50, discharge (lps): 19.5, driven by a 'KIRLOSKAR' make 440V squirrel-cage induction motor of 5.5 kW @ 1500 rpm. The dredge pump with its driving electrical motor was placed at a lower level than the test tank to allow the pump to be self-priming. Discharge from the dredge pump was directed to a discharge tank (length- 2.5 meter, width- 1.1 meter and height- 1.0 meter approximately) placed at a higher level than the test tank (Figure 47). There was a return pipe from the discharge tank to the test tank. Thus the water was re-circulated by gravity to the test tank after deposit of the dredged sand in the discharge tank.

All the electrical and hydraulic motors and the hydraulic cylinder were controlled from a console, which was placed on a higher level platform on the opposite side of the dredge-pump (Figure 47). The data acquisition system (DAQ) and the transducer stabilized power supplies were also fixed near to the console. Transducer power supplies were from a 12V car battery placed on the ground near the test tank and power supply boards. Signals received from the DAQ were recorded on a desktop computer placed on the console.

Analog pressure gauges were used to measure the pressures of the hydraulic systems for the auger drive motor and carriage feed cylinder. The feed cylinder travel time was measured by a stopwatch. The cutter RPM was measured by a hand held mechanical tachometer and rechecked with an optical tachometer. The depth of cut was measured by the rotations of the hand wheel, which were pre-calibrated and zeroed. For a single rotation of the hand wheel, the advancement of the slider (i.e. depth of cut) was equal to the pitch of the screw, which was 3 mm. The parameter and the sensors are shown in Table 9.

Sensors were required for the force measurements in the two orthogonal directions – one vertical and one horizontal. The cutter torque was estimated from the characteristic curves of the hydraulic motor, provided by the manufacturer and the pressure reading of the related hydraulic circuit. The pipeline losses between the hydraulic motor and the pressure gauge was small, hence the pressure loss for the pipe was neglected.

The force components in two orthogonal directions were measured by load cells, which were designed, built, instrumented and calibrated by the author. The following issues

were considered during the design of the load cell. The application of the load cell was the conversion of force into an electrical signal. The load nature was dynamic, i.e. the magnitude and direction would change with time. With a cutter diameter of 0.2 metre, maximum torque of the cutter hydraulic motor set as 320 Newton-meter, assumed transmission loss as 2%, and an overloading factor of 50%, the maximum tangential force acting in one direction at the cutter blade tips were expected to be 3,900 N respectively.

Considering the available data acquisition system input facility, signals could be in mV without pre-amplification. In this investigation, average force components were of importance. The DAQ system was a 16-bit converter. Interchange ability was taken into account to allow for easy replacement of the transducers from the system, hence the force transducers were modular and to the same design.

Table 9 Control parameters and sensors

Sl	Parameter	Sensor	Remarks
1	Cutter RPM	Tachometer	RPM of the cutter was measured above water by a hand held digital / optical tachometer and calibrated against the opening of hydraulic flow control valve. The average of the readings was taken for calibration.
2	Feed rate	Limit switches and stop watch	Start and stop times of the feed cylinder stroke was noted for a particular setting. Stroke of the cylinder being known, the velocity was calculated and calibrated with the related opening of the hydraulic oil flow control valve. The average of the readings was taken for calibration.
3	Depth of cut	Screw- nut mechanism with hand wheel rotation	Linear measurement of the slider movement fixed with the nut and screw mechanism was controlled by the known pitch of the square-thread of the screw nut mechanism, rotated by a hand wheel. The depth of cut was measured by the rotation of the hand wheel.

The load cell designed, built, instrumented and calibrated by the author (Bose 1985; Dally & Riley 1973; Perry & Lissner. 1962; Relay et al. 2007; RSData 1983a; RSData 1983b) (Bose 1985; Dally et al. 1973; Perry et al. 1962; Relay et al. 2007; Rsdata 1983a; Rsdata 1983b)(Bose 1985; Dally et al. 1973; Perry et al. 1962; Relay et al. 2007; Rsdata 1983a; Rsdata 1983b)is shown in Figure 51. Between two standard 150mm pipe flanges there were two 10 mm thick plates, which acted as the strain- elements. The design was very stiff along the axis passing through the centre of the two flanges and relatively flexible

along the axis perpendicular to the above axis and passing through the centre of the farthest flange from the strain gauges; hence the strain could be detected by the strain gauges fixed on the 10mm thick strain plate. Four strain gauges were fixed on two opposite faces of a strain plate and connected in a full Wheatstone bridge configuration. The power supply to the load cell was 5 volt. It was provided by a 12 V lead / acid battery and stabilized through electronics built by the author (Bose 1985).

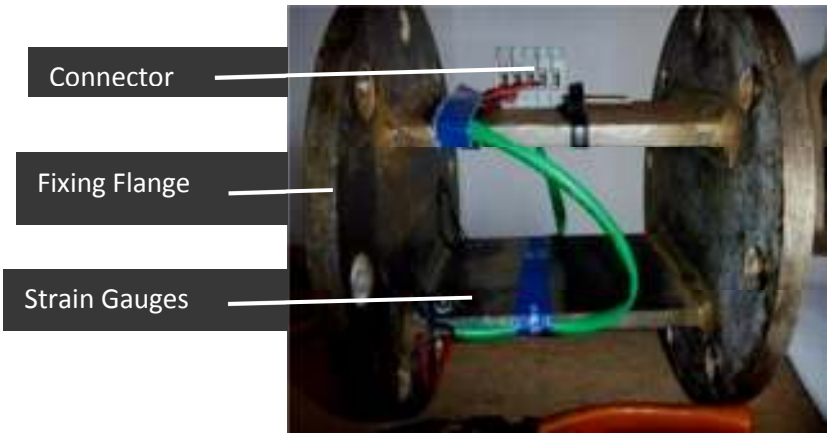

Figure 51 Load cell

Calibrations

Calibrations were necessary for correlating a) the signals and the forces measured by the load cells, b) the flow control valve opening and the RPM of the cutter c) the flow control valve opening and the extension of the hydraulic cylinder rod, which controlled the feed rate of the cutter and d) the pressure and torque of the hydraulic motor. For the limit switch, the manufacturers' calibration standards were applied.

Load cells were calibrated by using known weights applied in a random sequence with the maximum weight exceeding the expected experimental load. The average signal value for a known weight was taken and weight versus signal values were plotted using spread sheets. The application of loads was done very carefully to achieve a straight line curve fit with a R^2 value > 0.999. The slope of the line derived for a particular load cell was used to calculate the force from the signal value. A statistical normal equation was also formed (Spiegel 1992), which matches well with the equation formed by the spread sheet calculation. To investigate cross talk, the same weights were loaded at different lever arms from the flange face. The output did not show any discernible significant change in the signal values indicating that the transducer did not respond to change in moments. This

indicates that the distance of the cutter from the transducer would not affect the vertical force component.

Keeping one flange of the transducer on the ground and loading different weights on the other flange, no noticeable change in signal value outputs were observed. This showed the insensitivity of the load cell to axial loads.

The relationship between particular openings of the flow control valve in the hydraulic circuit and RPM of the dredging cutter were measured. The mean value of the readings was taken for use in the experiment. Hydraulic system pressures were recorded during the test runs. The torque of the cutter was calculated from the characteristic curves supplied by the hydraulic motor manufacturer with the help of the recorded system pressure and displacement per revolution of the motor (Editors Trade & Technical Press 1989). Considering frictional losses at the bearing of 2% (industry standard and also found from experiences), the available torque from the cutter is shown in Table 10 for the respective RPM of the cutter. Correlation between the flow control valve opening and the feed rate of the hydraulic cylinder is presented in Table 11.

Table 10 Correlation between flow control valve opening and hydraulic motor performance

Flow Control Valve open (rotation)	Pressure (kPa)	Torque (N-m)	Available Torque N-m)	Cutter RPM
1.67	7003	325	318	11
0.5	6473	233	228	25
1	4561	313	307	40

Table 11 Correlation between flow control valve opening and feed rate of hydraulic cylinder

Flow Control Valve open (rotation)	Feed rate hydraulic cylinder (m/ min)	Pressure (kPa)	Remarks
0.33	2.0	7847	Cutter tested under water
0.67	4.0	5885	-Do-
3.00	6.0	3825	-Do-

6.2.4. Data acquisition methods

For the data acquisition, an ADAM 4017, 16-bit, 12 channel DAQ system manufactured by ADVANTECH (ADVANTECH 2010) was used. The signals from the DAQ system were routed through a RS 232/ 485 converter and a shielded cable. A compatible power supply capable of suppressing surges was used for the DAQ and converter. This was important because mains power at the site suffered from frequent voltage spikes and load shedding with

power cuts common. Data were logged in a desktop computer placed on the control console with the help of the 'ADAMVIEW' (Advantech 2010) software (Figure 52).

Figure 52 Control console, computer with software window and DAQ with accessories

6.2.5. Test procedure

The test tank was placed on steel supports and the top of the rails at both the ends were levelled by a water level. River sand was collected, cleaned to exclude foreign materials, and compared with the sand scale (a standard field test procedure in dredging) to determine the particle size range. Then the test tank was filled to a depth of 500 mm with sand. Water was pumped into the test tank to fill it to a depth of 200 mm above the sand. The tank was left undisturbed for 48 hours to allow for sand saturation. The sand was hand rammed, levelled with a mould board and compaction tested at different locations within the test area with the penetrometer, to ensure that it did not exceed the slightly compacted state (less than 1 kg/ cm^2). A steel plate was put under water just below the auger to confirm that the cutter would just touch the sand level when lowered. This was the 'zero depth of cut' position. The depth of cut was decided by the rotation of the hand wheel fitted with the screw and nut mechanism.

The auger was rotated within the water without any depth of cut at a set RPM and feed rate of the cutter. Data from the two load cells were recorded on the computer. These gave the hydrodynamic frictional forces at the set rpm and feed rate of the cutter.

Afterwards the auger was lowered to a specific depth of cut and rotation with a set rpm was started. After allowing some time to stabilise the signals the feed cylinder was extended at the desired feed rate. Data were logged directly to the computer. Cutting tests of the saturated sand from loose to a slightly compacted state were done for different set up conditions as described above and the data were recorded.

6.3. Results & discussion

Variations of the vertical and horizontal force components for dredging loose to slightly packed sand with different depth of cuts and different rpm of the cutter at a feed rate of 2 m/ min and 6 m/ min are shown in Table 12and Table 13 respectively. The cutting force acts on the cutting edges at the auger circumference. The vertical and the horizontal reaction force components shown were positive upwards and forward of cutter feed directions respectively (Figure 53).

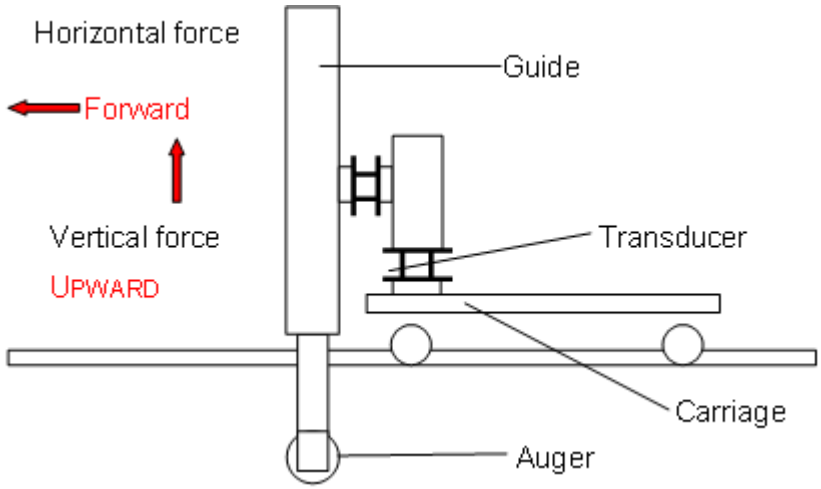

Figure 53 Force directions in the experiment

The hydrodynamic frictional force components in the vertical and horizontal directions encountered by the cutter were the force components with $\xi = 0$ ($\xi =$ depth of cut/ cutter diameter) i.e. depth of cut was zero. The plots of the vertical and horizontal force components at a feed of 2 m/ min are shown in Figure 54 and Figure 55 and those for a feed rate of 6 m/ min in Figure 56 and Figure 57 respectively.

The vertical and horizontal hydrodynamic frictional force components varied marginally with increased cutter RPM$\left(\xi = 0\right)$. For feed rates of 2 m/ min and 6 m/ min, the vertical force components showed a decreasing trend with increasing depth of cut when $\xi < 0.48$. The horizontal force components at 25 rpm of the cutter reduced from that at 11 rpm and again increased to 40 rpm for both the feeds of 2 and 6 m/ min with all the depths of cut. For $\xi = 0$ to $\xi = 0.24$, when the flights and the vane were engaged in cutting sand, the vertical force components increased almost linearly. When $\xi > 0.24$ part of the cutter shaft was submerged within the sand. Hence at $\xi = 0.48$ the force components were very high. These were not from the excavation force only, but mainly due to the frictional force between the cutter shaft and sand.

Table 12 Average vertical & horizontal force components for different ξ & rpm at 2 m/ min feed

Cutter RPM	ξ= (Depth of Cut / Cutter Diameter)							
	0		0.12		0.24		0.48	
	Vertical	Horizontal	Vertical	Horizontal	Vertical	Horizontal	Vertical	Horizontal
11	130	620	230	540	380	830	3400	1100
25	120	650	150	550	220	560	2880	1020
40	90	630	90	600	100	730	2950	1220

Table 13 Average vertical & horizontal force components for different ξ & rpm at 6 m/ min feed

Cutter RPM	ξ= (Depth of Cut / Cutter Diameter)							
	0		0.12		0.24		0.48	
	Vertical	Horizontal	Vertical	Horizontal	Vertical	Horizontal	Vertical	Horizontal
11	150	500	200	500	400	690	3420	1850
25	130	540	240	420	330	390	3050	1240
40	130	530	210	510	330	630	2610	1050

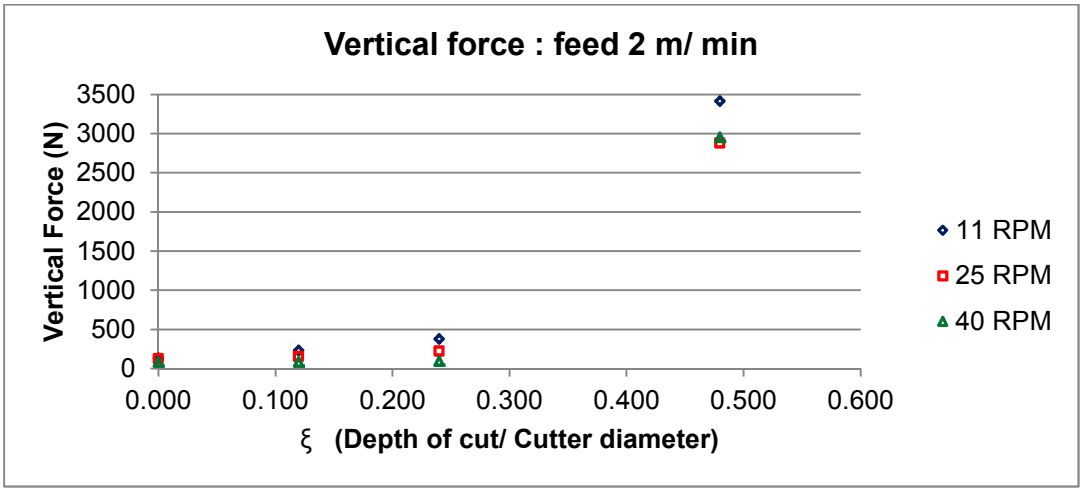

Figure 54 Average vertical force at different rpm and ξ at 2 m/ min feed

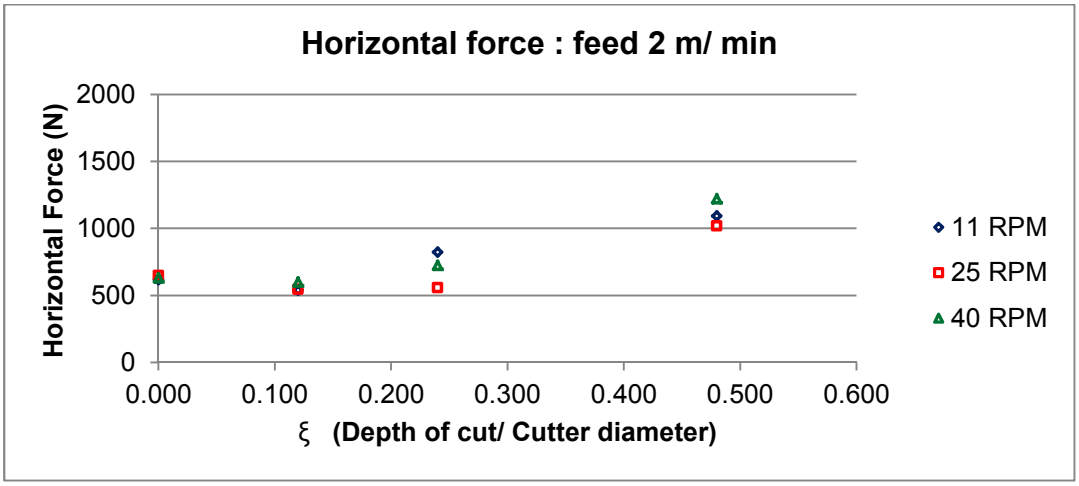

Figure 55 Average Horizontal force at different rpm and ξ at 2 m/ min feed

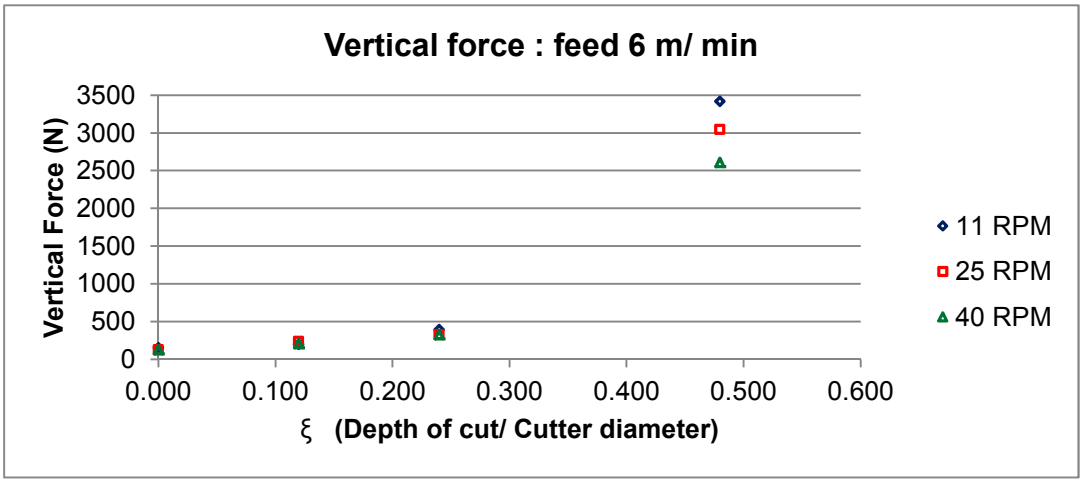

Figure 56 Average vertical force at different rpm and ξ at 6 m/ min feed

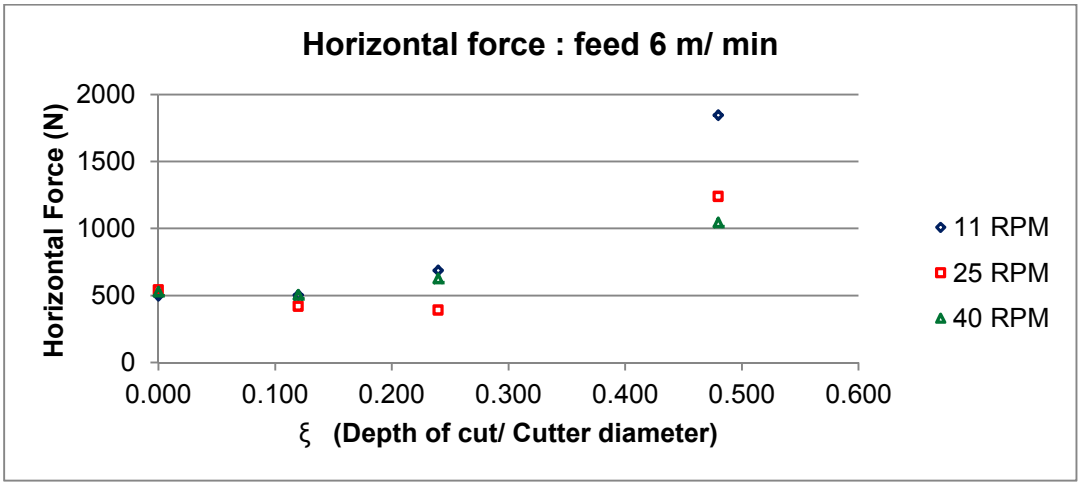

Figure 57 Horizontal force at different rpm and ξ at 6 m/ min feed

The total power absorbed by the cutter was dissipated in overcoming the hydrodynamic friction force, for excavation of the soil and for transporting the soil by the auger vane. Deducting the force component at a specific cutter rpm and without any depth of cut, from the force component at any depth of cut and at the same cutter rpm, gives the force component required for the soil excavation and transport of the soil at that specific depth of cut and the cutter rpm. The resultant of the vertical and horizontal force components yields the force necessary for excavation and transport of the soil.

After calculating the average torque from the force calculations depending on the auger radius and cutter RPM the power required for soil excavation and transport was determined. The transport power of the auger was calculated by considering the auger as a screw conveyor working under water.

Subtracting the transport power from the soil excavation and transport power, the soil excavation power was deduced. This power was compared to the power requirement based on the specific energy for dredging loose to slightly compacted sand.

The results for a feed rate of 6 m/ min and with 11, 25 and 40 rpm of the auger were plotted in Figure 58, Figure 59 and Figure 60. The lines shown in the graphs for loose and slightly packed sand were calculated by $E_{spec} = \frac{P_a}{Q_e}$

Equation 7, Chapter 4 and Table 6, Chapter 5. The combined power (soil cutting and transport power) was calculated from the experimental vertical and horizontal force components. The soil cutting power P_a was derived from the combined power (soil cutting

and transport powers) after deducting the calculated transport power from the combined power and shown in detail in Chapter 7. The excavated volume Q_e = (time of feed*developed length of auger circumference*auger length*depth of cut). This is described in the transport power calculation of the auger. The compaction of the saturated sand was done manually, which could not be closely controlled. Hence, the experimental power plots were done within the range of the field data of loose to slightly compacted sand, shown by the two lines in the figures. The error or the uncertainty is confined between the two lines due to probable uneven compaction of soil. As observed, the experimental powers were within the power range for dredging loose to slightly compacted sand based on the specific energy (please refer to Chapter 7).

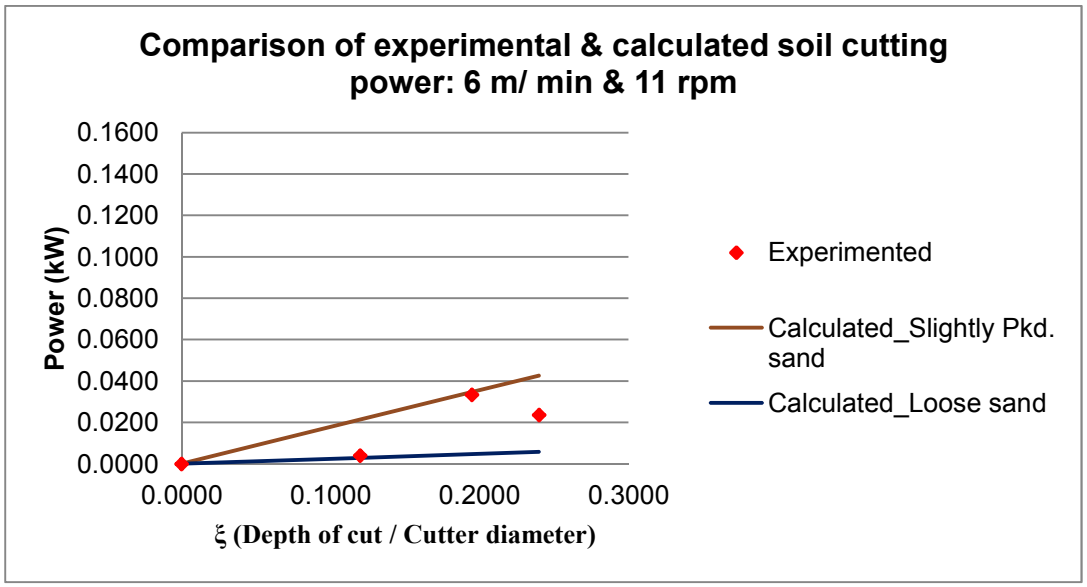

Figure 58 Power from experiment & specific energy for sand: 11 rpm

If the excavation at $\xi \geq 0.24$ is neglected (as this is not a practical dredging situation), then the average vertical and horizontal excavating force components for dredging loose to slightly compacted sand varied from 90 to 400 N and 390 to 830 N (Table 12 and Table 13). If these force components are unbalanced then the position keeping of the vehicle is disturbed and the auger deviates from the desired cutter trajectory. As depicted in the design by Sarkar (2011), the excavating force components are to be nullified by opposing position keeping forces, for effective dredging or mining, in the case of a marginally neutrally buoyant submersible dredger or miner. For position keeping of the type of submersible in question, one or a combination of a) vector thrusters, b) anchored spuds, c) VBT (Variable Buoyancy Tank and d) control planes can be used:

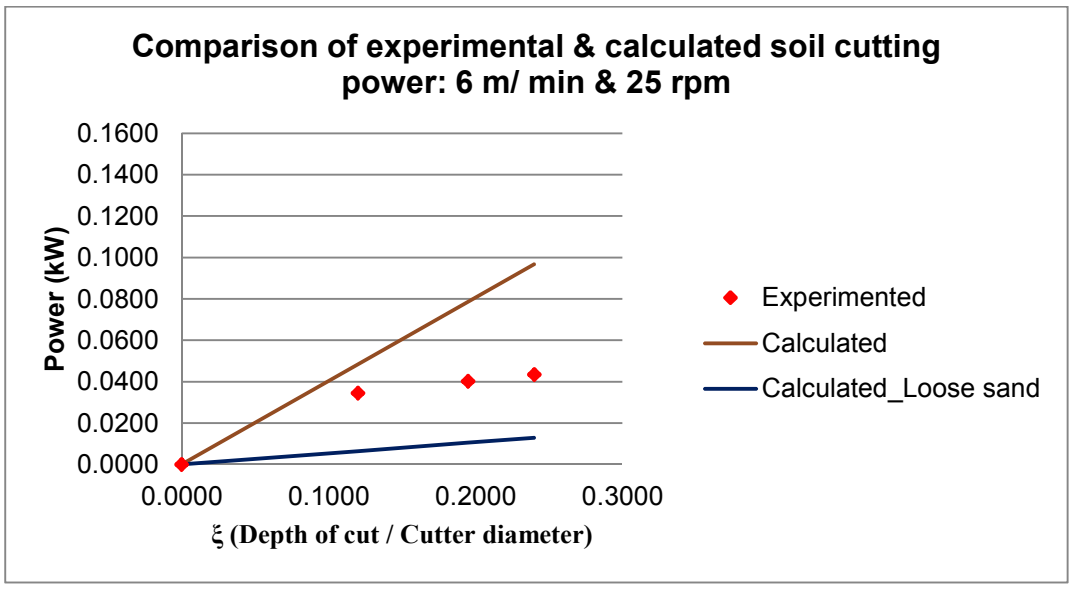

Figure 59 Power from experiment & specific energy for sand: 25 rpm

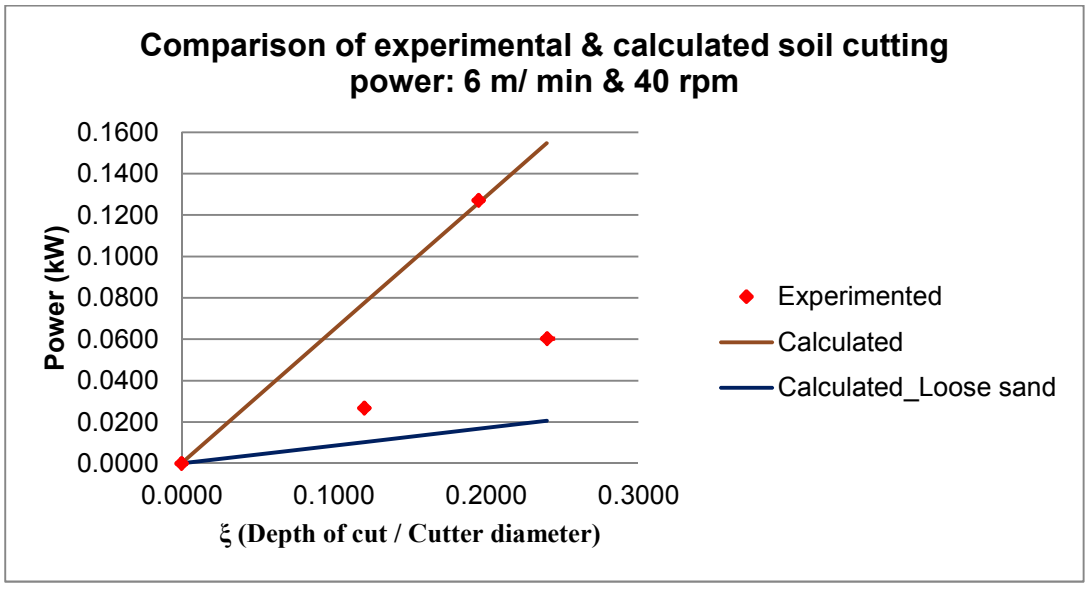

Figure 60 Power from experiment & sp. energy for sand: 40 rpm

The position keeping of the SROSD is a dynamic one, but the primary objective during dredging is to keep the vehicle in a static position without motion. Hence, the system was analysed as a static model at the point of threshold of motion.

Only the excavation forces and moments are considered in the analysis. Forces and moments are also produced by current, by impact with any foreign body. The vibrations of the pumps, risers and actuators also produce shaking forces and moments. These forces and moments are not considered in this analysis. Forces and moments due to gravity and

buoyancy are constant for a specific design of the vehicle. These are dependent on the vehicle geometry and the vehicle is designed to give a neutrally buoyant configuration.

The following analysis is done, considering all the counteracting forces are provided by the vector thrusters. The machine components are schematically shown in Figure 61 and a body-fixed coordinate system at the centre of mass of the vehicle was envisaged. The forces acting on the SROSD during dredging on underwater terrain are shown in Table 14.

Let,

F_{g_D} , weight force due of the vehicle acting along 'Z' axis at its centre of gravity

F_{g_a} , weight force of the actuator assembly, acting along 'Z' axis

F_b , buoyancy forces due to total submergence in water, acting along '-Z' axis

F_c , excavation forces acting at the cutter circumference, resolved into 'X', 'Y' and 'Z' axes as F_{ca}, F_{ch}, F_{cv} respectively

F_W , feed force, provided by the swing hydraulic cylinder to give necessary feed to the cutter

F_p , transport forces as vibrations felt at the mountings of the dredge pump, and at mountings of the delivery pipeline that are not considered for the present analysis

F_{ai} and M_{ai} , the shaking forces and moments due to various actuators (hydraulic cylinders, electrical motors) mounted at various positions and orientations on the vehicle body

F_s , force due to the currents at the place of operation that may not be in line with the vehicle at all times

$F_{g\_D} + F_{g\_a} + F_b = 0$, As neutrally buoyant when all the actuator links are retracted and the vehicle is floating without swimming

$F_{g\_ar\theta}$, vertical weight force component of the actuator during dredging, which changes position due to actuator movement, assumed constant at all positions for this analysis

Forces and moments generated by feed, vibrations from different sources, current and impact are excluded from this analysis. The balancing forces are, $\sum F_{T_i}$ where, F_{T_i} is the thrust provided by a thruster at position (i).

Table 14 Legend of forces

Symbol	Description	Symbol	Description	Symbol	Description
F_{g_D}	Vehicle weight force	F_{gL}	Actuator weight force	F_B	Buoyancy force
F_{Ti}	Thruster force	F_{Si}	Spud anchoring force	Fc_A	Cutter axial force
Fc_H	Cutter horizontal force	Fc_V	Cutter vertical force	F_W	Warping force

A simplified model was conceived for the force system. The following assumptions were made:

a) The vehicle is symmetrical around the 'X' axis. The actuator along with the cutter is considered working in the 'XZ' plane for the initial analysis hence all forces may be treated as two-dimensional

b) The forces due to currents can be superimposed later and are hence excluded for the initial analysis

   The excavation was done by the cutter fitted at the tip of a combination of a number of actuator links. The cutter occupied different positions both in horizontal and vertical planes. Initially, the cutter force and moment were analysed in the vertical plane at the two extreme operating positions, i.e. at the start of cut and at full depth of cut

c) The vehicle with all the components including the different links of the actuator system joined by rotary joints was actually flexible. But for the analysis the vehicle with actuators as a whole was treated as a rigid body

d) The force and moment vectors were assumed to operate at a specific point

e) All gravity forces were assumed to act at the centre of gravity of the respective members. These are sometimes treated as a resultant of all forces acting at the centre of mass of all masses.

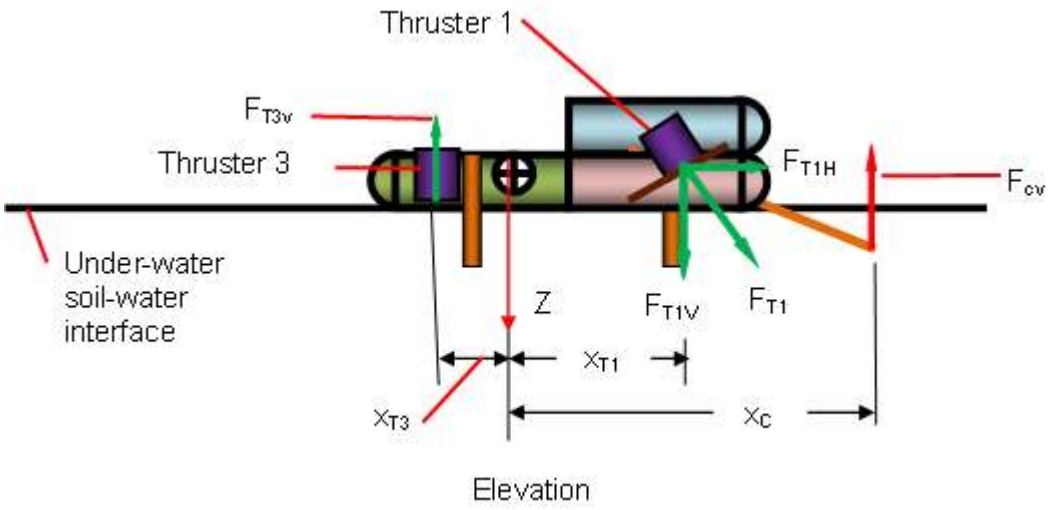

Figure 61 Vertical component of excavation force balancing by thrusters

If only thrusters are used for position keeping of the vehicle, then the resultant force and moment system should be zero. If the front wing thrusters and the rear vertical thruster are used for vertical position keeping (Figure 62) then,

$$\sum F_V = 0$$
$$F_{CV} - F_{T1V} - F_{T2V} + F_{T3V} = 0$$
$$\sum M_Y = 0$$
$$F_{CV} * x_C = F_{T1V} * x_{T1} + F_{T2V} * x_{T2} + F_{T3V} * x_{T3} \qquad \text{Equation 30}$$

$\sum F_V$ Resultant vertical force

F_{CV} Vertical component of the soil cutting force

F_{TiV} Vertical components of thruster force from thruster number i, when i = 1, 2, 3… etc.

M_Y Resultant moment around 'Y' axis

x_{Ti} Distance along 'X' axis from the centre of gravity of the vehicle and i = 1, 2, 3… etc.

Similarly, for horizontal position keeping (Figure 62):

$$\sum F_H = 0$$
$$F_{CH} - F_{T1H} - F_{T2H} - F_{T4H} - F_{T5H} = 0$$
$$\sum M_Z = 0$$
$$F_{CH} * y_C = F_{T1H} * y_{T1} + F_{T2H} * y_{T2} \pm F_{T4H} * y_{T4} \mp F_{T5H} * y_{T5}$$ Equation 31

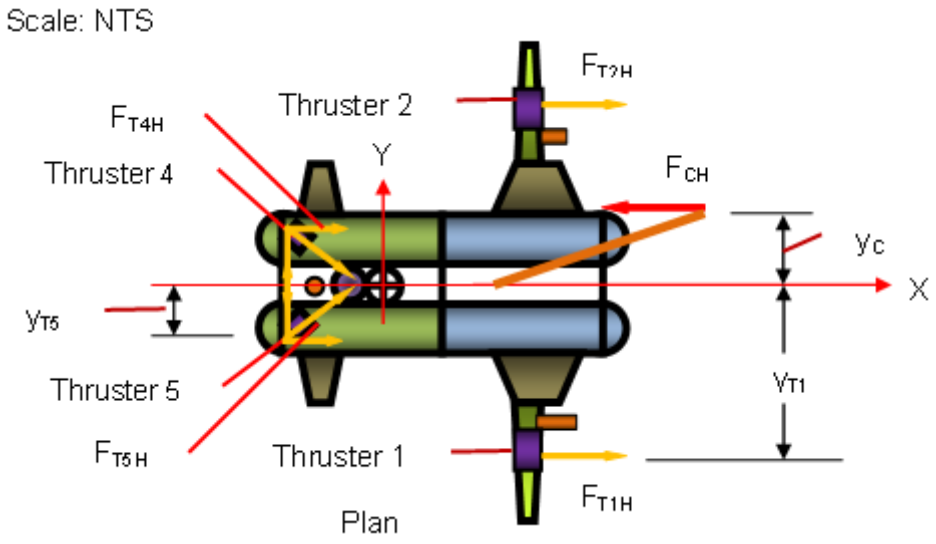

Figure 62 Horizontal component of excavation force balancing by thrusters

$\sum F_H$ Resultant horizontal force

F_{CH} Horizontal component of the soil cutting force

F_{TiH} Horizontal components of thruster force from thruster number i, when i = 1, 2, 3… etc.

M_Z Resultant moment around 'Z' axis

y_{Ti} Distance along 'Y' axis from the centre of gravity of the vehicle and i = 1, 2, 3… etc.

From the above equations the positions of the thrusters can be calculated provided the thrust of the thrusters are known. Thrusters are checked for swimming propulsion and the downward thrust necessary to counteract the anchoring force of the spuds. Supplemental forces provided by the spuds were calculated assuming the two forward and one rear spuds are of equal dimension. The vertical force acts along the axial direction of a spud. The counteracting force of a spud is dependent on the frictional force generated between embedded spud outer surface and soil. The horizontal force from a spud is assumed acting

at half the pushed in length of the spud. A VBT (Variable Buoyancy Tanks) offers extra downward weight force by the filled in water, acting through the centre of mass. Resultant of the two VBT placed in the forward top row of the vehicle contributes the extra downward force if necessary. The projected horizontal surfaces restrict upward motion by water drags and similarly, the vertical projected area of the vehicle resist backward movement. Collapsible control surfaces can be designed to deliver additional opposing forces if required.

6.4. Conclusions

A test facility was designed and built to generate test data during excavation of loose to slightly-packed saturated sand by an auger dredging cutter. Data were collected for the force components in vertical and horizontal directions during the test, which are important for the position keeping for a marginally neutrally buoyant submersible dredger or miner during dredging/ mining. Information about the nature of these two force components helps to design the counteracting devices necessary for position keeping of the vehicle.

Powers required for dredging loose to slightly compacted sand were derived from the vertical and horizontal components of forces recorded from the experiment. The experimental power requirement was within the power requirement based on specific energy required for dredging loose to slightly compacted sand. Hence, if the specific energy of a type of sand and the volume rate of dredging are known then, it is possible to derive the vertical and horizontal force components generated during dredging loose to slightly compacted sand.

Considerable vertical and horizontal forces were generated during excavations. These force components need counter-balancing for efficient dredging. Position keeping devices necessary for a swimming submersible dredger during dredging sand by an auger, can be designed based on the generated vertical and horizontal excavation force components.

The average vertical and horizontal excavating force components for dredging loose to slightly compacted sand for this experiment varied from 90 to 400 N and 390 to 830 N, which can be counteracted by commercially available thrusters. For higher production rate of dredging than the experimental one or with harder dredging materials, the spuds and/

or the VBT are to be used beside the thrusters. Depending on the soil condition, spud end could be embedded or vacuum- fixed to the terrain.

CHAPTER 7 EXPERIMENTAL RESULTS AND VALIDATION

7.1. Introduction

Power required for cutting loose to slightly compacted sand during dredging was recorded in the experiment. The particle size distribution (PSD) range for the sand was between 600 – 1000 μm . The experiment runs were undertaken with different RPM feed of the cutter and ξ (depth of cut/ cutter diameter). The development of the semi- empirical calculation method to derive soil-cutting power was done in this research. The calculation was done, partly with the data from the experiment runs and partly from theoretical model.

Based on the specific energy for dredging loose and slightly compacted sand, power requirements were calculated. Identical working parameters as the experimental runs were used in the power calculations by specific energy. These two results were compared for discussions and validation. With known specific energy of sand, calculation methods to predict the vertical and horizontal force components, generated during dredging sand, are also developed in this study.

7.2. Experimental assumptions

The total power supplied by the drive to the auger excluding the losses in transmission are, a) drag force felt by the cutter, consisting of the hydrodynamic resistance and the frictional forces from different moving component, b) transport force for transporting the material along auger-vane and c) soil cutting force.

The focus of this research was to investigate the soil cutting force components, which affect the position keeping of the vehicle during dredging. Considering a three axis orthogonal force system the force components are, a) vertical, b) horizontal and axial. The auger is divided from its centre to two geometrically 'mirror-image' parts. Axial force components produced by these two halves are equal and opposite in directions, cancelling each other. The resultant force of the remaining vertical and horizontal force components are originated from the torque, available at the auger circumference. The available power to the auger is dependent on the rpm and the torque of the auger. The hydrodynamic friction power was obtained from the experiment and the transport power from a

modified theoretical model of screw conveyor. Following assumptions were made during the analysis of the experimental results:

a) A two-dimensional force system was considered, as force in the other orthogonal direction was cancelled by the two opposite and equal forces produced by the left and right hand auger vane halves
b) The problem was analysed as a static one. The average of the excavation force was taken for analysis. It was also assumed that the soil-cutting force was acting at the circumference of the auger
c) The system was assumed in equilibrium, i.e. there was no accelerating motion of the system
d) Internal force systems were neglected, i.e. stresses produced within the structure were not considered
e) The structure was taken as a rigid body and the strains produced at the load cells were neglected
f) The carriage was moving with a constant velocity without any acceleration
g) For the instantaneous analysis, the auger was assumed to be stationary.

Schematic experimental arrangement with the envisaged force systems is shown in Figure 63.

Legends: (Figure 63)

F_{VC} *Vertical force component, Excavation force*

F_{HC} *Horizontal force component, Excavation force*

F_{VL} *Vertical force component measured at Load cell*

F_{HL} *Horizontal force component measured at Load cell*

X_C *Distance between cutter centre and cutter vertical component*

X_L *Distance between cutter centre and Load cell vertical component*

Y_C *Distance between cutter centre and cutter horizontal component*

Y_L *Distance between cutter centre and Load cell horizontal component*

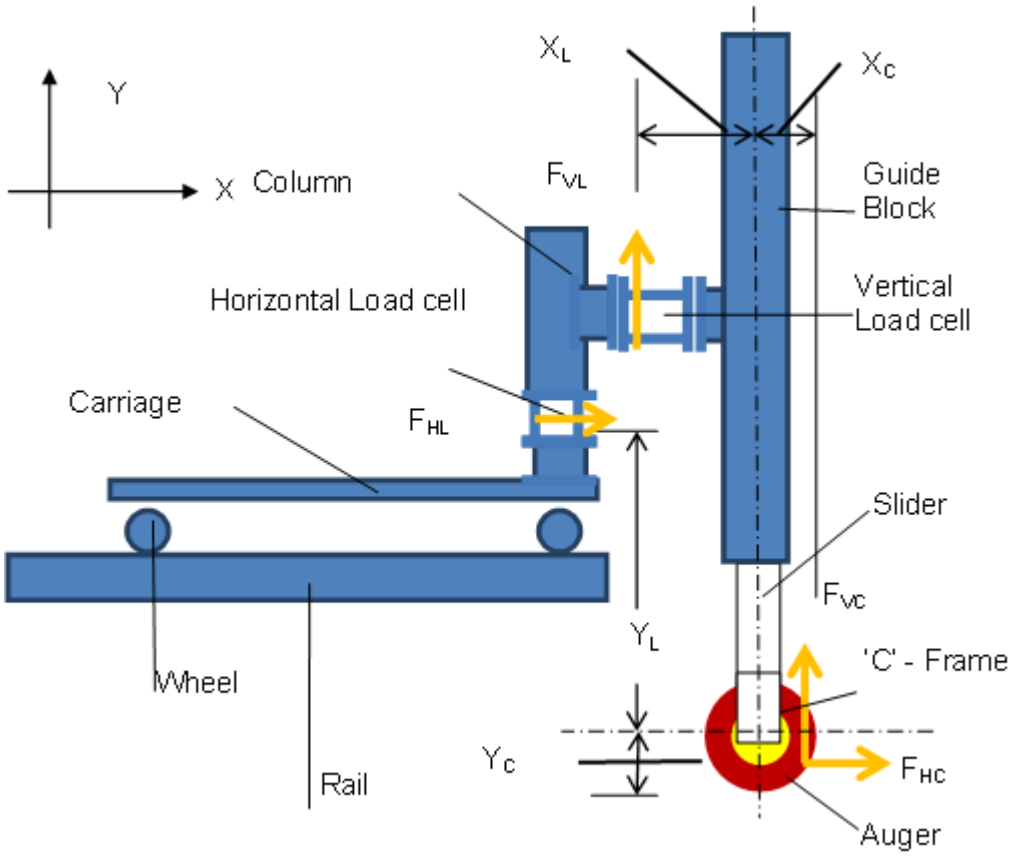

Figure 63 Schematic experimental set up

7.3. Experimental soil-cutting power

Horizontal and vertical components of the forces generated by the auger during excavation under water were recorded by the horizontal and vertical transducers. These force components were the vertical and horizontal force components working at the cutter circumference. Depending on the design of the auger no moments were recorded by the transducers. To derive the soil cutting power from the experiment, the following sequences were adopted:

a) The vertical and horizontal components recorded during a particular run were the components of the 'Total' force (Total force = Hydrodynamic friction force + Auger transport force + Soil cutting force)

b) Auger rotating and moving forward with a specific rpm and feed but without any depth of cut under water, recorded the vertical and horizontal components of the 'Hydrodynamic and friction' force
c) Deducting the respective vertical and horizontal force components of the 'Hydrodynamic and friction force' from those of the 'Total force' gave the force components of the 'Combined' force ('Transport' force + 'Soil-cutting' force)
d) By vectorial addition, of the 'Combined' vertical and horizontal force components, 'Combined' force for a specific operating condition was calculated
e) Assuming the 'Combined' force was acting at a distance of 'Effective radius' = [Cutter radius – (1/2* Depth of cut)] from the centre of the cutter, the 'Combined torque' of the cutter at the specific operating condition, was calculated as ['Combined' torque = 'Combined' force * Effective radius]
f) The experimental 'Combined' power required for (Auger transport and Soil cutting) was calculated by [kW = (Nm*RPM)/ 9549]
g) The auger transport power was calculated for the defined working condition considering auger as a screw conveyor and working under water (Carlos III University 2010; CEMA 2009; Roberts 2000)
h) Deducting the calculated 'Auger transport' power from the experimental 'Combined' power, the semi-empirical 'Soil cutting' power was derived.

7.4. Experimental results

The following section presents the data plots enable to assess the nature of forces. A raw data plot of the vertical component of an excavating force during a test is shown in Figure 64. Only the signals during the actual excavation period were used in the analysis. In the chart, Y axis represents the vertical component of the force in Newton and X axis represents the time in second. Four distinct sections are visible in the plot (Figure 64). The horizontal portion in section 'A' denotes the force when there was no rotation and feed of the auger. Portion 'B' represents the period when the cutter was rotating without feed. Portion 'C' represents the forces of excavation with the rotation and feed of the cutter. Start and finish of excavation data for the analysis are shown. The sudden rise and fall of signal values were due to the hydraulic oil surges, hence excluded. The fluctuations in the signal values within the excavation portion were for a combination of steady value due to

vane cutting and an intermittent value for flight cutting. In portion 'D' the feed was stopped but the auger was still rotating. Average value of the signals during excavation was considered for analysis. Outlier detection or elimination of spurious data was done (Figliola et al. 1995).

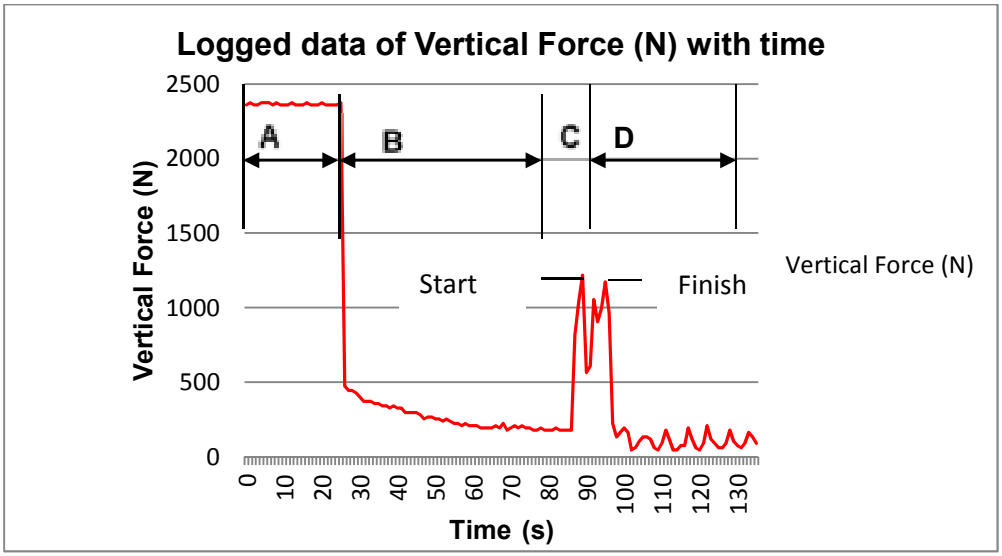

Figure 64 Vertical component of excavation force for a test run

The horizontal force component was also similar. Experimental results of the vertical and horizontal components for the 'Total' force for two feed rates and with different rpm of cutter and different ξ (Depth of cut / cutter diameter) are shown in Table 15 and Table 16. The vertical and horizontal components of the 'Hydrodynamic and friction' forces are the force components at zero depth of cut $(\xi = 0)$ and are shown in Table 17. The 'Combined' ('Auger Transport' and 'Soil-cutting') vertical and horizontal force components are shown in Table 18 and Table 19 at feed rates of 2 and 6 m / min respectively. Vectorial addition of these two force components gave the resultant 'Combined' force. The 'Combined' forces for feed rates of 2 and 6 m/ min are shown in Table 20 and Table 21 respectively.

Table 15 Components of 'Total' excavation force at different rpm and ξ at 2 m/ min feed

Cutter rpm	ξ= (Depth of Cut / Cutter Diameter)							
	0		0.12		0.24		0.48	
	Vertical	Horizontal	Vertical	Horizontal	Vertical	Horizontal	Vertical	Horizontal
11	130	620	230	540	380	820	3400	1100
25	120	650	150	550	220	560	2880	1020
40	80	630	90	600	100	730	2950	1220

Table 16 Components of 'Total' excavation force at different rpm and ξ at 6 m/ min feed

Cutter rpm	ξ= (Depth of Cut / Cutter Diameter)							
	0		0.12		0.24		0.48	
	Vertical	Horizontal	Vertical	Horizontal	Vertical	Horizontal	Vertical	Horizontal
11	150	500	200	500	400	690	3420	1850
25	130	540	240	420	330	390	3050	1240
40	130	530	210	510	330	630	2610	1050

Table 17 Components of 'Hydrodynamic and friction' force at different rpm and feed

Cutter rpm	11		25		40	
	Vertical	Horzntl.	Vertical	Horzntl.	Vertical	Horzntl.
Feed 2m / min	130	620	120	650	80	630
Feed 6m / min	150	130	130	540	130	530

Table 18 Components of 'Auger transport and Soil cutting' force: Feed 2 m / min (N)

ξ = (Depth of Cut / Cutter Diameter)	0.12		0.24		0.48	
	Vertical	Horzntl.	Vertical	Horzntl.	Vertical	Horzntl.
Cutter rpm 11	100	80	250	200	3270	480
Cutter rpm 25	30	100	100	90	2760	370
Cutter rpm 40	10	30	20	100	2870	590

Table 19 Components of 'Auger transport and Soil cutting' forces: Feed 6 m / min (N)

ξ = (Depth of Cut / Cutter Diameter)	0.12		0.24		0.48	
	Vertical	Horzntl.	Vertical	Horzntl.	Vertical	Horzntl.
Cutter rpm 11	50	0	250	190	3270	1350
Cutter rpm 25	110	120	200	150	2920	700
Cutter rpm 40	80	20	200	100	2480	520

Table 20 'Combined' force: Feed 2 m / min (N)

ξ = (Depth of Cut / Cutter Diameter)	0.12	0.24	0.48
Cutter rpm 11	128	320	3305
Cutter rpm 25	104	135	2785
Cutter rpm 40	32	102	2930

Table 21 'Combined' force: Feed 6 m / min (N)

ξ = (Depth of Cut / Cutter Diameter)	0.12	0.24	0.48
Cutter rpm 11	50	314	3538
Cutter rpm 25	163	250	3003
Cutter rpm 40	82	224	2534

Assuming, the 'Combined' force was acting at a distance R_e, from the centre of the auger, where,

$$R_e = \left(R_a - h/2\right)$$

R_e Moment arm of the torque

R_a Auger radius

h Depth of cut

The power necessary for the 'Combined force' is shown in Table 22 and Table 23.

Table 22 'Combined' power (kW): Feed 2 m / min

ξ = (Depth of Cut / Cutter Diameter)	0.12	0.24	0.48
Cutter RPM 11	0.0122	0.0262	0.1732
Cutter RPM 25	0.0227	0.0250	0.3317
Cutter RPM 40	0.0110	0.0303	0.5584

Table 23 'Combined' power (kW): Feed 6 m / min

ξ = (Depth of Cut / Cutter Diameter)	0.12	0.24	0.48
Cutter RPM 11	0.0048	0.0257	0.1854
Cutter RPM 25	0.0354	0.0465	0.3577
Cutter RPM 40	0.0287	0.0665	0.4830

The auger 'Transport' powers were calculated on the basis of the on land fully covered screw conveyor design principle (Section 5.4). As the water Drag due to feed and rotation of the auger and frictional forces in the bearings were already covered under the 'Hydrodynamic and friction' power, hence only the 'Transport' power was calculated. The auger 'Transport' powers were independent of feed rate and dependent on cutter rpm only and shown below in Table 24. Deducting the 'Transport' powers from the respective 'Combined' powers, 'Soil-cutting' powers were derived and shown in Table 25 and Table 26.

Table 24 Theoretical 'Auger transport' power (kW)

ξ (Depth of cut / Cutter diameter)	0.12	0.24	0.48
Cutter rpm 11	0.0006	0.0015	0.0038
Cutter rpm 25	0.0013	0.0034	0.0087
Cutter rpm 40	0.0020	0.0055	0.0140

Table 25 'Soil-cutting' power (kW) from experiment: Feed 2 m/ min.

ξ	0.12	0.24	0.48
11 rpm	0.0116	0.0247	0.1694
25 rpm	0.0214	0.0216	0.323
40 rpm	0.0090	0.0248	0.5444

Table 26 'Soil-cutting' power (kW) from experiment: Feed 6 m/ min.

ξ	0.12	0.24	0.48
11 rpm	0.0042	0.0242	0.1816
25 rpm	0.0341	0.0431	0.3490
40 rpm	0.0267	0.0610	0.4690

For validation of the experimental results, the experimental 'Soil-cutting' powers for loose to slightly-compacted sand were compared with the respective 'Soil-cutting' powers, calculated by the 'Specific Energy' at the same working conditions.

To derive the 'Soil-cutting' power based on the specific energy, the soil volume was estimated as, (length of auger*depth of cut*time of feed in sec*circumference of auger*auger rpm / 60). The powers required for cutting loose and slightly-compacted sand, at three different rpm (11, 25 and 40), with feed rates of 2 m/ min and 6 m/ min were calculated and shown in Table 27 and Table 28.

The experimental powers for cutting loose to slightly compacted sand are shown as points in Figure 65, Figure 66, Figure 67, Figure 68, Figure 69 and Figure 70. Depending on the specific energy, powers required for 'Soil-cutting' for loose and slightly-compacted sands are shown as two different lines in a figure.

Table 27 Soil cutting power (kW) from 'Specific energy': Feed 2 m/ min.

RPM	11		25		40	
Compaction ξ	Loose	Slightly packed	Loose	Slightly packed	Loose	Slightly packed
0.120	0.0028	0.0213	0.0064	0.0483	0.0103	0.0774
0.150	0.0035	0.0266	0.0081	0.0604	0.0129	0.0967
0.195	0.0046	0.0346	0.0105	0.0786	0.0168	0.1257
0.240	0.0057	0.0425	0.0129	0.0967	0.0206	0.1547
0.480	0.0113	0.0851	0.0258	0.1934	0.0413	0.3094

Table 28 Soil cutting power (kW) from 'Specific energy': Feed 6 m/ min.

RPM	11		25		40	
Compaction ξ	Loose	Slightly packed	Loose	Slightly packed	Loose	Slightly packed
0.120	0.0028	0.0213	0.0064	0.0483	0.0103	0.0774
0.150	0.0035	0.0266	0.0081	0.0604	0.0129	0.0967
0.195	0.0046	0.0346	0.0105	0.0786	0.0168	0.1257
0.240	0.0057	0.0425	0.0129	0.0967	0.0206	0.1547
0.480	0.0113	0.0851	0.0258	0.1934	0.0413	0.3094

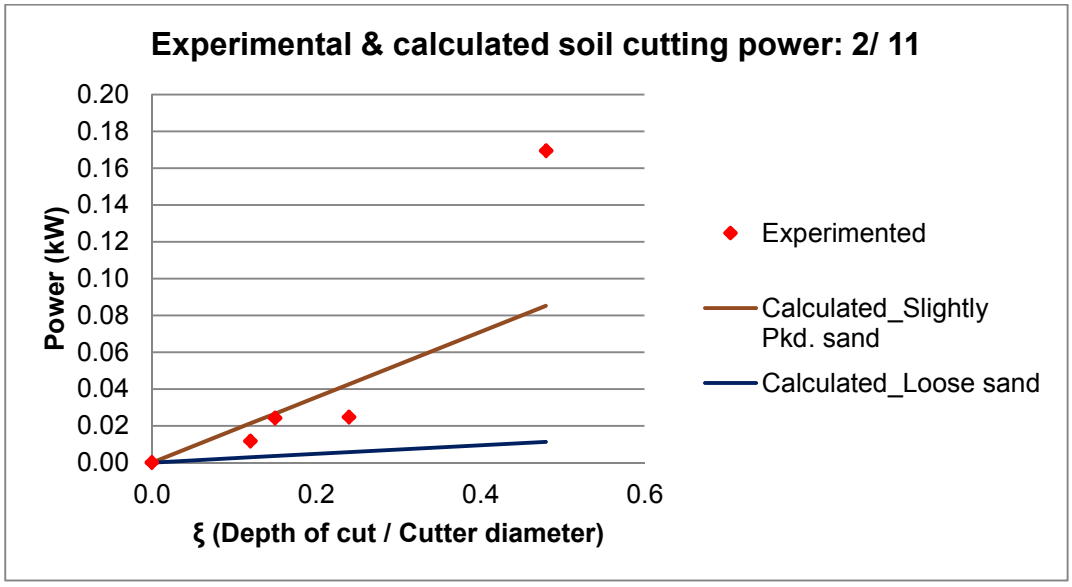

Figure 65 Experimental & calculated soil cutting power: 2m/ min & 11 rpm

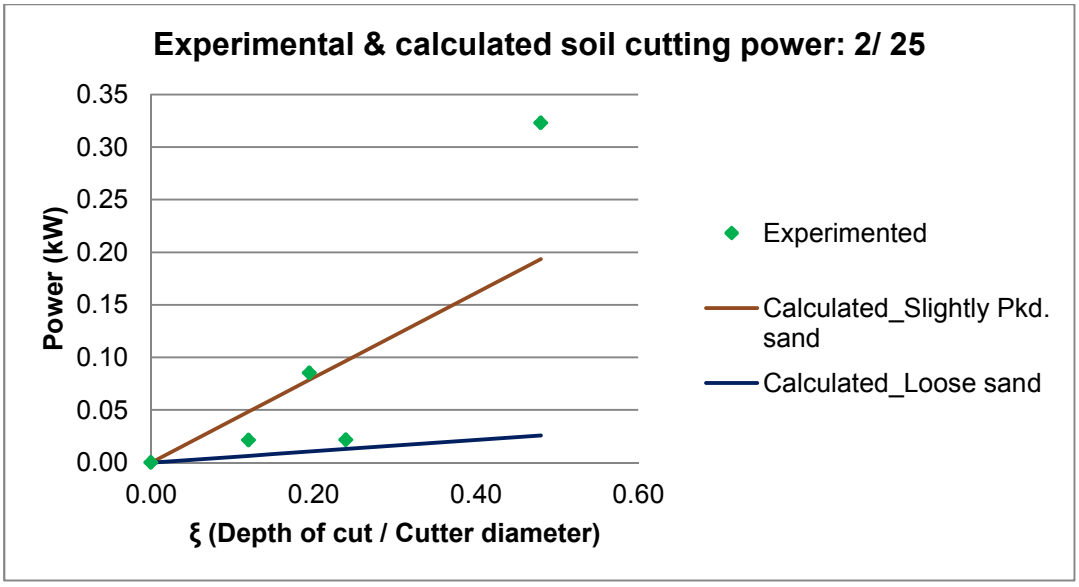

Figure 66 Experimental & calculated soil cutting power: 2m/ min & 25 rpm

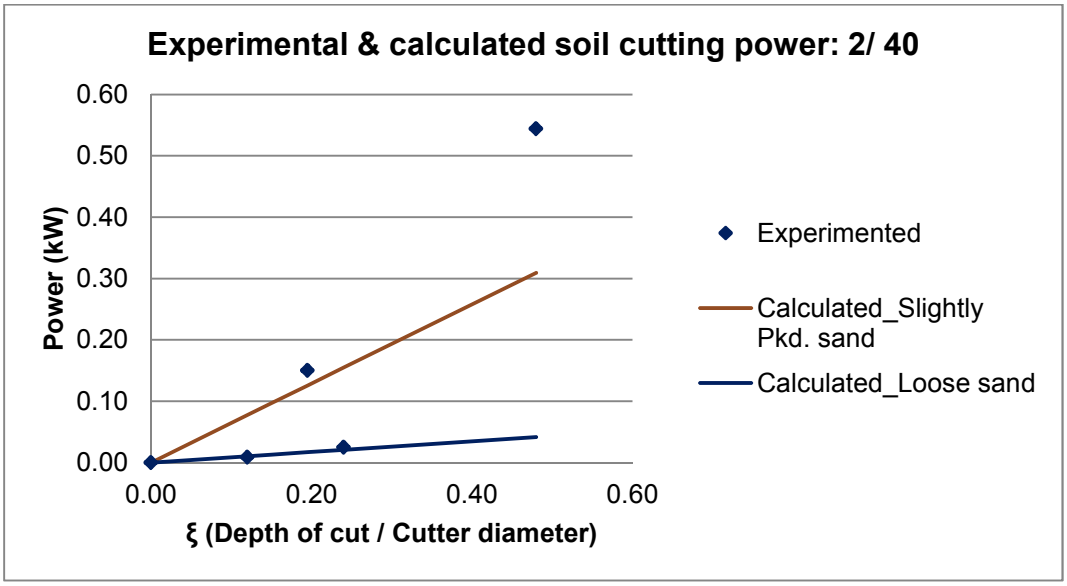

Figure 67 Experimental & calculated soil cutting power: 2m/ min & 40 rpm

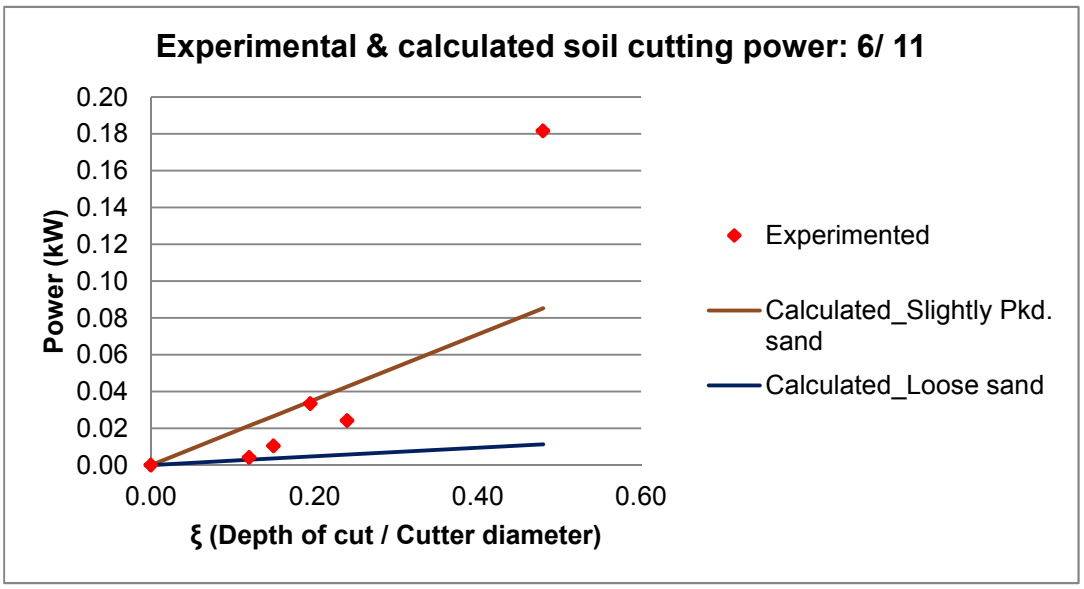

Figure 68 Experimental & calculated soil cutting power: 6 m/ min & 11 rpm

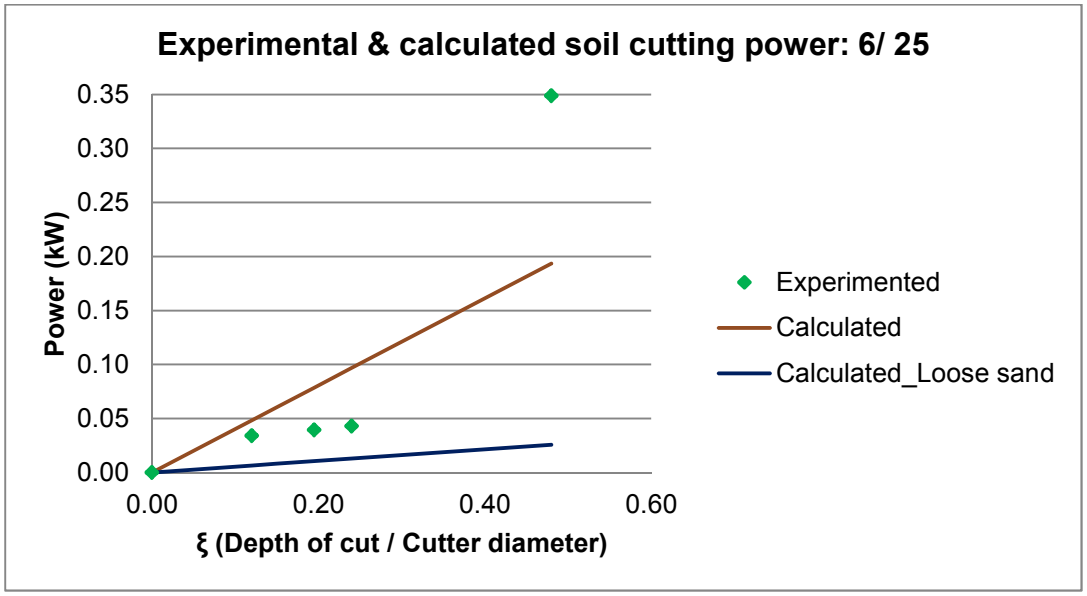

Figure 69 Experimental & calculated soil cutting power: 6 m/ min & 25 rpm

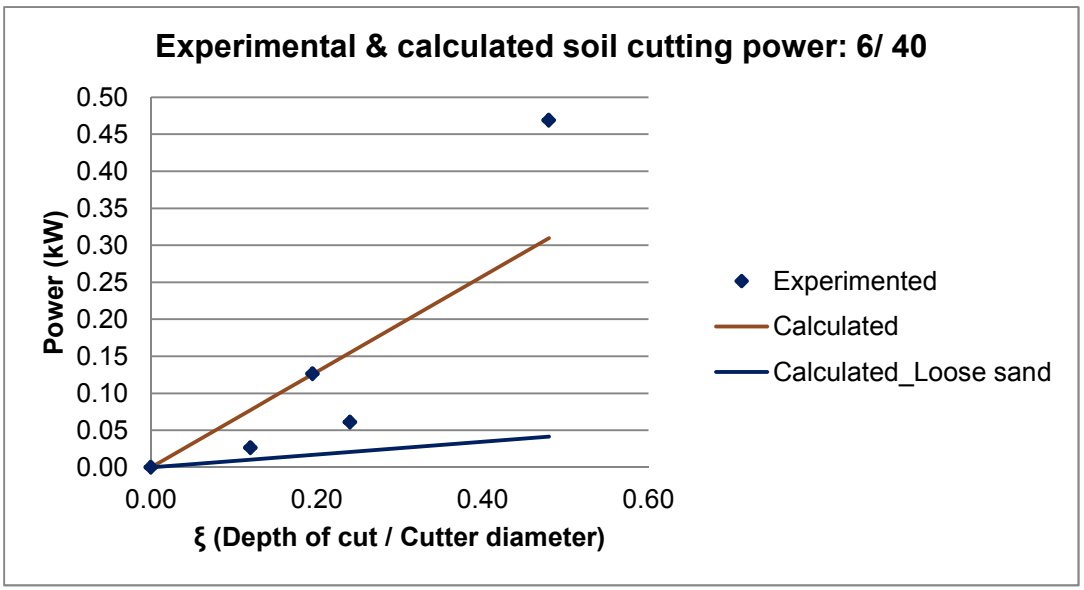

Figure 70 Experimental & calculated soil cutting power: 6 m/ min & 40 rpm

7.4.1. Uncertainty in the 'Soil-cutting' power

The aim of this work was to obtain excavation force components from experiment and to calculate the 'Soil-cutting' power for validation. The main equation used to calculate 'Soil-cutting' power was,

$$P_c = \left(P_{co} - P_H\right)$$

P_c Soil cutting power (kW)

P_{co} Power for combined excavation power (kW)

P_H Auger transport power (kW)

The 'Combined' excavation power consists of auger 'Transport' power and 'Soil-cutting' power. This was calculated from the experimental data of 'Total' and 'Hydrodynamic' vertical and horizontal force components. The auger 'Transport' power was derived from a modified theoretical model of the screw conveyor. The auger 'Transport' power is insignificant compared to the 'Soil-cutting' power. Hence, calculation of uncertainty analysis was done in this work based only on the 'Soil-cutting' power derived from experiments. For uncertainty analysis of the 'Combined' power the following data reduction equations were used.

$\overline{F_{vco}} = \left(\overline{F_{vt}} - \overline{F_{vhf}}\right)$ (Derived in Chapter 6, Section 6.3)

$\overline{F_{hco}} = \left(\overline{F_{ht}} - \overline{F_{hhf}}\right)$ (Derived in Chapter 6, Section 6.3)

$\overline{F_{co}} = \left(\overline{F_{vco}} + \overline{F_{hco}}\right)$ (Resultant is the vector addition of vertical and horizontal components)

$M_{co} = \left(R_a - h/2\right) * \overline{F_{co}}$ (Torque is the product of force and distance of action)

$P_{co} = M_{co} * \left(N / 9549\right)$ (Derived from the power torque equation with SI units)

Variables in the reduction equations are as follows:

$\overline{F_{vt}}$ Vertical component of 'Total' excavation force from the vertical load cell (N), obtained from experiment

$\overline{F_{ht}}$ Horizontal component of 'Total' excavation force from the vertical load cell (N), obtained from experiment

$\overline{F}_{vhf}$ Vertical component of 'Hydrodynamic friction' force from the vertical load cell (N), obtained from experiment

$\overline{F_{hhf}}$ Horizontal component of 'Hydrodynamic friction' force from the vertical load cell (N), obtained from experiment

$\overline{F_{vco}}$ Vertical component of 'Combined' excavation force (N), obtained by deducting $\overline{F}_{vhf}$ from $\overline{F_{vt}}$

$\overline{F_{hco}}$ Horizontal component of 'Combined' excavation force (N), obtained by deducting $\overline{F}_{hhf}$ from $\overline{F_{ht}}$

$\overline{F_{co}}$ 'Combined' excavation force (N), by vectorial addition of $\overline{F_{vco}}$ and $\overline{F_{hco}}$

M_{co} Torque for 'Combined' excavation force (Nm)

R_a Radius of auger (m)

h Depth of cut (m)

N Auger rpm (-)

Uncertainty in 'Combined' power calculation

'Combined' power is a function of 'Combined' torque and auger rpm.

$$P_{co} = f\left[M_{co}, N\right]$$

Uncertainty equation of the 'Combined' power is,

$$\left(\frac{UP_{co}}{P_{co}}\right)^2 = \left(\frac{UM_{co}}{M_{co}}\right)^2 + \left(\frac{UN}{N}\right)^2$$

The 'Combined' torque is a function of 'Combined' force, auger radius and depth of cut.

$$M_{co} = f\left[F_{co}, R_a, h\right]$$

The uncertainty equation for the 'Combined' torque is given by,

$$\left(\frac{UM_{co}}{M_{co}}\right)^2 = \left(\frac{UF_{co}}{F_{co}}\right)^2 + \left(\frac{UR_a}{R_a}\right)^2 + \left(\frac{Uh}{h}\right)^2$$

Uncertainty in 'Combined' force

Uncertainty in the 'Combined' force depends on the uncertainties of the a) bias error and b) precision errors of the load cells used for recording the vertical and horizontal force components signal values.

BIAS ERROR FOR THE LOAD CELL

Sources of bias error are from a) the 'Gauge factor' and 'Gauge resistance' of the strain gauges used in the load cells, b) the stabilised power supply to the load cells, c) resistors

used in the bridge and d) the digitisation of the analog signals in the data acquisition system. To measure the force components, load cells were designed, calibrated and instrumented. The strain gauges specifications were, Make: MEM (Measurements Group Inc. Raleigh, Carolina, USA; Model: CEA-06-250UW-120; Gauge resistance in Ohms at $24^0 C : 120.0 \pm 0.3\%$; Gauge Factor at $24^0 C : 2.065 \pm 0.5\%$ and Transverse sensivity at $24^0 C : (+0.4 \pm 0.2)\%$. Error values of these variables are shown below:

Table 29 Error values of variables

Symbol	Description	Error value	Unit
GF_{sg}	Gauge factor at 24^0 C	$2.065 \pm 0.3\%$	(-)
R_{sg}	Gauge resistance at 24^0 C	$120.0 \pm 0.5\%$	(Ω)
V	Stabilised supply voltage	5 ± 0.01	(V)
R	Bridge resistance	$120 \pm 2\%$	(Ω)
D	Digitisation error	5 ± 0.000076	(V)
L_{lc}	Length of load cell	0.2 ± 0.003	(m)
B_{lc}	Width of load cell	0.1 ± 0.003	(m)
t_{lc}	Thickness of load cell	0.01 ± 0.0001	(m)

ERROR IN DIGITISATION

DAQ recording voltage is 5 Volts. Taking half a step for the 16 bit AD converter, error is,

$$\frac{1}{2}\left[\left(\frac{2 * 5}{2^{16}}\right)\right] = 7.62939453 \times 10^{-5} = 0.000076$$

Hence,

$$\left(\frac{UD}{D}\right)^2 = \left(\frac{0.000076}{5}\right)^2 = 0.00000000023$$

The bias error of the load cell is,

$$\left(\frac{ULC_b}{LC_b}\right)^2 = \left(\frac{UGF_{sg}}{GF_{sg}}\right)^2 + \left(\frac{UR_{sg}}{R_{sg}}\right)^2 + \left(\frac{UV}{V}\right)^2 + \left(\frac{UR}{R}\right)^2 + \left(\frac{UL_{lc}}{L_{lc}}\right)^2 + \left(\frac{UB_{lc}}{B_{lc}}\right) + ^2\left(\frac{Ut_{lc}}{t_{lc}}\right)^2 + \left(\frac{UD}{LD}\right)^2$$

$$\left(\frac{ULC_b}{LC_b}\right)^2 = 0.003659$$

Precision error of the load cell

Precision error sources are from, a) the measured signal values during calibration and b) variation of sand density during excavation process. For uncertainty analysis in the signal values during calibration, different weights were placed at random sequence up to a total value of 3438 N. Signal values were recorded for all the individual weights. Standard deviations for limited number of samples for the signal values related to each load were calculated with the following formula (Coleman & Steele).

$$\widehat{S_r} = \left[\frac{1}{M-1} \sum_{k-1}^{M} (r_k - r)^2 \right]^{1/2} \qquad \text{Equation 32}$$

M Number of readings

r_k Individual reading

r Mean of the readings

Precision index of the mean of M tests is,

$$S_{\bar{r}} = \frac{\widehat{S_r}}{\sqrt{M}}$$

Precision limit of the M tests are,

$$p_{\bar{r}} = tS_{\bar{r}}$$

t Value from the t-distribution for a 95% confidence level.

RSS (Root-Sum-Square) value of all the precision limits was calculated, which gives the calibration error of the load cell. Precision error from the measurements of calibration for the vertical load cell is,

$$p_{\overline{rlcv}} = \pm 0.0021$$

Hence,

$$\left(\frac{ULC_{cpv}}{LC_{cpv}} \right)^2 = \left(p_{\overline{rlcv}} \right)^2 = (\pm 0.0021)^2 = 0.0000044$$

Similarly, precision error from the measurements of calibration for horizontal load cell is,

$$p_{\overline{rlcv}} = \pm 0.0023$$

and

$$\left(\frac{ULC_{ph}}{LC_{ph}}\right)^2 = \left(p_{\overline{rlch}}\right)^2 = \left(\pm 0.0023\right)^2 = 0.0000053$$

Uncertainty expression for the variation of sand density is,

$$\left(\frac{U\gamma_s}{\gamma_s}\right)^2 = \left(\frac{142}{1758}\right)^2 = \pm 0.006524$$

The propagated uncertainty due to precision error for the vertical load cell is,

$$\left(p_{lcv}\right)^2 = \left(\frac{ULC_{pv}}{LC_{pv}}\right)^2 = \left(\frac{ULC_{cpv}}{LC_{cpv}}\right)^2 + \left(\frac{U\gamma_s}{\gamma_s}\right)^2 = \left(0.0000044 + 0.006524\right) = 0.006528$$

The propagated uncertainty due to precision error for the horizontal load cell is,

$$\left(p_{lch}\right)^2 = \left(\frac{ULC_{ph}}{LC_{ph}}\right)^2 = \left(\frac{ULC_{cph}}{LC_{cph}}\right)^2 + \left(\frac{U\gamma_s}{\gamma_s}\right)^2 = \left(0.0000053 + 0.006524\right) = 0.006529$$

Uncertainty in the 'Combined' vertical force components measurements were the propagated errors, from the bias and precision errors of the vertical load cell and is given by,

$$\left(\frac{UF_{\mathrm{cov}}}{F_{\mathrm{cov}}}\right)^2 = \pm\left[\left(b_{\overline{rlc}}\right)^2 + \left(p_{\overline{rlcv}}\right)^2\right] = \pm\left[\left(0.003659\right) + \left(0.006528\right)\right] = \pm 0.010187$$

Similarly, the uncertainty in 'Combined' the horizontal force components is,

$$\left(\frac{UF_{\mathrm{co}h}}{F_{\mathrm{co}h}}\right)^2 = \pm\left[\left(b_{\overline{rlc}}\right)^2 + \left(p_{\overline{rlch}}\right)^2\right] = \pm\left[\left(0.003659\right) + \left(0.006529\right)\right] = \pm 0.010188$$

$$\left(\frac{UF_{co}}{F_{co}}\right)^2 = \left(\frac{UF_{\mathrm{cov}}}{F_{\mathrm{cov}}}\right)^2 + \left(\frac{UF_{coh}}{F_{coh}}\right)^2 = 0.020375$$

$$\left(\frac{UM_{co}}{M_{co}}\right)^2 = \left(\frac{UF_{co}}{F_{co}}\right)^2 + \left(\frac{UR_a}{R_a}\right)^2 + \left(\frac{Uh}{h}\right)^2 = \left(0.020375 + 0.000225 + 0.01148\right) = 0.03208$$

Uncertainty in vertical force is,

$$\left(\frac{UF_v}{F_v}\right) = 0.1009 = 10.09\%$$

Uncertainty in horizontal force is,

$$\left(\frac{UF_h}{F_h}\right) = 0.1009 = 10.09\%$$

F_v is in Newton.

Error in rpm

Auger rpm is a function of hydraulic flow control valve opening and the bias error of the rpm.

$$N = f(\alpha, T)$$

$$\left(\frac{UN}{N}\right)^2 = \left(\frac{U\alpha}{\alpha}\right)^2 + \left(\frac{UT}{T}\right)^2$$

Error in valve rotation $\pm 7.5^0$

Average error in valve rotation,

$$\left(\frac{U\alpha_{av}}{\alpha_{av}}\right)^2 = 0.00998$$

Tachometer: Make: 'Clas Ohlson' 'CIELO'; Model: 100 MT; Precision: ± 0.01 sec (Variation in time in 1 minute is 60 ± 0.01 sec). Average rpm of the tachometer = 1/3(40.2+25.2+11.4) = 25.6

T_b Average bias error of the tachometer= ±0.0043

$$\left(\frac{UT_b}{T_b}\right)^2 = \left(\frac{0.0043}{25.6}\right)^2 = 0.00017$$

T_p Average precision error of measurements of the tachometer= ±0.20 rpm

$$\left(\frac{UT_p}{T_p}\right)^2 = \left(\frac{0.2}{25.6}\right)^2 = 0.00006$$

$$\left(\frac{UT}{T}\right)^2 = \left(\frac{UT_b}{T_b}\right)^2 + \left(\frac{UT_p}{T_p}\right)^2 = 0.00023$$

$$\left(\frac{UN}{N}\right)^2 = \left(\frac{U\alpha}{\alpha}\right)^2 + \left(\frac{UT}{T}\right)^2 = 0.01021$$

Uncertainty in 'Soil-cutting' power

The 'Transport' power is insignificant compared to 'Soil-cutting' power. Hence, uncertainty in 'Soil-cutting' power is,

$$P_c = f[M_{co}, N]$$

$$\left(\frac{UP_c}{P_c}\right)^2 = \left(\frac{UM_{co}}{M_{co}}\right)^2 + \left(\frac{UN}{N}\right)^2 = \pm(0.03208 + 0.01021) = \pm 0.04229$$

$$\left(\frac{UP_{co}}{P_{co}}\right) = 0.2056 = 20.56\%$$

Error bars

Uncertainties are shown as error bars for vertical force, horizontal force and soil cutting power at 11 rpm, in Figure 71, Figure 72 and figure 73 respectively.

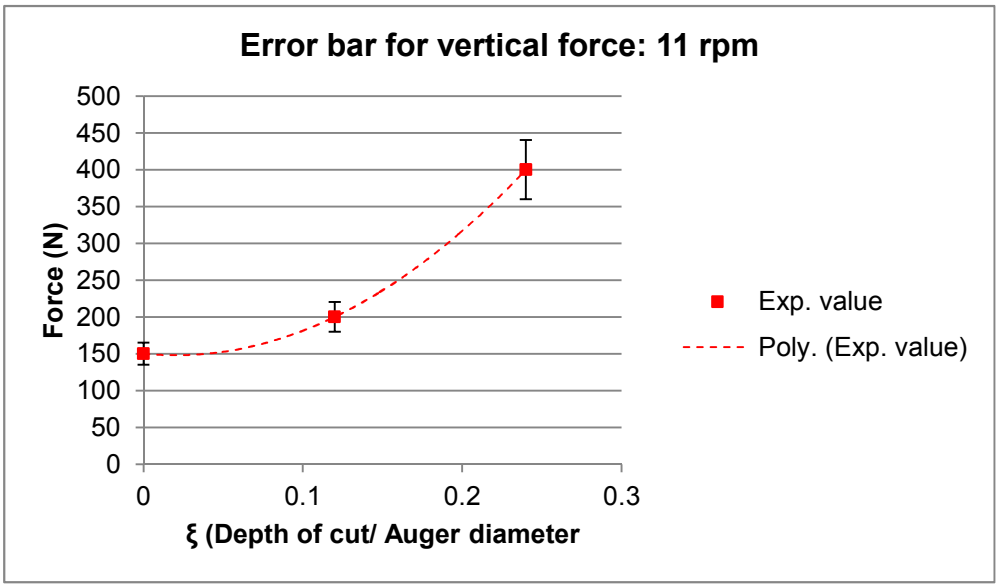

Figure 71 Error bars for vertical force: 11 rpm

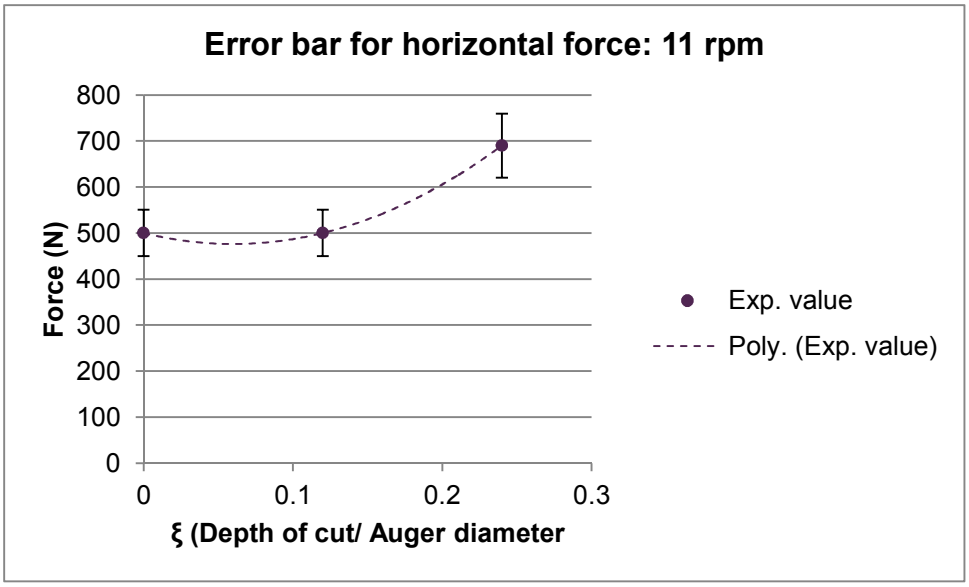

Figure 72 Error bars for horizontal force: 40 rpm

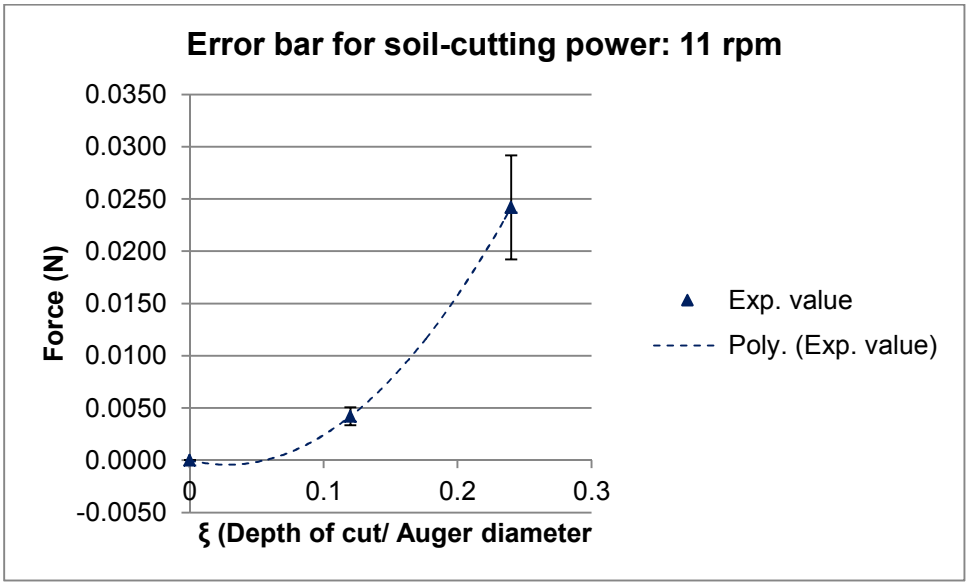

Figure 73 error bars for soil-cutting power: 11 rpm

7.5. Force components and Specific Energy

A method to predict the vertical and horizontal force components produced during dredging of sand, with known specific energy is described in this section. As described in Section 7.3, power requirement calculated from the experimental data for cutting sand, matched closely with the power requirement calculated from the specific energy of cutting sand. Hence, it can be concluded that, for practical purposes, the 'Soil-cutting' power to cut a known volume rate of particular sand can be computed from the specific energy. Sand cutting power is,

$$P_c = E_{spec} * Q_c$$

The volume rate of sand cutting depends on the auger length, depth of cut and the auger rpm. Volume rate of production per sec,

$$Q_c = \frac{\pi D_a * N * L_a * h}{60}$$

The 'Transport' power can be calculated as discussed previously.

$$P_H = c_0 * \frac{Q * \gamma_s * L_a * g}{3600} kW$$

Addition of the 'Soil-cutting' and 'Transport' powers results to the 'Combined' power.

$$P_{co} = P_c + P_H$$

The vertical and horizontal components of the 'Hydrodynamic and friction' force for an auger with a specific rpm and feed can be found from the experiment. By vectorial addition of the 'Hydrodynamic and friction' force components 'Hydrodynamic and friction' force can be obtained.

$$\overline{F_{hf}} = \overline{F_{hhf}} + \overline{F_{vhf}}$$

Assuming that the hydrodynamic friction force is acting on the auger circumference, the hydrodynamic torque is,

$$M_{hf} = \overline{F_{hf}} \bullet R_a$$

and the 'Hydrodynamic friction' power is,

$$P_{hf} = \frac{M_{hf} * N}{9549}$$

[kW = (Nm*RPM)/ 9549]

The average 'Total' power used during excavation process of dredging is obtained by adding all the above powers.

$$P_u = P_c + P_H + P_{hf}$$

The 'Total' torque, M_u and subsequently the 'Total' circumferential force, $\overline{F}_u$ acting tangentially at the effective radius can be derived from the average 'Total' power.

$$M_u = \frac{P_u * 9549}{N}(Nm)$$

$$\overline{F}_u = \frac{M_u}{\left(R_a - h/2\right)}$$

E_{spec} Specific energy of a particular sand (kW/m3)

Q_c Volume of sand cut per sec (m3)

h Depth of cut (mm)

θ_e Effective angle (Radian)

P_c 'Soil-cutting' power (kW)

P_H	Auger 'Transport' power (kW)
P_{co}	'Combined' power (kW)
P_u	'Total' power (kW)
P_{hf}	'Hydrodynamic friction power (kW)
M_u	'Total' torque (Nm)
N	Auger rpm (-)
F_u	'Total' circumferential force (N)
F_{uv}	'Total' vertical force (N)
F_{uh}	'Total' horizontal force (N)

To get the vertical and horizontal components of the total force, the orientation of the circumferential force is estimated as described below. The acting point of the circumferential reaction force varies with the angle of cutting as shown in Figure 74.

Let O_1 and O_2 be the centre of the auger at the start and finish of a cut, A_0 be the initial position on the $X-axis$, from where the angle of rotation is measured. A_1 and A_2 be the cutting point at the start and finish of cut by a cutting point of the auger. Let, θ_1 and θ_2 are the angles at the start and finish of a cut as shown.

The circumferential force provided by the auger torque acts normal to the cutter radius at that point, hence the direction of the force indicated by θ_i with the horizontal, changes with time. A normalized equation was formed from the experimental data (Table 30 and Figure 75) to find the effective angle (degree) θ_e at which the average tangential force $F_{u_{av}}$ was acting. The equation relates θ_e to ξ (depth of cut/ auger diameter) as shown below, for ξ from 0 to 0.48,

$$\theta_e = 114.2\xi^2 + 50.005\xi + 15.282 \qquad \text{Equation 33}$$

The equation to calculate the effective angle θ_e is a polynomial fit and derived from the mean values of experimental values. The equation is non-dimensional and a general one applicable to auger of any dimension.

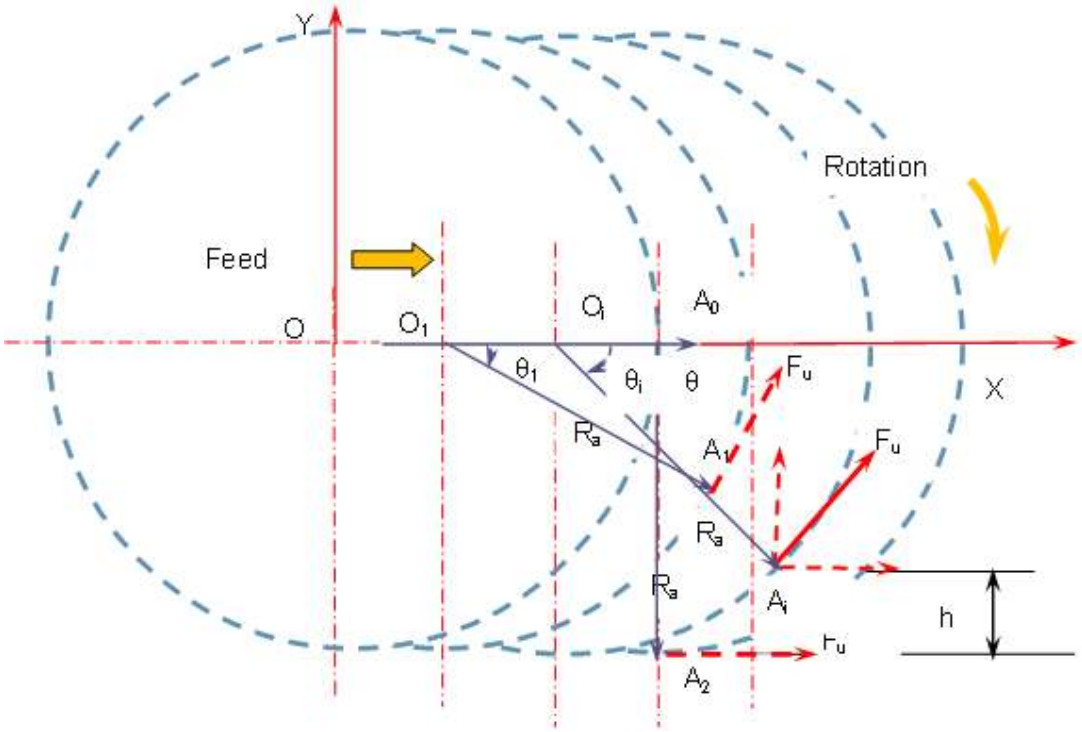

Figure 74 Circumferential force of an auger during sand cutting

Table 30 Depth of cut and Force orientation

ξ (depth of cut/ auger diameter)	0	0.12	0.24	0.48
theta (deg)	14.65	24.61	32.60	65.80

During excavation with an auger, the average circumferential reaction force $F_{u_{av}}$ acts normal to the radius R_a and at an angle θ_e with the vertical. Hence the average vertical and the horizontal force components are,

$$F_{uv} = F_u * \sin\theta_e (upward)$$ Equation 34

$$F_{uh} = F_u * \cos\theta_e (forward)$$ Equation 35

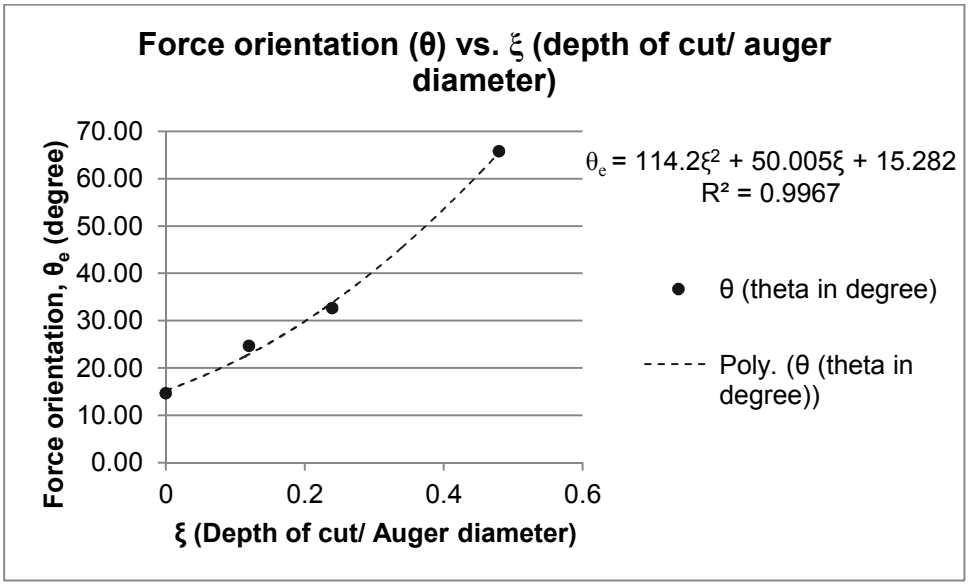

Figure 75 Depth of cut and force direction with vertical

No theoretical equation was found in the literature for comparison. This equation can be used as a basis to calculate the vertical and horizontal force components when the specific energy of the sand and the depth of cut are known. It could be refined or modified with more practical data. The steps to calculate the vertical and horizontal force components, produced during dredging sand of known *specific energy*, by an auger, are summarised below:

a) 'Soil-cutting' power for an auger, to dredge a known volume rate of sand, can be calculated from the *specific energy*
b) 'Transport' power for the auger with specific geometry can be calculated, treating the auger as a screw conveyor working under water with the modified factors of virtual casing
c) The 'Hydrodynamic and friction' power requirement of the auger, for the set conditions can be calculated from the vertical and horizontal force components data from an experiment
d) 'Total' power used by the auger during dredging can be derived by addition of all the above powers
e) The average 'Total' torque necessary for excavation, can be calculated from the total power

f) Average 'Total' force working near the circumference of the auger is calculated, assuming 'Total' force acts normal to the auger radius, at a distance of [auger shaft radius - ½(depth of cut)] from the auger axis
g) Orientation of the 'Total' force is calculated from the empirical equation
h) The 'Total' force is resolved into vertical and horizontal components.

7.6. Discussions and conclusions

Position keeping of a marginally neutrally buoyant submersible dredger / mining vehicle during dredging is largely affected by the excavation force components. In a three directional orthogonal force system, vertical and horizontal direction force components produced by an auger are important, for position keeping. Two mirror imaged halves of an auger produces equal and opposite axial forces cancelling each other, hence the axial force component was not considered.

The 'Total' force components consists of the a) 'Hydrodynamic friction' force components b) 'Transport' force components and c) 'Soil-cutting' force components. The 'Hydrodynamic friction' force components for an auger with specified rpm and feed can be found from an experiment. The 'Hydrodynamic friction' force components deducted from the 'Total' force components gives the 'Combined' force components. 'Combined' power can be calculated by vectorial addition of the 'Combined' force components. The 'Combined' power is the addition of 'Transport' power and 'Soil-cutting' power. The 'Transport' power can be calculated by considering the auger as a screw conveyor working under water with a virtual casing as discussed previously. The 'Soil-cutting' power can be calculated from the *specific energy* of sand with the known auger rpm, auger length and depth of cut. 'Soil-cutting' powers derived from the experiment and calculated from the specific energy were compared in this work for validation.

As observed from the experiments, the 'Total' forces as well as the 'Hydrodynamic friction' force vary directly with the length and diameter as well as the rpm and feed of the auger. The force will also increase with the volume rate of dredging, which varies directly with the depth of cut, auger length and rpm of the cutter. Harder materials have higher specific energy. Hence dredging harder material will produce higher force components.

In the experiment, during excavation of saturated sand, with three cutter RPM (11, 25 and 40), two cutter feed (2 and 6 m/ min) and for ξ (Depth of cut/ Cutter diameter) values varying from zero to 0.48, an upward average total vertical force from 80 to 3400 Newton were generated The backward average total horizontal forces were from 390 to 1850 Newton, produced during the same tests. The average upward vertical and backward horizontal component of 'Combined forces' (Auger 'Transport' and Soil cutting') forces were from 10 to 3200 Newton and from 30 to 1490 Newton respectively.

To find the relationship between the depth of cut and the vertical/ horizontal force components, recorded vertical/ horizontal force components (N) were plotted against h (depth of cut in mm) for the three auger rpm used in the experiment (Figure 76, Figure 77 and Figure 78).

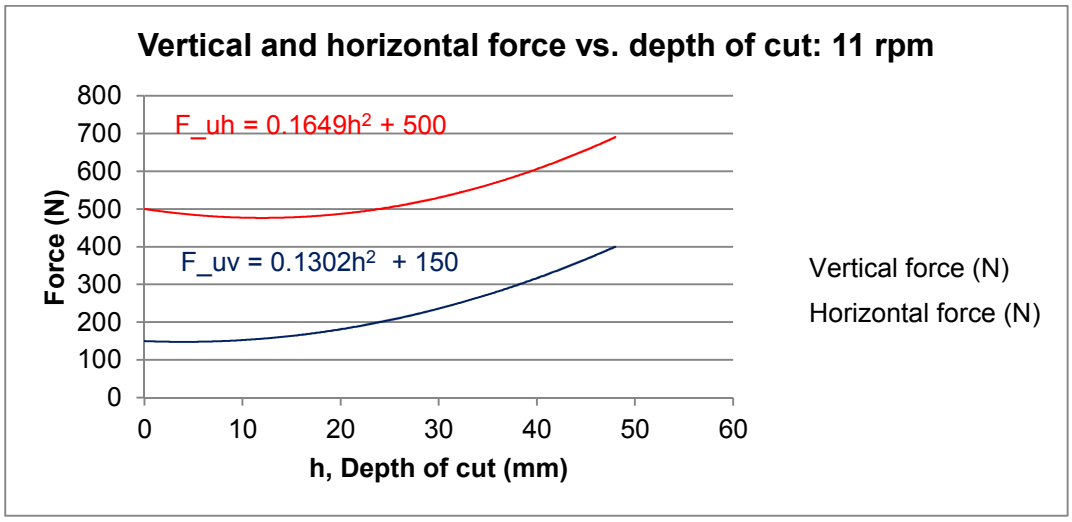

Figure 76 Force components with different depth of cut : 11rpm

Normalised equations with $R^2 = 1$ were formed from the plots. From the trend line it was observed that the force components increased with increasing depth of cut and auger rpm.

Most of the experimental values for 'Soil-cutting' power for dredging loose to slightly-compacted sand for ξ (Depth of cut/ Cutter diameter) values up to 0.25 were closely within the range of the power calculated by *Specific Energy*. Major deviations were found with all the runs when $\xi \geq 0.48$. These were due to the submergence of the auger shaft within the soil during excavation. The powers used here, did not contribute to the excavation of the soil but were mostly lost in extra friction between the auger shaft and

sand. The power requirement with a depth of cut of 96 mm (ξ = 0.48) is not a practical situation for dredging with this auger. Hence, those values were excluded in the plots of the previous chapter.

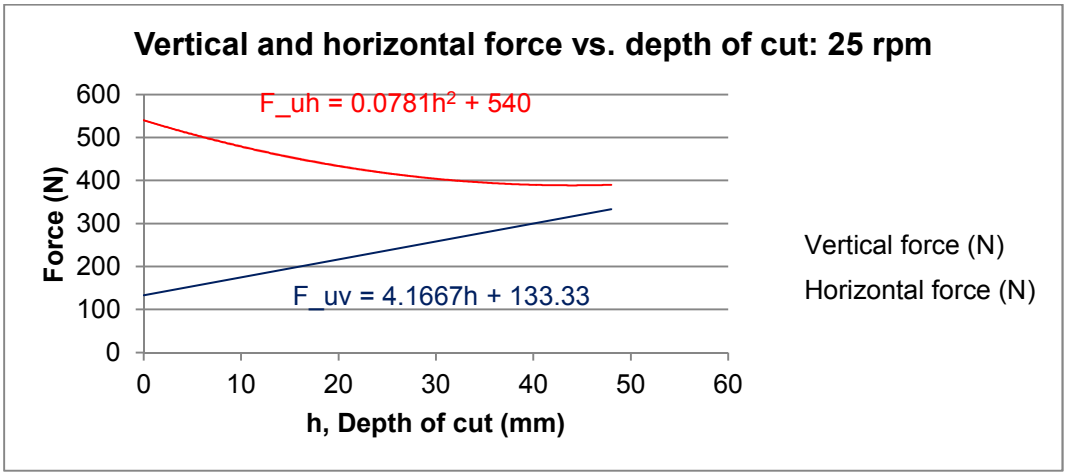

Figure 77 Force components at different depths of cut: 25 rpm

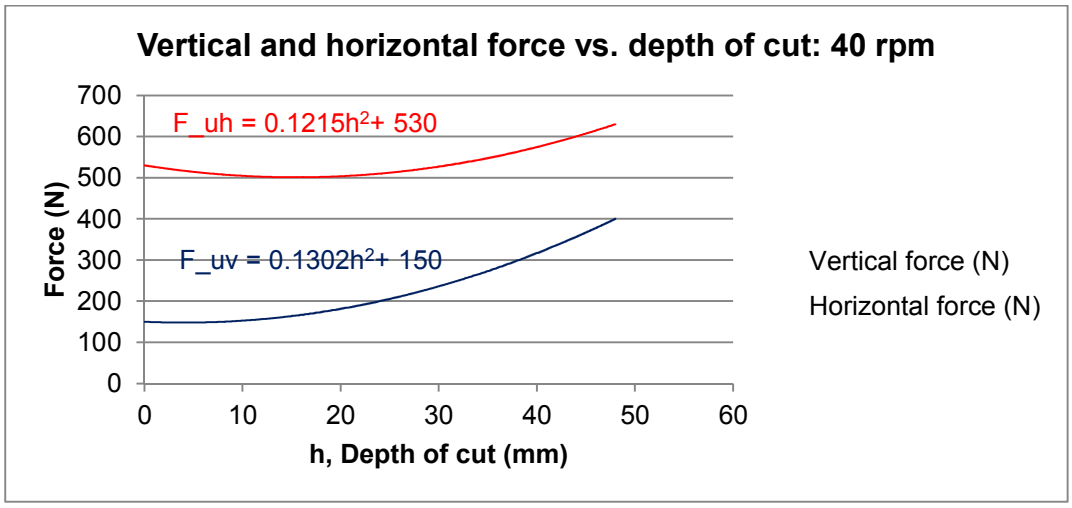

Figure 78 Force components at different depths of cut: 40 rpm

The powers increased with increasing rpm of the auger, higher ξ values (with increasing depth of cut) and increasing feed rate. The powers required at a depth of cut of 96 mm (ξ = 0.48), are shown in previous plots to have an idea about the power requirement if the auger shaft is inadvertently, submerged within the sand due to careless operation or ground undulation. In the later plots this points were excluded with a different vertical scale to show the details of the points with lower ξ values.

In actual dredging situation, shaking forces and moments originated from the transport system (pump, pipeline), locomotion and positioning systems also contribute to these vertical, horizontal and axial force components. The effect of current can be superimposed on these force components to simulate practical situations. These issues were beyond the scope of this work.

A semi-empirical model was proposed, to predict the 'Total' vertical and horizontal force components, generated by the excavation process of dredging sand of known specific energy, with an auger. Force components data calculated by the above method, is useful to design position keeping devices for neutrally buoyant submersible dredgers/ miners. Without any published literature in this area, this method can be used as a starting point to predict these force component values for other similar or different sized cutters without doing experiments every time.

Further research is necessary to extend the method to different types of materials, various shapes and sizes of transverse-axis cutters and to correlate feed with the vertical and horizontal force components.

CHAPTER 8 ENVIRONMENTAL IMPACTS OF SUBMERSIBLE DREDGING

8.1. Introduction

Operation of a machine interferes with the environment and its operation affects the environment. Impacts of operation of the submersible dredger/miner on the environment are described in this chapter. The underwater environment is very complex and potentially sensitive. Dredging has significant possibility to impact the environment and it is important that we develop simple measures to assess environmental effects. Turbidity can be used as an indicator of environmental impact. In this experiment, turbidity generated by an auger during dredging within a test tank was measured at various locations, to assess the environmental impact of dredging with the auger fitted with the SROSD.

8.2. Environmental disturbances by dredging

Environmental disturbances produced by dredging process, depends on its sub-processes, which are, a) excavation, b) gathering and mixing, c) transport and d) disposal. The dredging machine during operation affects both the *biotic* and *abiotic* components of the surrounding environment with the above sub-processes. In the following picture, various living creatures including snails are visible around the sampling robotic hand, dredging in a subsea environment. (Figure 79: Reproduced with permission from Nautilus Minerals Inc.).

Figure 79 Sampling in a subsea environment

Gathering of the soil to the suction mouth and mixing of the soil with water, as well as excavation could physically injure the biotic population, be responsible for turbidity generation, release the locked in harmful elements from the sediment and generate sound and vibration. In the transport system there can be leakages of slurry from the pump and the pipeline and the inherent vibrations are present. Disposal of dredged material are equally harmful to the environment as the excavation process. The potential oil leakage from the different systems in the dredger is also significant and may prove detrimental to the environment. Activities of dredging disturbing the environment are populated in Table 31.

Table 31 Disturbances produced on environment by dredging

Activity Disturbance	Excavation	Transport	Disposal
Mechanical shock	YES	YES	YES
Vibration	YES	YES	YES
Noise	YES	YES	YES
Contamination: oil leak	YES	NO	NO
Turbidity	YES	YES	YES
Gas & chemical release	YES	NO	YES
Temperature rise	YES	NO	NO
Pressure variation	YES	YES	NO

8.3. Environmental Effect of dredging

Many countries including Australia and India have significant ocean bed resources. Deposits such as sea-floor massive sulphide (SMS) deposits, manganese nodules, high technology elements like lithium, diamonds and sea floor muds are all of interest to dredging industries (Giurco et al. 2009). Exploration of these resources requires subsea dredging and potential mining activities. During underwater dredging and mining operations, most of the cutting devices result in spillage from the cutter and suction configurations. The sea-floor including the mineral-rich sites, support various communities of life (Drew 2000). The environmental impacts of dredging can be severe, causing change and often degradation in habitat for both pelagic and benthic (Lindeman & Snyder 1999). The fragmented loose solids are re-suspended during dredging or mining, increasing the total suspended solid (TSS) in water making the water unclear. This non-clarity of water is known as turbidity (IADC 2007). All aquatic habitats are susceptible to fluctuations in turbidity. Increased turbidity adversely affects the environment and the existence and growth of flora and fauna. With increased turbidity natural light is blocked that impacts all

aspects of an organism's life cycle. Significant reduced light penetration reduces photosynthesis and day-time oxygen release into the water. The dredging cutters, implements and suction can cause injuries to the organism, which may lead to greater susceptibility to disease. While dredging causes an increase in turbidity levels it can also release metals and other contaminants into the water column. These may be components of ore or legacy deposits lying at the bottom of water beds that are released during dredging (EPA 2012; Queensland Government 2012; Walker et al.1997). A recent report on the increase in turbidity levels in the Port of Gladstone, Australia (Gooch 2012), emphasizes the importance of minimizing environment disturbances during dredging operations. Increase of turbidity from the initial condition can be transported by density current or settle down in favourable conditions. Even in inland dredging environments, an increase of turbidity associated with dredging, can be a health hazard to the community using the water. It was observed by (Schwartz & Goldstein 2000) that increased turbidity is directly linked to increased gastrointestinal illness for elderly people. From the above discussions, it is apparent that 'Turbidity' produced during dredging or subsea mining can be a suitable indicator for assessing the environmental impact.

During project implementation, turbidity levels must be carefully checked. Before undertaking any dredging or subsea mining project, normally, three variables are usually considered. They are, a) the nature of the sea, lake or river bed (inclusive of the soil and rock) in the area to be dredged, b) the nature of the surface water in and around the area to be dredged and c) the dredging technique and type of dredger to be used inclusive of loosening, gathering, mixing, transport and disposal.

8.4. Dredging Regulations

Before forty years, environmentalists and people from the maritime industry thought about the protection of the sea environment from pollutions made by man,. The 'Convention on the Prevention of Maritime Pollution by Dumping of Wastes and Other Matter, 1972' or popularly known as the 'London Convention' was the first important international convention to protect the sea from man-made (anthropogenic) pollutions. .

Impact of dredging on the environment was realised at that time. Dredging of contaminated sediments from the port of Rotterdam and disposal by encapsulation, (Gandrass & Salomons 2001) shows the concerns about the impact of dredging and

disposal on the environment. Environmental considerations for dredging both for inland and offshore conditions are discussed in great detail in the publications of International Association of Dredging Companies and Central Dredging Association, (IADC & CEDA 1996 to 2001) and later edited by Bray (2008).

The 'London Convention' was updated in 1996 to 'London Protocol' and enacted into force in 2006 for the international maritime community. All dumping in the sea is prohibited under this protocol except the acceptable waste shown in the 'reverse list'. They are, a) dredged material; b) sewage sludge; c) fish wastes; d) vessels and platforms; e) inert, inorganic geological material (e.g. mining wastes); f) organic materials of natural origin; g) bulky items primarily comprising of iron, steel and concrete; and carbon dioxide streams from carbon dioxide capture processes for sequestration (Department of Sustainability 1981).

Action lists and action levels are codified for sea disposal of dredged material in the 'Guidance for the Development of Action Lists and Action Levels for Dredged Materials' adopted in 2008. Other important International Maritime Conventions relevant to pollution control for dredging activities are:

a) 'International Convention for the Prevention of Pollution from Ships 1973' later modified in 1977 and 1978 (known jointly as MARPOL)
b) 'International Convention on the Control of Harmful Anti-fouling Systems on Ships (AFS)' adopted in 2008
c) The pending 'International Convention for the Control and Management of Ships' Ballast Water and Sediments' (BWM Convention).

Among the regional programs the followings are noteworthy:

a) 'United Nations Environment Programme' (UNEP) launched in 1974
b) 'Arctic Region' (www.pame.is)
c) 'Antarctic Region' (CCAMLR, www.ccamlr.org)
d) 'OSPAR Commission' representing the European Union and others.

Except the UNEP all these conventions aim towards pollution control in local and regional ways. Dredging activities for various purposes are increasing; however, as evidenced from the above references, the environmental program related to dredging is still area- specific.

A picture of the existing scenario about remediation of contaminated dredged material is discussed by Spadaro (2011).

Australia follows formal sediment management framework and regulations (Department of Sustainability 1981). To assess the integrated social and environmental effect of mining under water, CSIRO are doing research and organizing workshops with stakeholders (Parr et al. 2009).

Dredging or subsea mining increase the existing turbidity level and in many countries it is now essential to conduct an Environmental Impact Assessment (EIA) before the execution of a dredging project. Natural turbidity fluctuations at the prospective dredging site should be assessed beforehand, as part of an environmental baseline study.

Environmental benchmarks for subsea mining have not been clearly defined (IADC 2006) and the environmental sustainability of ocean mining has been poorly studied. Public policies related to environmental impact assessment for subsea dredging and mining are still country-based and inadequate (IADC 1997, 2006). Many countries are formulating their own policies regarding environmental issues related to dredging.

EIA information related to dredging projects was published by the International Association of Dredging Companies (IADC 2006). Statutory regulations about subsea mining and dredging are in their infancy and vary from country to country.

The ambitious Marine Strategy Framework Directive (MSFD) (adopted in June 2008) aims to protect the marine environment across Europe. The Directive requires Member States to prepare national strategies to manage their seas to achieve or maintain Good Environmental Status (GES) by 2020, and to protect the resource base upon which marine related economic and social activities depend. To implement issues related to dredging under MSFD, CEDA formed the Marine Strategy Navigation Group (MSNG) consisting of the following members:

CEDA - Central Dredging Association, EBA - European Boating Association, EBI - European Boating Industry, ECSA - European Community Ship-owners Association, EuDA- European Dredging Association (Corresponding Member), ESPO - European Seaports Organisation, ICOMEA - International Council of Marine Industry Associations, ISU - International Salvage Union and PIANC - International Navigation Association.

Without a unified international standard, there are conceivable conflicts between the EU directives and the international conventions (Mink et al. 2006). For example, the European Commission argued that the dredged material is a waste, whereas, the EuDA feels it as a natural resource. Other directives, in particular the 'Habitats and Birds Directives' is a concern to many dredging people. The specifications require a long project time with strict rules for disposal and long-time monitoring, which may lead to delays, project cost increase and even cancellation of project (Gooch 2012). Due to the difference of opinions, dredging activities are delayed. Accepting that the dredging activities are essential for development, reconciliations are happening. An example is a compromise wording for a new Waste Framework Directive (WFD) which excluded dredged material from the Directive's jurisdiction made in the European Parliament in June 2008. As a result about 90% of all materials dredged in Europe were eliminated from the category of 'waste'. Now, only the hazardous materials are within the 'waste' category. A new hi-tech, environmentally sound approach of "flexible disposal" has been undertaken in a project located on the maritime border of Belgium and the Netherlands (IADC 2012).

8.5. Assessment of turbidity in the test environment

Turbidity is postulated to be a suitable indicator to predict the environmental impact from dredging on the subsea environment. Turbidity generated within a test tank, during dredging loose to slightly-compacted sand, by the auger used in the tests, at set values of auger rpm, feed rate and (depth of cut/cutter diameter) ratio, were monitored by sensors and 'Secchi discs'. 'Secchi disc' is a disc alternately painted white and black on its surface. The pattern is distinguishable at fixed depth of water, depending on the turbidity of water. This experiment was conducted to determine the increase of turbidity at different positions with respect to the auger and generate data to assess the environmental impact.

8.5.1. Sensor and calibration

Two types of sensors were used, which are, a) a OBS3+ turbidity sensor manufactured and calibrated by Campbell Scientific Inc., designed on the principle of light scattering, which was re-calibrated with a synthesized 'Formazin' solution at different NTU (Nephelometric Turbidity Unit) values (Figure 80) and b) 'Secchi disc' made in house by EEM. Re-calibration data of the OBS3+ turbidity sensor (in volt) with the synthesized 'Formazin' are shown in Table 32.and Figure 81. For measuring nominal turbidity by Secchi disc Table 33 was

followed (Myre et al. 2006). In this table the depth of water at which the Secchi disc pattern is vanished is shown against NTU.

Table 32 Calibration & recalibration curves of turbidity sensor OBS3+

NTU	10	50	500	1000
RC_16NOV	0.055	0.077	0.271	0.430
RC_27NOV	0.048	0.066	0.299	0.509

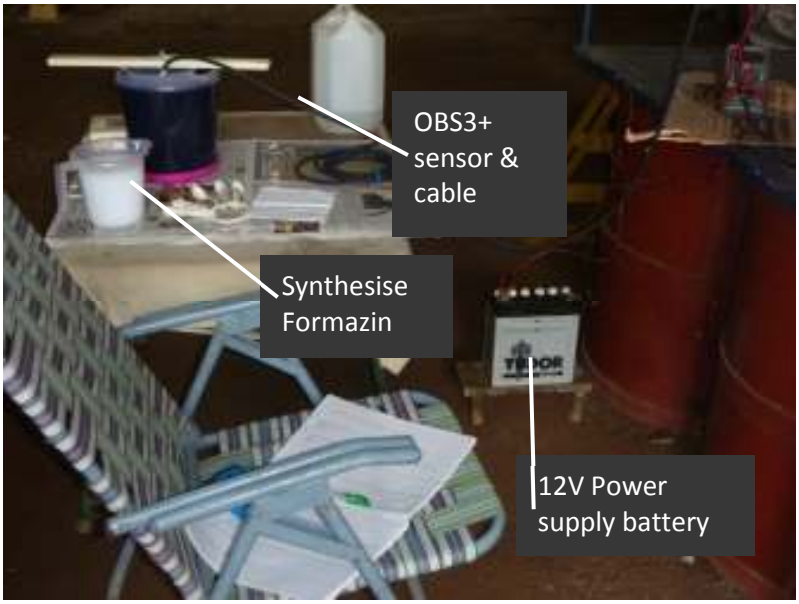

Figure 80 Calibration of OBS3+ with synthesised Formazin

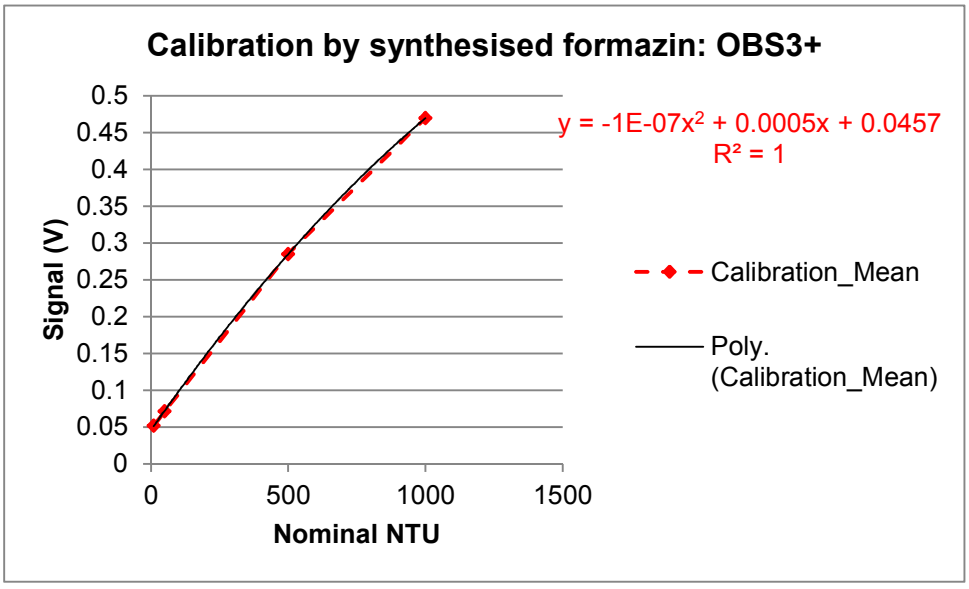

Figure 81 Plots of recalibration of turbidity sensor OBS3+

Table 33 Depth to turbidity conversion for 'Secchi disc'

Depth in centimetres	Turbidity (NTU)
6.7	240
7.3	200
8.9	150
11.5	100
17.9	50
20.4	40
25.5	30
33.1	21
35.6	19
38.2	17
40.7	15
43.3	14
45.8	13
48.3	12
50.9	11
53.4	10
85.4	5

8.5.2. Test procedure and turbidity sensing

Using the test set up described in Chapter 6, turbidity was observed at different positions with reference to a shrouded auger. The data were analysed to ascertain the in-field turbidity levels around the auger as well as at some chosen locations in the test tank during dredging. All the tests were done with the OBS3+ sensor placed serially at different locations (positions 1 to 6) within the test tank as shown in Figure 82. Locations are indicated as small circles and numbered for clarity. All measurements are given in millimetres. Insert illustrates the relationship between the sensor and the cutter.

The probe was fixed with the cutter for positions 1 to 4 and moved with the cutter. It was fixed in the tank at positions 5 and 6. The cutter was rotated at 40 rpm at a feed rate of 6 m/ min and with a depth of cut of 100 mm (ξ=0.5). All these working parameters were the highest values, possible in the test set up, assumed to represent maximum turbidity. Six separate 'Secchi disc' measurements were taken simultaneously, at the start positions from 1 to 4 and at positions 5 and 6 just before and after dredging.

With the start of the computer and the DAQ system the recording cycle started for a test run. After the start of the recording cycle, the OBS3+ sensor was kept in the fixed position for some time and the initial average turbidity was recorded, before starting the auger driving motor, feed hydraulic cylinder and the dredge pump motor. The auger drive hydraulic motor was started first. After the signal was stable (as the auger was rotating at the same position without feed and without suction of the dredge pump), the feed

hydraulic cylinder and the dredge pumps were started simultaneously. Time of feed is the actual dredging. After the dredging, the feed hydraulic cylinder, the auger drive motor and the dredge pump were stopped together. The signal was recorded till it comes down near the initial value.

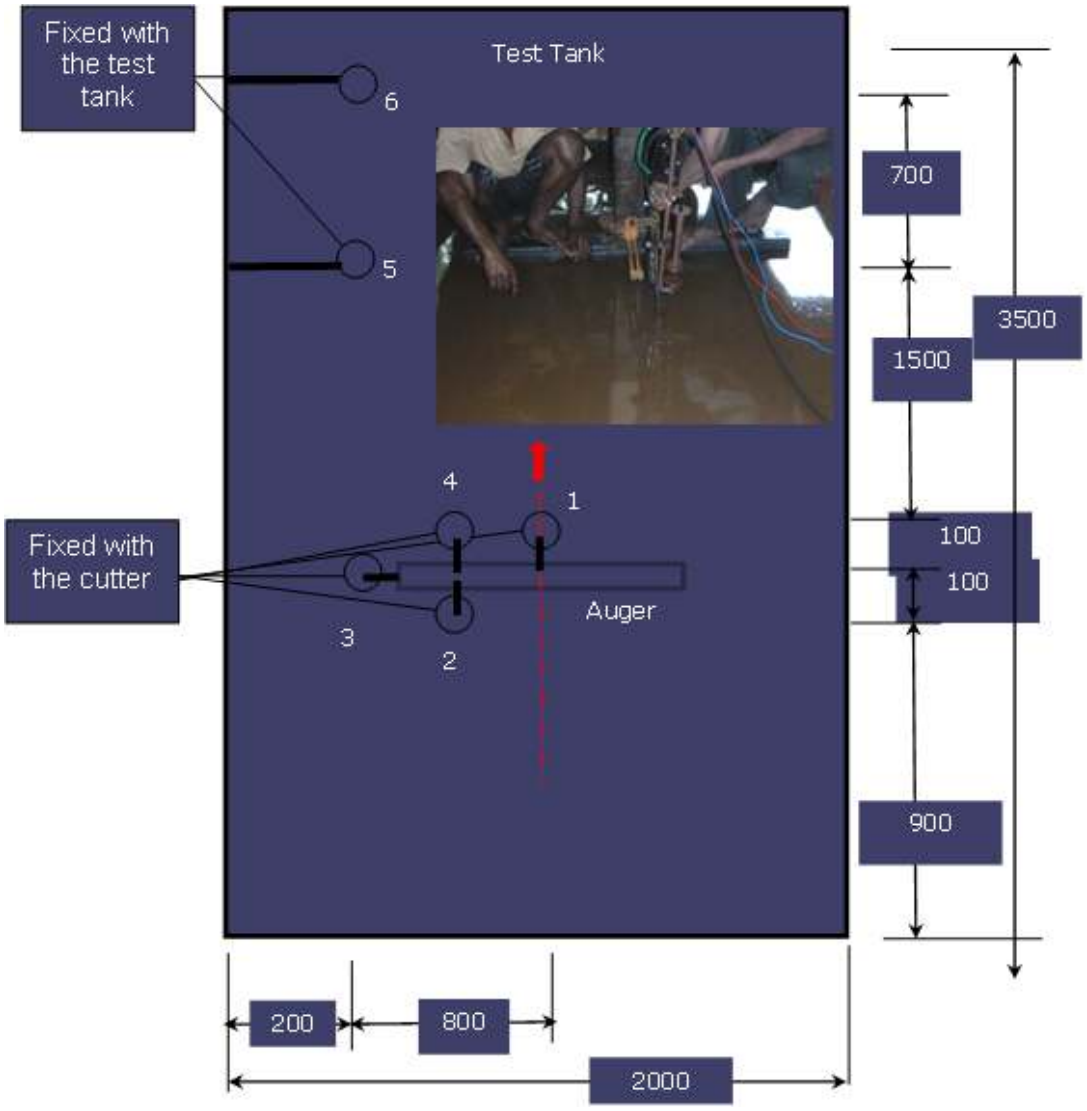

Figure 82 OBS3+ sensor locations for turbidity measurements

8.5.3. Analysis of data

Plots of nominal turbidity values in NTU, with respect to time for positions 1 to 6 are shown in Figure 83, Figure 84, Figure 85, Figure 86, Figure 87 and Figure 88. To have an idea, about the relationship between the sequential activities and generated turbidity,

activities are shown by points in the plots, for positions 1, 2 and 3 (Figure 83, Figure 84 and Figure 85). Start of auger motor is shown by point 'A', start of dredging (both feed and pumping) by point 'B', stop of dredging by point 'C' and the final nominal average turbidity calculations are taken from point 'D' onwards, in the plots. The complete cycle of run is shown in all the plots. The initial value of turbidity is the mean of the values before the start of the auger motor. During the dredging (when the auger motor was running, feed was given to the auger and the dredge pump was running), there is a maximum and an average value of turbidity. After stop of dredging and stabilisation the mean of the turbidity values yields to the final value of turbidity.

The variations in shape of the plots in Figure 83, Figure 84, Figure 85, Figure 86, Figure 87 and Figure 88 were partly due to the difference in start-up time of the cutter for each experimental run. Shape difference is also attributed to position in the experimental set up.

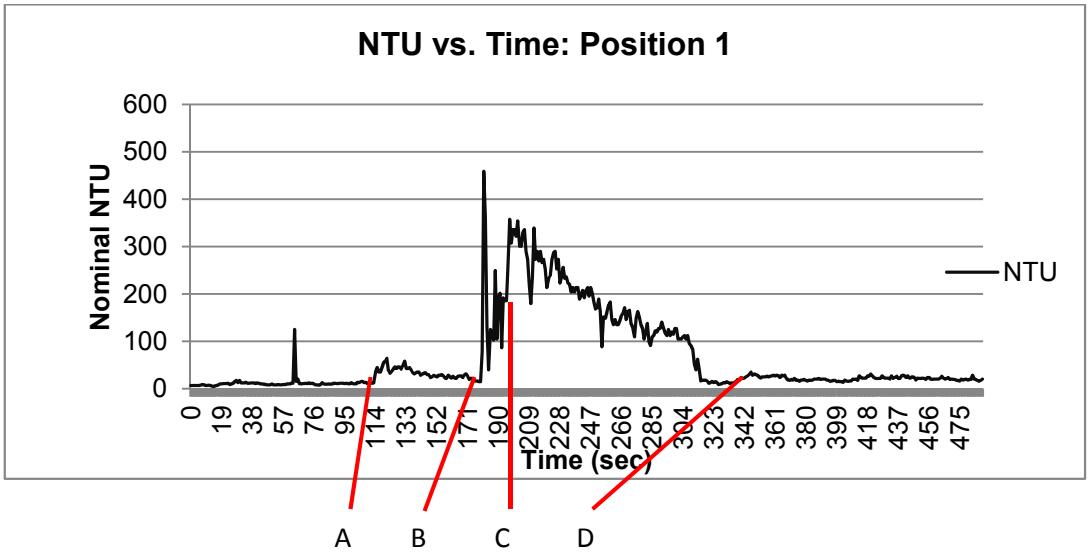

Figure 83 NTU values: Position 1

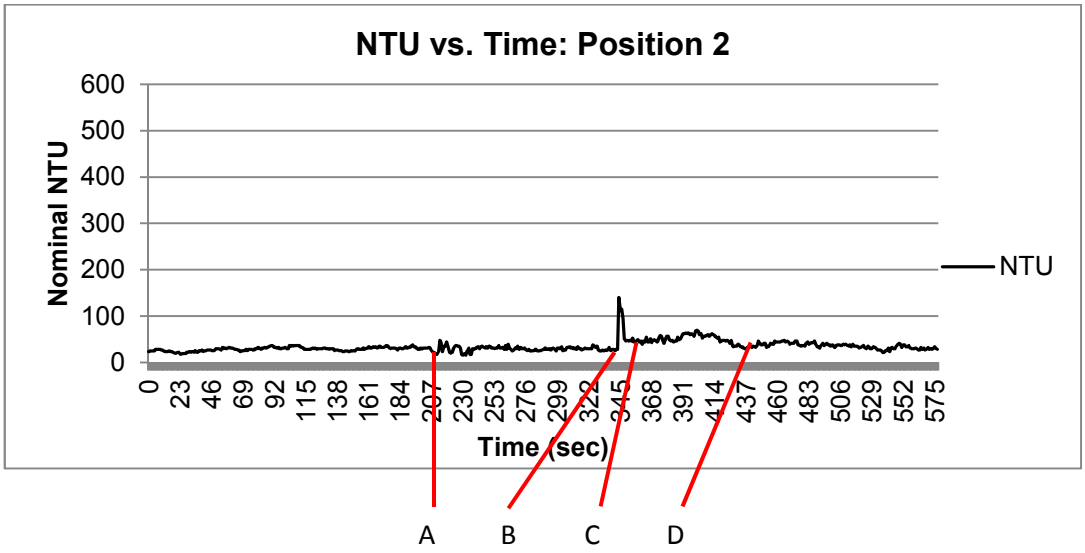

Figure 84 NTU values: Position 2

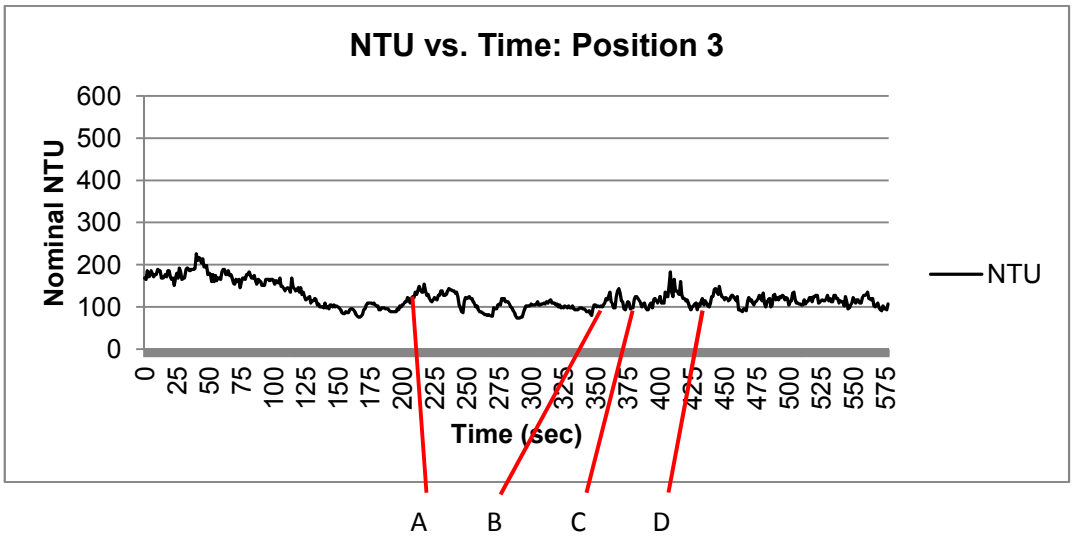

Figure 85 NTU values: Position 3

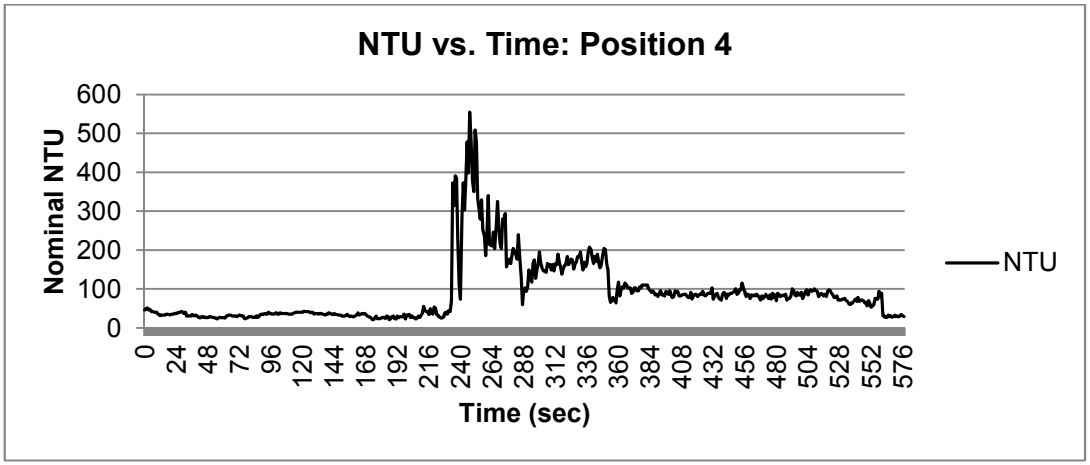

Figure 86 NTU values: Position 4

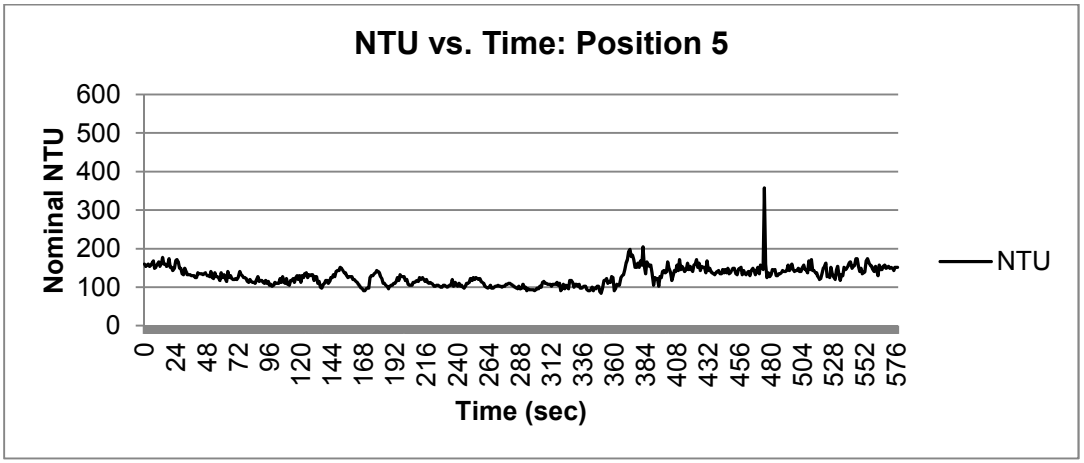

Figure 87 NTU values: Position 5

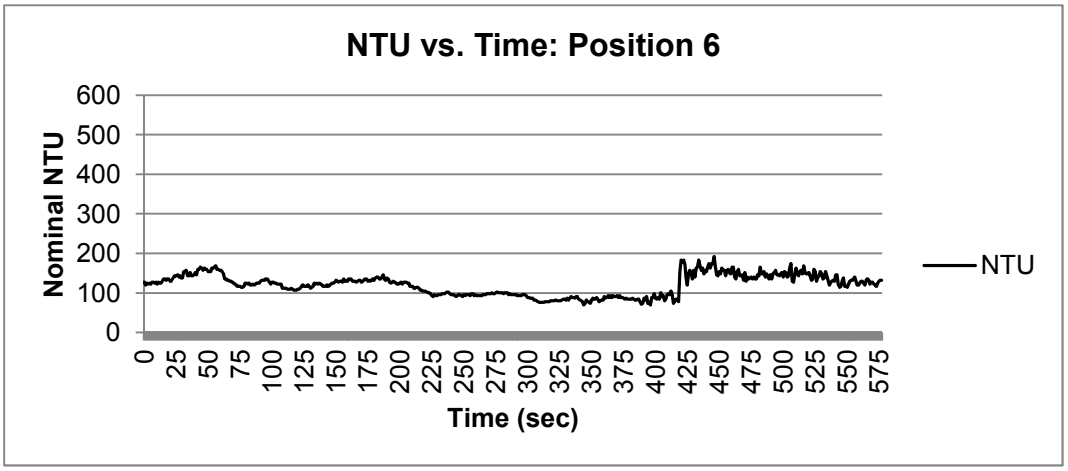

Figure 88 NTU values: Position 6

The salient observations were tabulated in Table 34. The table shows the initial average turbidity, Final average turbidity, maximum turbidity, average turbidity during dredging and settling time required after dredging to come down near to the initial average turbidity with respect to a position.

For position 3 (Figure 85), the initial value is high and there is a low value after the start of the auger motor and before dredging starts. This was attributed to the reflective waves from the side of the tank; however, the cutter motor was started after stabilization. The cause of sudden peak in Figure 87 is not exactly known, hence neglected in the calculations.

As observed from the Table 34, there were alternate values of low and high turbidity values, for positions 3, 5 and 6 shown as (a), (b) and (c) in the remarks column of the Table. These were attributed to the swirling about water due to reflection, from the sides of the test tank. These alternate high and low values of turbidity in positions 3, 5 and 6 showed a very slow rate of attenuation. Initial, average, final and maximum values of nominal turbidity at different positions related to auger and tank are shown in Figure 89. The average nominal turbidity values in NTU against time are plotted in Figure 90 to show the fluctuations of turbidity at position 5.

Table 34 Summary of turbidity generated by the auger during dredging

	Initial av. turbidity	Final av. turbidity	Max. turbidity	Av. Turbidity during excavation	Settling time	Remarks
Position 1	19	21	459	188	125	
Position 2	29	36	140	54	87	
Position 3	177		226	105		(a)
Position 4	33	30	554	131	326	
Position 5	117		177	144		(b)
Position 6	129		174	117	220	(c)

8.5.4. Error level in measurement

Turbidity is not a directly measurable quantity. The NTU values indicate nominal values depending on a standard testing condition, material in suspension, type of data acquisition system, type of Light Dependent Resistor (LDR), scattering or absorption of light and other conditions. The OBS3+ sensor was recalibrated twice and the calculated error level (standard deviation) was approximately ±2%. The mean of the two readings

was taken and the equation was taken as the standard, which aligns well with the calibration curve of the manufacturer. For the 'Secchi disc', minimum measurement possible was ±3 mm. Hence the error level was approximately ±5%.

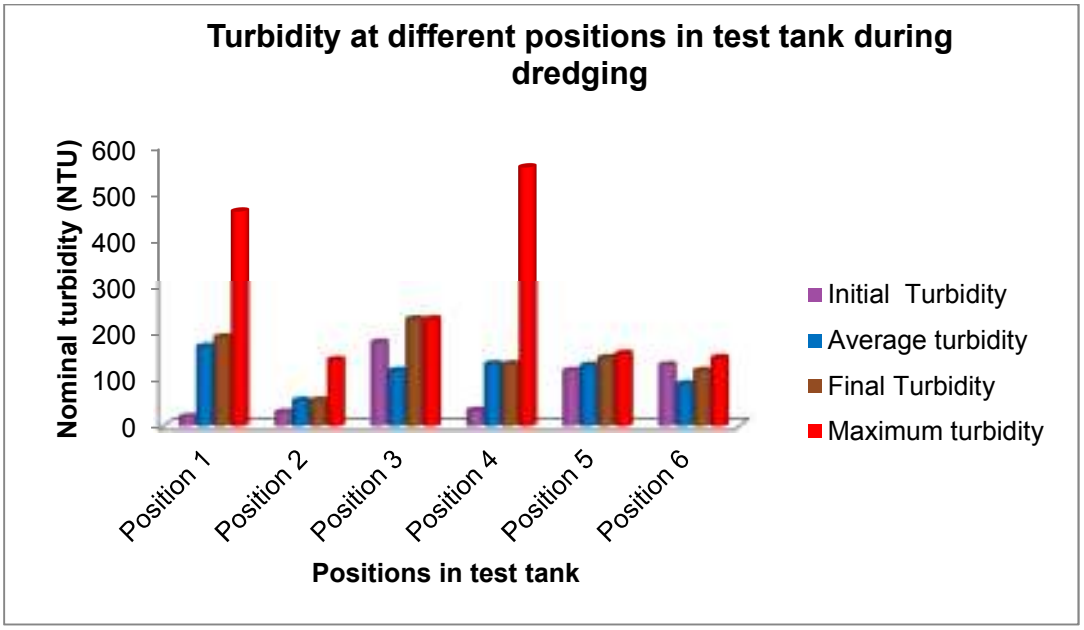

Figure 89 Initial, average, final and maximum values of turbidity at different positions

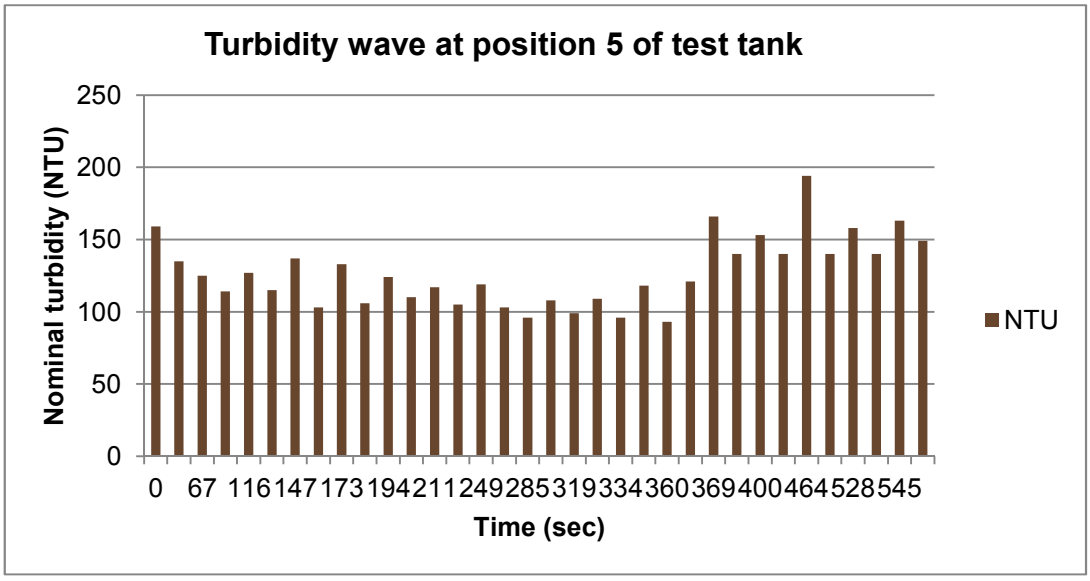

Figure 90 Nominal turbidity with respect to time for position 5 in test tank

8.6. Discussions & Conclusions

The global economy insists on more demands that are fulfilled by exploiting new natural resources, which disturb a particular eco-system. On the contrary environmentalists are more concerned about the protection and maintenance of the existing ecological system either in a local or in global perspective. It is true that any machine activity and intervention affects the dynamic environment. The convergence of these two opposite perception is difficult but necessary. Dredging or mining in the inland underwater and subsea conditions would create disturbances in the underwater environment. Suitable, sustainable and unified methods for subsea dredging or mining are to be developed to keep the environmental disturbances to a minimum. Relevant environmental parameters, as well as the impact of operation of the machine on the environment were discussed in this chapter. A test tank used for excavation force components measurements was also used to measure turbidity in the near and far-field of an auger. Analyses were done for the different positions in the test tank about the increase of the nominal average turbidity increase.

Position 1 is at the front and centre of the auger. Here the suction effect is at its maximum. Sands are also transported and delivered by the two halves of the auger. Assuming, suction capacity of the dredge pump and the transported and delivered sand rate are equal, then the turbidity level is constant at this position. It is assumed that there is enough water available at the suction mouth, to form slurry. If the material delivery rate is higher than the suction capacity, then there is spillage of the excess material resulting in increased turbidity. On the contrary, if suction capacity is higher, the turbidity level comes down. In a practical situation, it was found that an equilibrium position is seldom reached and there is fluctuation of the turbidity level.

Position 2 is at the back of the auger and almost at the centre. Due to the shroud of the auger the turbidity level did not show any significant variation. The influence of the shroud is significant.

Position 3 was at the side of the auger outside the shroud on the opposite side to that of the auger drive motor. Minor turbidity level variations were observed, which are due to less effective suction power in this region and intermittent cutting actions of the auger blades.

Position 4 is in front of the auger halfway from the auger end to auger centre. The turbidity level during excavation is highest here. It is significantly higher than the position 1, which is at the centre of the cutter and materials from both sides are thrown to that position. This is due to less effective suction and more excavated and transported material than at any other position.

The distance of position 5 and position 6, from the dredging zone was reduced gradually with advancement of the auger. There was a time lag in these positions for the increase of turbidity level after excavation was started. Disturbances were generated, with the forward movement of the auger along with the guide and slider. These swirling were reflected by the tank front and back walls which produces alternate high and low values of turbidity.

With the modular design, the vehicle is supposed to work with different materials generating different type of turbidity flumes. Apart from turbidity level increase by excavation, improper suction mouth design can increase the turbidity level in the dredging area. Leakage from the pumps and transport system and locomotion and movement of actuators are also responsible for increasing turbidity. Acceptable turbidity levels are different for different locations depending on the biotic and abiotic components of the micro-ecological system in question. In a particular location, an intelligent design of the suction mouth and shroud over the cutter, enclosed transport system and low disturbance level due to smaller size of the vehicle, would be an eco- friendly option for dredging.

From the above discussions it can be concluded that:

a) Turbidity can be an indicator to assess environmental impact during submersible dredging or mining
b) The shroud is effective to control turbidity dispersions and there is possible scope for better shroud design,
c) The increase in turbidity is greater in the front of the auger than the sides (more than 3 times),
d) Maximum turbidity was observed halfway between the side and centre of the auger,
e) Turbidity may be generated due to obstacles in the near field as observed in positions 5 and 6 due to swirling and turbulence caused by the movement of water.

More research is necessary to predict the turbidity flume generation for, a) different types of materials, b) augers with different geometries and c) different rpm, feed and depth of cut for an auger.

CHAPTER 9 CONCLUSIONS, LIMITATIONS AND RECOMMENDATIONS

9.1. Conclusions

Dredging at greater depths is required to facilitate increased resource acquisition and construction of infrastructures, where diver assisted dredging equipment and surface floating dredger capacities are limited. Available submersible dredgers with tracks or legs are constrained by their slow speed and inability to negotiate steep slopes. For subsea mining and dredging of hard materials, more power for cutters is required, which obviously produces huge forces. For efficient dredging or mining, these forces are to be counter-balanced to keep vehicle and the cutter in the desired position and trajectory.

To overcome the limitations of existing equipment, a conceptual design for a new type of submersible remotely operated swimming dredger (SROSD) was presented in this research. This dredger can dredge in ground-contact condition, when counterbalancing the excavation forces by vector thrusters, anchored spuds, Variable Buoyancy Tanks and even with drag control surfaces as necessary. Thrusters and the spuds can be used as dual functional devices. The thrusters can be utilized for excavation force balance as well as, for the normal function of propulsion for free swimming vehicles. Spuds can be used for excavation force equilibrium as well as for locomotion during working.

A transverse axis auger is an effective excavating tool for dredging on a vehicle of this type. It is capable of dredging thin slices (surgical cutting) of material required for mining with minimum spillage, minimum dilution and minimal environmental disturbance. The contra-directional mirror-image halves of the auger vane cancel the axial forces generated during excavation and make it easier to control the vehicle during dredging.

A test setup was designed, fabricated and instrumented by the author, to investigate the excavation force components produced and turbidity generated by a transverse-axis full scale cutter during dredging. This setup was significant in the following ways:

a) The mechanism of the generation of cutting forces by an axial cutter was explored. This experiment was done to investigate about the excavating reaction force components generated, as a function of cutter rpm, feed rate and depth of cut, during dredging loose to slightly compacted sand by an auger. No such published literature was found for transverse axis augers either

for surface floating or submersible dredgers. Vertical and horizontal directions of the excavation force components were recorded in the experiment for counterbalancing the generated excavation forces. The two halves of the auger cutting edge geometry from the centre are a mirror image of each other. The generated axial force components in the two halves cancel each other, hence they were neglected.

b) In previous research done with axial cutters, cutter positioning was done through a linkage system, joined to the carriage by a pinned joint. In this experiment, a transverse-axis auger cutter attached to the carriage through a sliding link was used.

c) In the former research, strain gauges were fixed to the cutting edges/ points of a cutter working under water, to measure the cutting forces, making them difficult to maintain or replace. In this experiment, the strain gauges were fixed to the de-mountable load cells designed built and calibrated in-house, which were placed above water. The load cells can be easily replaced either for repair or for changed requirement.

d) The strain gauged force transducers give the vertical and horizontal force components explicitly. Whereas, those mounted on blades do not. In the latter case it is very difficult to get overall loads acting along the 'X' and 'Y' axes.

Instead of a scaled model, a full-scale actual inland dredging auger was used in the experiment. The vertical and horizontal force components generated during dredging loose to slightly compacted sand, were measured by two load cells, data processed by a data acquisition system and recorded in a micro-computer.

Data were gathered for three different rotational speeds of the auger, three different depths of cut and two different feeds of the auger. In general, cutter force components were found to increase linearly for practical purposes with rpm for rates of rotation between 11 and 40 per minute

Possibilities of counterbalancing the excavating forces by vector thrusters were also discussed. With the commercially available thrusters at present, the above vertical and horizontal excavation force components can be easily balanced. When the volume rate of excavation is more or the dredging material is harder (with higher specific energy), then thrusters with higher thrust would be required. Thruster balancing is limited by the

maximum capacity of available thrusters at present, which is approximately 11,000 N (SMD 2012).

A theoretical model based on the auger geometry was developed to predict the excavation forces generated by the auger in two orthogonal directions during dredging of loose to slightly compacted sand as a function of cutter rpm, feed and depth of cut.

Validation of the experimental data was done by comparing the semi-empirical power derived from experiment and the power calculated empirically from the specific energy of loose to slightly compacted sand. The average experimental power for dredging loose sand was approximately 1.5 times the calculated power based on specific energy.

$$P_{e_{ls}} = 1.5 * P_{se_{ls}}$$

Equation 36

For dredging slightly packed sand, the average experimental power was half the power requirement based on specific energy.

$$P_{e_{scs}} = 0.5 * P_{se_{scs}}$$

Equation 37

$P_{e_{ls}}$ Power requirement calculated from experiment for loose sand

$P_{se_{ls}}$ Power requirement calculated from specific energy for loose sand

$P_{e_{scs}}$ Power requirement calculated from experiment for slightly-compacted sand

$P_{se_{scs}}$ Power requirement calculated from specific energy for slightly-compacted sand.

From the above equations, power requirement for a transverse axis auger cutter can be predicted, provided the specific energy of the sand is known.

Attachments were designed and built for fixing a turbidity sensor (OBS3+) at six different positions. Three positions moved with the cutter and the other three positions were fixed with the tank. A shroud covering the back, two sides and the top was designed and built to reduce dispersion of the turbidity flume during dredging.

Maximum turbidity increase was observed in front of the auger at a distance of one-fourth of the auger length from its both ends. This was due to lesser suction force than the

centre and more material dredged at this location than at the end. The centre of the auger showed the second highest turbidity, where the suction was maximum. The minimum turbidity at the back of the cutter showed the effectiveness of the shroud. The position at the side of the auger outside the shroud showed less turbidity increase than the front two positions but more than the position at the back. The sensor was attached to the moving auger at these positions. The other two positions were fixed near the tank side ahead of the cutter. One was almost at the tank end and the other quarter-way from the end. These positions showed alternate high and low values of turbidity by the swirling of water produced by the movement of the auger and water reflected by the side walls of the tank.

9.1.1. Possible application of the conceptual design

The possible application and advantages of the conceptual design are:

a) The Submersible Remotely Operated Swimming Dredger (SROSD) conceptual design is shown to be viable and is postulated to be a quick moving device appropriate for subsea dredging.

b) The excavation forces during dredging of sand by an auger could be counterbalanced by vector thrusters, and if required by means of other devices such as anchoring spuds, Variable Buoyancy Tank (VBT) and control planes.

c) For mining and dredging hard materials an auger is expected to be more suitable than an axial cutter, as for the form of an auger, the excavation forces are more even than an axial cutter and controlled surgical cuts (dredging in thin layers) with minimum dispersion of loosened materials are possible.

d) The vector thrusters are used for propulsion and control during swimming and as counterbalancing devices during dredging.

e) During dredging or locomotion in ground-contact condition, the forward spuds fitted with the forward wing tips can be rotated anti-clockwise from the initial position to an angle less than 90^0 and embedded into the ground by means of hydraulic cylinders. Further anti-clockwise rotation of the forward spuds with the wing tips can move the vehicle forward. Lifting the spuds out of the ground and rotation of the spuds in the clockwise direction and pushing them again to the ground would start the second step of walking. The rear spring-loaded spud when embedded would follow the motion of the front spuds and would be vertical with the help of the spring when lifted up. The spuds also counterbalance the excavation forces and during locomotion and dredging.

f) If the excavation rate and dredging material properties demands forces higher than the counteracting forces provided by vector thrusters and the anchored spuds, the Variable Buoyancy Tank (VBT) and the control planes can be used as secondary position keeping devices .

9.1.2. Main findings

To summarise the findings of this work:

a) As a result of this work, a method was found to estimate the excavation reaction force components, provided the geometry of the auger, excavation production rate and the specific energy of the dredging material are known. Hence, it can be concluded that, for practical purposes, the 'Soil-cutting' power to cut a known volume rate of particular sand can be computed from the specific energy.

b) The method used to calculate the vertical and horizontal force components are narrated in section 7.5 and briefly described below. 'Soil-cutting' power is $P_c = E_{spec} * Q_c$ where the specific energy of sand is E_{spec} and the volume rate of production per sec is Q_c. The empirical 'Transport' power is P_H kW. The 'Combined' power $P_{co} = P_c + P_H$. Vectorial addition of the vertical and horizontal components of the 'Hydrodynamic and friction' force $\overline{F_{vhf}}$ and $\overline{F_{hhf}}$ (found from experiment) gives the 'Hydrodynamic and friction' force, $\overline{F_{hf}} = \overline{F_{hhf}} + \overline{F_{vhf}}$. The 'Hydrodynamic friction' torque M_{hf} and power P_{hf} are calculated for the auger having a radius of R_a and rotating at N rpm. The average 'Total' power P_u used during excavation process of dredging is, $P_u = P_c + P_H + P_{hf}$. The 'Total' torque M_u is calculated and the 'Total' circumferential force is derived as, $\overline{F}_u = \dfrac{M_u}{\left(R_a - h/2\right)}$. The effective angle of orientation of the 'Total' circumferential force with the vertical is $\theta_e = 114.2\xi^2 + 50.005\xi + 15.282$ and the vertical and horizontal force components are, $F_{uv} = F_u * \sin\theta_e$ and $F_{uh} = F_u * \cos\theta_e$ respectively.

c) With the screw conveying system, transverse axis rotation, controlled depth of cut and environmental shroud, the auger is found to be an effective eco-friendly tool.

9.2. Limitations

The experiment was done with one type of material, i.e. loose to slightly compacted sand and with a single geometry of the auger. Effect of size and shape of the dredging material were not included in this research. Effect of auger pitch to auger diameter and the auger length to auger diameter were out of scope of the work. Compaction of the material could not be closely controlled. Hence relationship between compaction and the excavation reaction force components were out of scope. No actual operating data was available for such category of vehicle. Hence, comparison with actual operating data was not possible.

9.3. Recommendations for future work

Recommendations for future work can be outlined as,

a) Further experiments on excavation reaction force components for different variations of the granular, cohesive soils and rocks could be undertaken.
b) Steady state nature of turbidity experiments can be done.
c) For precision of the experimental data, longer test tank with winch feed mechanism could be adopted in future.
d) Shaking forces and moments for pumps, pipelines, actuators were not undertaken in this experiment. Investigations of the impacts of these forces and moments along with the input of environmental forces (e.g. current) for more severe conditions on position keeping of the vehicle could be done.
e) Effect of positional and orientation variations of vector thruster, spuds, Variable Buoyancy Tanks on position keeping of the vehicle could be investigated.
f) For remote control and operation of the vehicle quick decision making is necessary. It is possible by comparing any actual subsea working environment with a known global database of subsea environment. Hence, creation of a standard subsea environment global database, useful for dredging or mining is necessary.

g) In dredging and mining the spoils are removed and the water is returned to the surrounding area. How turbid is this water and is this a major contributor to the generation of turbidity in the region? Should the returning water be filtered and if so, how is this done?

h) An actual model of the conceptual design can be fabricated and tested for future data generation.

References

Abelev, A. V. Valent, P. J. & Holland, K. T. 2007, 'Behavior of a Large Cylinder in Free-Fall Through Water ', *Oceanic Engineering, IEEE,* vol. 32, no. 1, pp. 10-20.

Adrian, E. 1999, 'Deep Dredging Equipment for Mega – size Hopper Dredgers', *Proceedings of the CEDA Dredging days 1999*, Amsterdam, the Netherlands.

ADVANTECH 2010, 'ADAMView, Sl. 4233232863, Computer program, Milpitas, CA, <www.advantech.com/products/ADAMview/>.

Alvarez Grima, M. 2011, 'Deep Sea Mining With an Archimedes Screw Driven Vehicle', *Proceedings of the OMAE2011, 30th International conference on Ocean, Offshore an Arctic Engineering*. Rotterdam, The Netherlands, pp. 1-8.

Anderson, E. P. 1969, *Electronic Circuits,* 3rd. Indian edition, D. P. Taraporevala Sons & Co. Ltd. Bombay.

Bachmayer, R. Whitcomb, L. & Grosenbaugh, M. 2000, 'An accurate four-quadrant non- linear dynamic model for marine thrusters-Theory and experimental validation ', *Journal of Oceanic Engineering, IEEE*, pp. 146-159.

Barnes, G. 2000, *Soil Mechanics Principles and Practice,* Second edn, Macmillan Press Ltd., London.

Bindt, A. 1994, 'Quantitative & Qualitative Research on the Snow Plough Effect in Water Saturated Sand', in, Report no. 94.3.GV.4336, Delft University of Technology, Delft, the Netherlands.

Bose, N. 1985, 'A simple DC strain gauge, amplifier and torque transducer circuit', Report no. NAOE-85-51, Naval Architecture and Ocean Engineering, University of Glasgow, Glasgow.

Bose, N. 2008, *Marine Powering Prediction and Propulsor*, The Society of Naval Architects and Marine Engineers, Jersey City, New Jersey.

Boskalis, O. 2000, *White Rose project glory hole excavation*, accessed 23 November, <www.boskalis.com/.../Projecten/.../Canada >.

Brandner, P. 1998, 'An experimental investigation between two closely spaced azimuthing thrusters', in, Launceston, Tasmania, p. 82, AMECRC reports: C - 98/ 2 - C 00/12.

Bray, R. N. 2008, *Environmental Aspects of Dredging*, Taylor and Francis, London, UK.

Burcher, R. & Rydill, L. 1998, *Concepts in submarine design,* Reprint 1998 edn, Cambridge University Press, Melbourne 3166.

Carlos III University, M. E. 2010, 'Screw Conveyor', in, Mechanical Engineering Department, Carlos III University, Madrid.

CEDA, Environment Commission Working Group 2011, 'Underwater sound in relation to dredging', *Terra et Aqua,* vol. 125, no. December 2011, p. 6.

CEMA (ed.) 2009, *Screw conveyors for bulk materials, Conveyor equipment manufacturers' association book no. 350,* Conveyor Equipment Manufacturers Association, Naples, Florida, USA.

Coleman, H. W. & Steele, W. G. 1989, *Experimentation and uncertainty analysis for engineers*, Wiley Interscience, John Wiley & Sons, NewYork.

Craig, R. F. 1992, *Soil Mechanics,* Fifth edition edn, Chapman & Hall, London.

Cross, N. 2000, *Design Methods, Strategies for Product Design* John Wiley & Sons Ltd., West Sussex, England.

Dally, J. & Riley, W. 1973, *Experimental stress analysis,* International student edition edn, McGraw-Hill Kogakusa.

Damen 2010, *Product Ranges, Mussel Dredger*, accessed 28 June 2010, <http://www.damen.nl/PRODUCTS/mussel_dredgers.aspx?mId=8625>.

Dekker, M. A. Kruyt, N. P. Den Burger, M. Vlasblom, W. J. 2003, Experimental and numerical investigation of cutter head dredging flows, *Journal of Waterway Port Coastal and Ocean Engineering*, vol. 129, Issue 5, pp. 203-209.

Department of Sustainability, E. W. P. a. C. 1981, *Sea Dumping*, Canberra, Australia, accessed 13 May 2011, <http://www.environment.gov.au/coasts/pollution/dumping/index.html>.

Desa, E. 1999, 'Opportunities for offshore mineral exploration in the Indian Ocean', *Proceedings of the 3rd. ISOPE Ocean Mining Symposium, ISOPE,* 8-11 November 1999, Goa, India.

DeWijs, B. 2000, 'AUV/ ROV propulsion thrusters', *Proceedings of the OCEANS 2000 MTS/IEEE*, 06 August 2002, Providence, RI.

Drew, L. 2000 'The promise and peril of seafloor mining', *Oceanus Magazine,* vol. 47.

ECOR, Engineering Committee for Oceanic Researches 2011, 'MARUM crawler',Conveyed by e-mail by N. Bose to M. K. Sarkar on 11 June 2011.

EDF, Environmental Defense Fund 2009, *Global warming*, accessed 13 November 2009<http://www.edf.org/page.cfm?tagID=65>.

Editors Trade & Technical Press (ed.) 1989, *Hydraulic Handbook,* Trade & Technical Press Ltd., Surrey, England.

Endicott, L. 2001, *Fast track construction of the airport platformat Chek Lap Kok through geotechnical/ civil engineering planning and design*, books.google.co.in, accessed 23 November 2009, <http://books.google.co.in/books?id=75sZNS7cOe4C&pg=PA303&lpg=PA303&dq=Lap+Kok+airport+dredging&source >.

EPA, USA. 2012, 'Contaminated Sediments Program - Great Lakes Monitoring ', in, ed. U. S. E. P. Agency, U.S. Environmental Protection Agency, Great Lakes National Program Office, 77 W. Jackson Boulevard (G-17J), Chicago, IL 60604-3511 Chikago, accessed on 19 May 2012 <http://www.epa.gov/greatlakes/contact.html>.

Evans, J. & Nahon, M. 2004, 'Dynamics modelling and performance evaluation of an autonomous underwater vehicle', *Ocean Engineering,* vol. 31, pp. 1835-1858.

Faltinsen, O. 2003, *Sea loads on ships and offshore structures*, Cambridge University Press.

Fichter, G. 1978, 'The Future Sea', in, Sterling Pub. Co., NewYork.

Figliola, R. & Beasley, D. 1995, *Theory and design of mechanical measurements,* Second edition edn, John Wiely & Sons Inc., New York.

Fossen, T. & Ross, A. 1994, *Guidance and control of ocean vehicles*, Wiley, New York.

Fossen, T. & Ross, A. 2002, *Marine control systems : guidance, navigation and control of ships, rigs and underwater vehicles* Marine Cybernetics, Trondheim, Norway.

Gandrass, J. & Salomons, W. 2001, 'Dredged Material in the Port of Rotterdam – Interface between Rhine Catchment Area and North Sea', in, GKSS Research Centre, Institute for Coastal Research, Geesthacht, accessed on 19 May 2012, <www.sednet.org/.../Part_A_Executive_summary_and_introduction_http://w3g.gkss.de/i_a/dredged_material/index.html>.

Garg, S. 2010, *soil mechanics and foundation engineering,* 7th edn, Khanna Publishers, New Delhi.

Giurco, D. Prior, T. Mudd, G. Mason, L. & Behrisch, J. 2009, ' Peak minerals in Australia: a review of changing impacts and benefits ', in, Institute for Sustainable Futures (University of Technology, Sydney) and Department of Civil Engineering (Monash University), March 2010.

Goldewijk, K. 2001, 'Estimating global land use change over the past 300 years', in *Global Biogeochemical Cycles 2001*, pp. 417-434.

Gooch, N. 2012, 'Gladstone dredging resumes'*, Lloyd's List Australia,* 9 february 2012, p. 2.

Hanson, T. Johnson, H. P. & Young, D. F. 1966, 'Dynamic shearing resistance of soils'*, Proceedings of the Winter Meeting of the American Society of Agricultural Engineers*, Chikago.

Hatamura, Y. & Chijiiwa, K. 1975, 'Analyses of the mechanism of soil cutting 1st report', *Bulletin of the JSME,* vol. 18, no. 120.

Hatamura, Y. & Chijiiwa, K. 1976a, 'Analyses of the mechanism of soil cutting 2nd report', *Bulletin of the JSME,* vol. 19, no. 131.

Hatamura, Y. & Chijiiwa, K. 1976b, 'Analyses of the mechanism of soil cutting 3rd report', *Bulletin of the JSME,* vol. 19, no. 139.

Hatamura, Y. & Chijiiwa, K. 1976, 'Analysis of the mechanism of soil cutting', *Bulletin of The JSME,* vol. 19, no. 137, p. 9.

Hatamura, Y. & Chijiiwa, K. 1977a, 'Analyses of the mechanism of soil cutting 4th report', *Bulletin of the JSME,* vol. 20, no. 139.

Hatamura, Y. & Chijiiwa, K. 1977b, 'Analyses of the mechanism of soil cutting 5th report', *Bulletin of the JSME,* vol. 20, no. 141.

He, J. Miedema, S. A. & Vlasblom, W. J. 2005, 'FEM Analyses Of Cutting Of Anisotropic Densely Compacted and Saturated Sand'*, Proceedings of the WEDAXXV & TAMU37*, June 2005, New Orleans, USA.

Henriksen, J. 2009, 'Investigation of turbulance characteristics for modelcutter suction dredging operation', *PIANC,* vol. March 2009, no. 1.

Herbich, J. B. (ed.) 1992, *Handbook of dredging Engineering,* McGraw-Hill Inc., NewYork.

Herbich, J. B. & Lou, Y. K. 1975, 'Stable Catamaran Hulls for Cutterhead Dredges', *Proceedings of the Offshore Technology Conference*, 5-8 May 1975, Houston, Texas.

Hettiaratchi, D. R. P. 1965, *The present state of the theory of soil cutting,* PhD thesis, The University of Newcastle upon Tyne, Newcastle upon Tyne, England.

Hettiaratchi, D. R. P. & Reece, A. R. 1967, 'Symmetrical Three-Dimensional Soil Failure', *Journal Terramechanics,* vol. 4 (3) pp. 45-67.

Hettiaratchi, D. R. P. Witney, B. D. & Reece, A. R. 1966, 'The calculation of passive pressure in two dimensional soil failure', *Journal Agricultural. Engineering,* vol. 11 (2), p. 19.

Hettiaratchi, D. R. P. & Reece, A. R. 1974, 'The calculation of passive soil resistance', *Geotechnique,* vol. 24, no. September, pp. 289-310.

Hettiaratchi, D. R. P. & Reece, A. R. 1975, 'Boundary wedges in two-dimensional passive soil failure', *Geotechnique,* vol. 25, no. 2, pp. 197-220.

Hisao, T. Sadayosi, Y. 1999, 'Dredging robot "No.2 Futaba"', *Workvessel,* vol. 246 no. 1999, pp. 4-11.

Hoagland, P. Beaulieu, S. Tivey, M. A. Eggert, R. German, C. Glowka, L. & Lin, J. 2010, ' Deep-sea mining of seafloor massive sulphides', *Marine Policy,* vol. 34.

Hofstra, C. Hemmen van, S. A. Miedema, S. & Hulsteyn van, J. 2000, 'Describing the position of backhoe dredge buckets', *Texas A & M 32 nd. Annual dredging seminar,* 25-28 June 2000, Warwick, Rhode Island.

Hope, K. G. 2000, 'Marine propellers & computer methods for small vessels', in, I. MarE & RINA, Sydney, NSW.

Humphreys, D. 1976, 'Development of the equations and transfer functions for underwater vehicles', in, NCSL, Panama City, Florida, Document no. 287-76, pp. 1-27.

IADC 2006, 'Environmental Law on Dredging ', *Terra et Aqua,* vol. Number 104

IADC 2007, 'Facts about Turbidity - Information update', *Terra et Aqua,* vol. 2, p. 4.

IADC 2012, 'Selecting a destination for dredged material', in *Tera et aqua - Information update*, Number 1 - 2012, International Association for Dredging Companies, The Netherlands.

IADC, (ed.) 1997, *Conventions, Codes, and Conditions: Land Disposal,* IADC, The Hague, The Netherlands.

IHC 2011, 'Piling with a pencil', in *Ports and Dredging*, Spring 2011, IHC Merwede, The Hague, Netherlands, p. 4.

IWMI 2009, *General Brochure*, accessed 13 November 2009,< http://www.iwmi.cgiar.org/Publications/Other/index.aspx>.

Jackson, E. Clarke, D 2007, 'Subsea Excavation of Seafloor Massive Sulphides', *Proceedings of the OCEANS 2007*, Sept. 29 -Oct. 4 2007 Vancouver, BC.

Joanknecht, L. W. F. 1974, 'Cutting Forces in Submerged Soils', in, Technische Hogeschool Delft, Delft, the Netherlands.

Joanknecht, L. W. F. 1975, 'Results of Tests on Two Cutterheads operating in Sand', *Proceedings of the First Inernational Symposium Dredging Technology*, Canterbury, England.

Joanknecht, L. W. F. 1976 'A Review of Dredge Cutterhead Modelling and Performance', *Proceedings of the WODCON VII*, San Francisco.

Jones, D. A. Clarke, D. B. Brayshaw, I. B. Barillon, J. L. Anderson, B. A. 2000, 'The calculation of hydrodynamic coefficients for underwater vehicles', Report no.AMECRC IR 00/ 37, AMRL, Launceston.

Kermode, A. 1963, 'Mechanics of Flight', in, Seventh Edition edn, Sir Issac Pitman & Sons Ltd., Bath, UK.

Kurimoto 1994, 'Kurimoto high efficiency sand dredging system©', *Proceedings of the AAPH'94*, 20-22 September 1994 Regent Hotel, Kuala Lumpur, Malaysia.

KWS 2008, *Design Engineering Manufacturing*, accessed 29 July 2010, C:\AMC_UTAS\Knowledge\Integrated\Excavation\Auger\Important\Important_Screw Conveyor Engineering Guide - Horsepower Calculation.mht.

Leer van, J. 2000, *Small Catamaran Research Vessels*, accessed 09 July 2010, <http://www.unols.org/publications/manuals/SBCompendium/12SmCat.pdf>.

Lindeman, K. C. & Snyder, D. B. 1999, 'Nearshore hardbottom fishes of southeast Florida and effects of habitat burial caused by dredging', *Fishery Bulletin [Fish. Bull.],* vol. Vol. 97, no. no. 3, Jul pp. 508-525.

Lunne, T. Robrtson, P. K. 1997, *Cone penetration testing in geotechnical practice* Blackie Academic & Professional, London EC4P 4EE, books.google.com

Luth, H. J. Wismer, R. D. 1969, 'Performance of plane soil cutting blades in sand', *Proceedings of the Annual Meeting of the American Society of Agricultural Engineers*, Purdue University, Lafayette, Indiana, June 1969, pp. 255-262.

Ma, Y. N., F & Miedema, S. A. 2006, 'Calculation of the Blade Cutting Force for small Cutting Angles based on MATLAB', *Proceedings of the The 2nd China Dredging Association International Conference & Exhibition, themed 'Dredging and Sustainable Development'*, May 17-18 2006, Guangzhou, China.

Matsuo, T. & Ishii, K 2007, 'Neural Oscillator Based Motion Control System for Snake-like Robot', *Proceedings of the Underater Technology and Workshop on Scientific use of Submarine Cables and Related Technologies, 2007*, Tokyo.

McKyes, E. & Ali, O. S. 1977, 'The cutting of soil by narrow blades', *Journal of Terramechanics,* vol. 14, no. 2, pp. 43-58.

Mero, J. 1964, *The Mineral Resources of the Sea*, google Books, accessed 13 November 2009, <http://books.google.co.in/books?id=LbTDLa_2opsC&dq=Mero,+John.+L.+The+mineral+resources+of+the+sea&printsec=frontcover&source=bl&ots=cbFZJsFBD0&sig=tccJAQ87poC9xlG8qp6wlzHbQ8w&hl=en&ei=idX8SuD3DIqBkQWKqO34Cw&sa=X&oi=book_result&ct=result&resnum=1&ved=0CAgQ6AEwAA#v=onepage&q=&f=false>.

Miedema, S. 1985a, 'Derivation of the differential equation for sand pore pressures', *Dredging & Port Construction*, no. September 1985, p. 1.

Miedema, S. 1985b, 'Mathematical modelling of the cutting of densely compacted sand under water', *Dredging & Port Construction*, no. July, p. 4.

Miedema, S. 1987, *The Calculation of the Cutting Forces when Cutting Water Saturated Sand, Basic Theory and Applications for 3-Dimensional Blade Movements with Periodically Varying Velocities in Dredging for Usual Excavating Elements',* PhD thesis, Delft University of Technology, Delft, the Netherlands.

Miedema, S. 1989, 'On the Cutting Forces in Saturated Sand of a Seagoing Cutter Suction Dredger', *Terra et Aqua,* vol. 41, no. December, p. 10.

Miedema, S. 1994, 'On the Snow-Plough Effect when Cutting Water Saturated Sand with Inclined Straight Blades'*, Proceedings of the ASCE Proc. Dredging 94* Orlando, Florida, USA, November 1994.

Miedema, S. 2000, Calculation of the Cutting Forces when Cutting Water Saturated Sand-Basic Theory and Applications for 3-Dimensional Blade Movements, unpublished Class Notes of MSc in Dredging Technology, 2000.

Miedema, S. 2009, 'New Developments Of Cutting Theories With Respect To Dredging, The Cutting Of Clay And Rock'*, Proceedings of the WEDA XXIX & Texas A&M 40*, June 14-17 2009, Phoenix Arizona, USA.

Miedema, S. 2010a, 'The influence of the strain rate on cutting processes'*, Proceedings of the ISOPE 2010*, June 2010, Beijing China.

Miedema, S. 2010b, 'New developments of cutting theories with respect to offshore applications, the cutting of sand, clay and rock'*, Proceedings of the ISOPE 2010*, June 2010, Beijing China.

Miedema, S., Lu, Z & Matousek, V 2003, 'Numerical Simulation of the development of density waves in a long pipeline and the dynamic system behaviour', *Tera et Aqua,* Number 93, issue- 04, p. 13.

Miedema, S. Frijters, D. D. J. 2004, 'The wedge mechanism for cutting of water saturated sand at large cutting angles'*, Proceedings of the WODCON XVII*, September 2004, Hamburg Germany.

Mink, F. D. Van Raalte, W. Vlieger, De. Hugo, G. Russell, M. 2006, 'Impact of European Union Environmental Law on Dredging', *Terra et Aqua,* vol. Number 104

Myre, E. Shaw, R. 2006, *The Turbidity Tube: Simple and Accurate Measurement of Turbidity in the Field,* written for the requirements of CE 5993 Field Engineering in the Developing World and FW 5770 Community Planning and Analysis, MSc. thesis, Michigan Technological University, Michigan.

Nakheel 2009, *The World - Dredging and Reclamation*, accessed 23 November 2009
< http://www.zawya.com/projects/project.cfm>.

Nautilus, Minerals Inc. 2009, *Solwara 1 Development Project Update*, Toronto, accessed 28 June 2010, <http://www.marketwire.com/press-release/Nautilus-Minerals-Inc-Solwara-1-Development-Project-Update-TSX-NUS-991772.htm>.

Negahban, M. 2002, *Equations of motion for a rigid body (Euler's laws)*, Department of Engineering Mechanics, University of Nebraska, Lincoln, NE 68588-0526.

NIOT (National Institute of Ocean Technology) 2002, *Technology Projects > Deep Sea Mining* Chennai, accessed 28 June 2010, <http://www.niot.res.in/projects/dsm/dsm_facilities.php>.

Odong, J. 2007, ' Evaluation of empirical formulae for determination of hydraulic conductivity based on grain-size analysis', *The Journal of American Science,* 3(3).

Palmer, C. A. King, R. A. 2008, 'Subsea Pipeline Engineering', 2 edn, Pennwell Books, Oklahama.

Paragon International, bv 1991, 'Reservoir dredging - Temporary management and technical assistance' Document no. IBTA IN 91.506-01 P11006, Oud-Alblas, The Netherlands.

Paragon International, b. 1993, 'Opening the horizon', Document no. IBTA IN 91.506-03 P11006, Oud-Alblas, The Netherlands.

Parr, J. Mason, C. Boughen, N. Fulton, B. Griffiths, C. Johns, S. Paxton, G. Sweetapple, M. & Yeats, C. 2009, 'Marine mining: Integrated social and environmental research in the design of a NSW test case.', *Proceedings of the Coastal Conference 2009*, Sydney, NSW.

Payne, P. 1954, *The relationship between the mechanical properties of soil and the performance of simple cultivation implements,* PhD thesis, National Institute of Agricultural Engineering, Reading, UK.

Payne, P. C. J. & Tanner, D. W. 1959, 'The relationship between rake angle and the performance of simple cultivation implements', *Journal of Agricultural Engineering Research*, p. 14.

Peire, K. Neman, H. & Bosschem, E. 2009, 'Gravity base foundations for the Thornton bank offshore wind farm', *Terra et Aqua,* vol. 115, no. June, pp. 19-29.

Perry, C. C. Lissner, H. R. 1962, *The strain gage primer*, McGraw-Hill.

PIANC (Permanent International Association of Navigation Congresses) (ed.) 1984, *Classification of soils and rocks to be dredged*, Brussels, Belgium.

Primidi 2009, *Forget Space Tourism Go Underwater,* accessed 13 November 2009, <http://www.primidi.com/Forget_Space_Tourism_Go_Underwater>,.

Queensland Government 2012, 'Gladstone harbour dredging not releasing contaminants', ed. Media Room, released on 4 May 2012,Research centre, Queensland Government.

Reece, A. R. Grinsted, T. W. 1986, 'Soil mechanics of submarine ploughs', *Proceedings of the Offshore Technology Conference*, Houston, Texas, May 5-8 1986.

Reece, A. R. Hettiaratchi, R. P. 1989, 'A slip-line method for estimating passive earth pressure', *Jounal of Agricultural Engineering,* vol. 42, pp. 27-41.

Reese, L. C. 2001, *Single pile and pile groups under lateral loading*, Taylor & Francis group plc, London, UK.

Relay, W. Sturges, L. & Morris, D 2007, *Mechanics of materials,* 6th edn, John Wiley & Sons.

Roberts, A. W. 2000, 'Design considerations and performace evaluation of screw conveyors', accessed on 23 June 2010 <www.saimh.co.za/beltcon/beltcon11/beltcon1114.htm>.

Rocke, S. 2003, 'Subsea Power Transfer - What is the Challenge', *Proceedings of the Applied Technology Workshop,* Oslo.

RSData 1983a, *Fixed voltage series regulators*, accessed on 24 January 2011, < ww.alldatasheet.com/?gclid=CLCEroj3tbACFUZ76wodYWHm8A>.

RSData 1983b, *Instrumentation Amplifier RS AD524A*, accessed on 24 January 2011, <www.alldatasheet.com/?gclid=CLCEroj3tbACFUZ76wodYWHm8A>.

Sarkar, M. K. 2011, 'Conceptual Design of a Submersible Remotely Operated Swimming Dredger (SROSD) - [49868]', *Proceedings of the OMAE2011*. Rotterdam, The Netherlands.

Sarkar, S. 2007, *Submersible walking dredger/ miner,* Ph D thesis, Faculty of Engineering and Applied Science, Memorial University of Newfoundland St. Johns, Newfoundland,Canada.

Schmertmann, J. H. 1978, 'Guidlines for cone penetration test. (Performance and design)', TRIS and ITRD database, Accession no. 00302192, accessed on 23 february 2010, <http://ntl.bts.gov/lib/35.../0/35414/FHWA-TS-78209.pdf>.

Schwartz, J. L., R Goldstein, R 2000, 'Drinking water turbidity and gastrointestinal illness in the elderly of Philadelphia', *Epidemiol Community Health,* vol. 54, p. 7.

Slinn, T. 2009, 'Top of the world', *Dredging and Port Construction,* October 2009, <www.dpcmagazine.com>.

SMD 2009, *Soil Machine Dynamics-Our Products*, Soil Machine Dynamics, NewCastle upon Tyne, <http://smd.co.uk/products/>, accessed 12 September 2009.

SMD 2012, *Products, Hydraulic thrusters*, SMD, Newcastle upon Tyne, <http://www.smd.co.uk/products/curvetech/hydraulic-thruster.htm>, accessed 06 March, 2012.

Smedley, P. L. & Kinniburgh, D. G. 2009, *Source and behaviour of arsenic in natural waters*, World Health Organisation Wallingford, Oxon OX10 8BB, U.K., accessed 13 November 2009, <www.who.int/entity/water_sanitation_health/dwq/arsenicun1.pdf.>.

Spadaro, P. A. 2011, 'Remediation of contaminated sediment: A worldwide status survey of regulation and technology', *Terra et Aqua,* vol. 123, no. June 2011, p. 10.

Spiegel, M. 1992, *Theory and problems of statistics,* Metric edition edn, McGraw-Hill Book Company, Singapore.

Tangirala, S. & Dzielski, J. 2007, 'Variable buoyancy control system for a large AUV', *Journal of Oceanic Engineering, IEEE ,* vol. 32, no. 4, p. 10.

Teferra, A. 1975, 'Beziehungen zwischen Reibungwinkel und Sondierwiderstanden', *F.B.G. Aachen,*

Terzaghi, K. 1925, 'Principles of soil mechanics IV-Settlement and consolidation of clay', in *Engineering News-Record*.

TID (ed.) 1993, *Cutter Suction Dredging Handbook Part I* Training Institute for Dredging, Kinderdijk, the Netherlands.

Van Leussen, W. 1983, 'Theorie snijden van zand onder water', Delft Hydraulic Laboratory, Delft, the Netherlands, p. 35.

Van Leussen, W. & Nieuwenhuis, J. D. 1984, 'Soil mechanics aspects of dredging', *Geotechnique,* vol. 34, no. 3, p. 23.

Van Os, A. G. 1977, 'Behaviour of soil when excavated under water', Document no. D.2, Delft Hydraulics Laboratory, Delft, The Netherlands.

Van Os, A. G. & Van Leussen, W. 1987, 'Basic research on cutting forces in saturated sand', *Journal of Geotechnical Engineering,* vol. 113, no. 12

Van de Velde, M. 2008, *Dredging- The past two decades*, accessed 23 November 2009, < http://www.theartofdredging.com/20years.htm >.

Verheul, O. Vercruijsse, P. M. & Miedema, S. A. 2004, 'The development of a concept for accurate and efficient dredging at great water depths', *Proceedings of the WODCON XVII*, Humburg, Germany.

Verruijt, A. 1985, *Offshore Soil Mechanics*, Delft University of Technology, Delft, the Netherlands.

Verruijt, A. 1999, *Soil Mechanics*, Delft University Press, Delft, the Netherlands.

Verruijt, A. 2001, *Soil mechanics*, Delft University of Technology, geotech.pe.kr., Delft, the Netherlands.

Vlasblom, W. 1999, College WB3413 Baggerprocessen, College notes, MSc. Dredging Technology, Delft University of Technology, Delft, The Netherlands.

Vlasblom, W. 2000, 'Relation between cutting, sidewinch and axial forces for cutter suction dredgers', in, *Delft University of Technology*, Delft, the Netherlands, p. 16.

Waldmann, C. R., L 2007, 'Traction properties of the wheels of an underwater crawler on different soils', *Proceedings of the OCEANS 2007*, Sept. 29 2007-Oct. 4 2007 Vancouver, BC.

Walker, T.I. Fabris, G. J. Knuckey, I. A. Sporcic, M. I. & Hudson, R. J. 1997, 'Webb Dock Marine Ecology Study, Interim report to Melbourne Port Corporation by Marine and Freshwater Resources', ed. V. G. EPA, Melbourne, Australia.

Whitcomb, L. L. & Yoerger, D. R. 1999, 'Development, comparison, and preliminary experimental validation of non-linear dynamic thruster models', *IEEE Journal of Oceanic Engineering,* vol. XX, no. XX 1999, pp. 1-15.

Whitlow, R. 1998, *Basic soil mechanics,* Third edition, Reprint edn, Addison Wesley Longman Ltd.

WHO 2001, *Leaching behavior of arsenic from various rocks by controlling geochemical conditions*, accessed 13 November 2009, <http://www.who.int/mediacentre/factsheets/fs210/en/index.html>.

Wikipedia 2009, *Palm Islands*, accessed 23 November 2009, <en.wikipedia.org/wiki/Palm_Islands>.

Wikipedia 2012, *Moon pool*, accessed 24 March 2012, <http://en.wikipedia.org/wiki/Moon_pool>.

Wikipedia 2010, *Population growth*, accessed 16 July 2010, <http://en.wikipedia.org/wiki/Population_growth>.

Williams, G. L. & Visser, K. G. 1997, 'The Punaise: A Remotely Operated Submerged Dredging System', *Terra et Aqua,* vol. December 1997, no. 69, p. 9.

Winkelman, M. 2011, 'A dredging revolution', *Dredging & Port Construction,* vol. 2011, no. July, p. 4.

Wong, J. Y. 2001, *Theory of ground vehicles,* Second edn, John Wiley & Sons, New York.

Yatsuk, E. P. Panov I. M. Efimov D. N. Marchenko O. S. & Chernenkov A. D. 1984, *Rotary soil working machines Construction, calculation and design*, Amerind Publishing Co. Pvt. Ltd. , New Delhi.

Zhao, Y. 2001, *Calculation of pressure and force in water saturated sand cutting with boundary edge pattern,* MSc. thesis, Technical University of Delft, Delft, The Netherlands.

Zwanenburg, M. 2004, 'The exploitation of cockle shells', *Terra et Aqua,* vol. 94, no. March 2004, p. 13.